HEINRICH HEINE
UNIVERSITÄT DÜSSELDORF

Characterisation of the Hepatitis C Virus protein NS5A interaction with human SH3 domains

Inaugural-Dissertation

zur Erlangung des Doktorgrades
der Mathematisch-Naturwissenschaftlichen Fakultät
der Heinrich-Heine-Universität Düsseldorf

vorgelegt von

Amine Betül Aladağ

aus Krefeld

Düsseldorf, März 2012

Aus dem Institut für Physikalische Biologie

der Heinrich—Heine—Universität Düsseldorf

Gedruckt mit der Genehmigung der

Mathematisch-Naturwissenschaftlichen Fakultät der

Heinrich—Heine—Universität Düsseldorf

Referent: Prof. Dr. Dieter Willbold

Koreferent: Prof. Dr. Georg Groth

Tag der mündlichen Prüfung: 24.04.2012

To My Sisters

Zehra and Fatıma

Index

I. Introduction

I.1 Hepatitis C Virus

The family of *Flaviviridae* includes numerous pathogens such as the Hepatitis C Virus (HCV) and the dengue virus. *Flavi* is the Latin word for "yellow" and is named after the famous member "Yellow Fever Virus". The family is a small group of enveloped RNA viruses that consists of the *Hepacivirus*, *Flavirus* and *Pestivirus*. HCV is the sole member of the *Hepacivirus* genus. The hepatocyte is the primary target cell although various lymphoid populations may also be infected at lower levels (Hiasa, 1998). HCV was discovered after specific diagnostic tests for Hepatitis A (HAV) and B (HBV) revealing that most of the post transfusion hepatitis could not be linked to HAV or HBV. Molecular cloning of the viral genome identified HCV as the causative agent for chronic human non A, non B hepatitis NANBH (Kuo et al. 1089). Currently about 130 to 170 million people worldwide are infected by HCV and 350 000 die each year (WHO 2000), representing a growing public health burden. The viral isolates are classified into eleven genotypes and a varying number of subtypes. The most common genotypes are listed in the table I.1 featuring the geographic distribution of the different types. The most common genotypes are the isolates 1a and 1b. The majority of the patients (80%) develop a chronic infection which can lead to liver cirrhosis, hepatic failure and hepatocellular carcinoma (HCC). The current therapy is based on interferon–α (IFN–α) and ribavirin combined medication, which gives a response rate of 48% for the genotypes 1, 4, 5 and 6 and around 88% for the genotypes 2 and 3 (NA for the other genotypes)(Poynard et al. 2003). HCV is classified as an oncovirus, which causes together with HBV worldwide 4.9 % of human cancers (Parkin; 2006).

Table I.1 Global distribution of the most common HCV geno– and subtypes (Maertens and Stuyver, 1997)

Most common HCV genotypes	Global distribution
1a	North and South America, also common in Australia
1b	Europe and Asia
2a	most common genotype 2 in Japan and China
2b	most common genotype 2 in USA and Northern Europe
2c	most common genotype 2 in Western and Southern Europe
3a	prevalent in Australia (40%) and South Asia
4a	prevalent in Egypt
4c	prevalent in Central Africa
5a	prevalent only in South Africa
6a	restricted to Hong Kong, Macau and Vietnam

7a and 7b	Thailand
8a,8b, and 9a	prevalent in Vietnam
10a and 11a	Indonesia

One of the main obstacles in finding a vaccine for HCV infection HCV replicase has no proof–reading ability and hence several so called quasi–species will be detected in the same patient during the disease development. Despite the fact that the virus has been already discovered for more than 20 years, knowledge about HCV lifecycle is limited due to the lack of efficient cell culture and small animal models for the infection.

I.1.1 Structural and genomic organisation of HCV

The members of the *Flaviviridae* virus family have three structural proteins involved in the creation of new viral particles. As a result, the viral surface is a mix of the glycosylated envelope proteins E1 and E2, which are anchored to the membrane. Underneath the envelope layer the nucleocapsid is located. It is composed of the core protein and contains the viral positive strand RNA genome. *Flaviviridae* follow a receptor mediated endocytosis into host cells, utilising several host receptors. Fusion of the viral envelope with the cellular membrane leads to nucleocapsid release into the cytoplasm. After this entry event, the precursor polyprotein is produced and cleaved by cellular and viral proteases into the structural (S) and non–structural proteins (NS).

Fig. I.1 I. Shown is the schematic genome organization of HCV virus with the 5' UTR site which contains the internal ribosome entry site (IRES). The HCV ORF encodes for 10 (11) proteins. The structural proteins are located in the N–terminal region of the ORF, denoted as S and highlighted in lighter grey. This region includes three structural proteins Core (C), E1 and E2, a small protein, p7, whose function has not yet been determined. The C–terminal segment highlighted in a darker grey encodes the 6 non–structural (NS) proteins, NS2, NS3, NS4A, NS4B, NS5A and NS5B, including the 3'UTR region. (Rijnbrand and Lemon, 2000.) Protein "F" is the 11th protein which results from a frameshift in the C protein region.

Despite the mentioned similarities between the members of the *Flaviviridae*, HCV does exhibit a number of differences. HCV translation is not cap–dependent. The HCV 5' untranslated region (UTR) folds into a complex RNA secondary structure, including a small part of the core coding region, which

is an internal ribosome entry site (IRES) that directly binds the 40S ribosomal subunit without the need of canonical translation initiation factors (Lemon and Honda, 1997)(figure I.1).

The HCV open reading frame, (ORF) contains 9094 to 9111 bp depending on the genotype. The ORF encodes at least 11 proteins, including 3 structural proteins Core , E1 and E2, a small protein, p7, whose function has not yet been definitely defined, 6 nonstructural (NS) proteins, NS2, NS3, NS4A, NS4B, NS5A and NS5B, and the so called "F" protein which results from a frameshift in the core encoding region (Xu et al. 2003). The resulting polyprotein is cleaved by cellular and viral proteases.

I.1.2 HCV nonstructural protein NS5A: subcellular localisation and structural features

The localisation of NS5A has been studied fairly well, screening liver biopsy samples from chronic HCV patients as well as overexpressing NS5A in human hepatoma cells. NS5A localises in the cytoplasm, the perinuclear membrane fraction and at the ER/Golgi membrane (Polyak et al. 1999, Tanji et al. 1995a). When expressed in context of the HCV replicon system in Huh cells, NS5A co–localises with the HCV core protein, as well as associates with human apolipoprotein A1 on the surface of globular structures containing lipid droplets (Shi et al. 2002). It is typical for plus strand RNA viruses to replicate their genome in close association with host intracellular membranes. These membrane platforms can either be pre–existing membrane organelles or membrane structures induced *de novo* by the virus (Egger et al. 2002). These globular membrane structures were analysed and described by Moradpour et al. 2004 as "membranous web". Given the evidence that NS5A colocalises in such specialized cytoplasmic membrane fractions and associates with the HCV core protein, HCV nonstructural proteins (Shirota et al. 2002) and the nascent viral RNA, it is clear that NS5A indeed participates in a multiprotein virus replication and assembly complex. However, the molecular structure and function of this complex remains elusive and a challenge for future research.

The HCV nonstructural protein NS5A is a proline–rich protein without transmembrane helices. It is predicted to be hydrophilic. The understanding of the functional properties of NS5A was limited for a long time due to the lack of structural information. However, in the recent years an increasing number of structural features have been derived experimentally. NS5A does not show any ER retention domains or evidence for lipid modifications. The initial N–terminal 30 amino acids were predicted to form an amphipathic helix (Brass et al. 2002). The structure was experimentally verified by nuclear magnetic resonance spectroscopy (NMR) by Penin et al. 2004. The amphipathic helix is conserved throughout all HCV subtypes emphasizing its importance for the NS5A function. Hydrophobic amino acids on one side of the helix facilitate its attachment to intracellular membrane

compartments, buried within the cytosolic leaflet of the lipid bilayer. Mutation studies on the helix showed that it is crucial for membrane association of NS5A protein. Disruption of the conserved hydrophobic nature of the amphipathic helix resulted in localisation of NS5A predominantly in the nucleus. The delocalisation of NS5A shows that in addition to the membrane–anchoring function, the helix is important for HCV replication (Elazar et al. 2003). Different localisation in different compartments may contribute to different biological functions of NS5A.

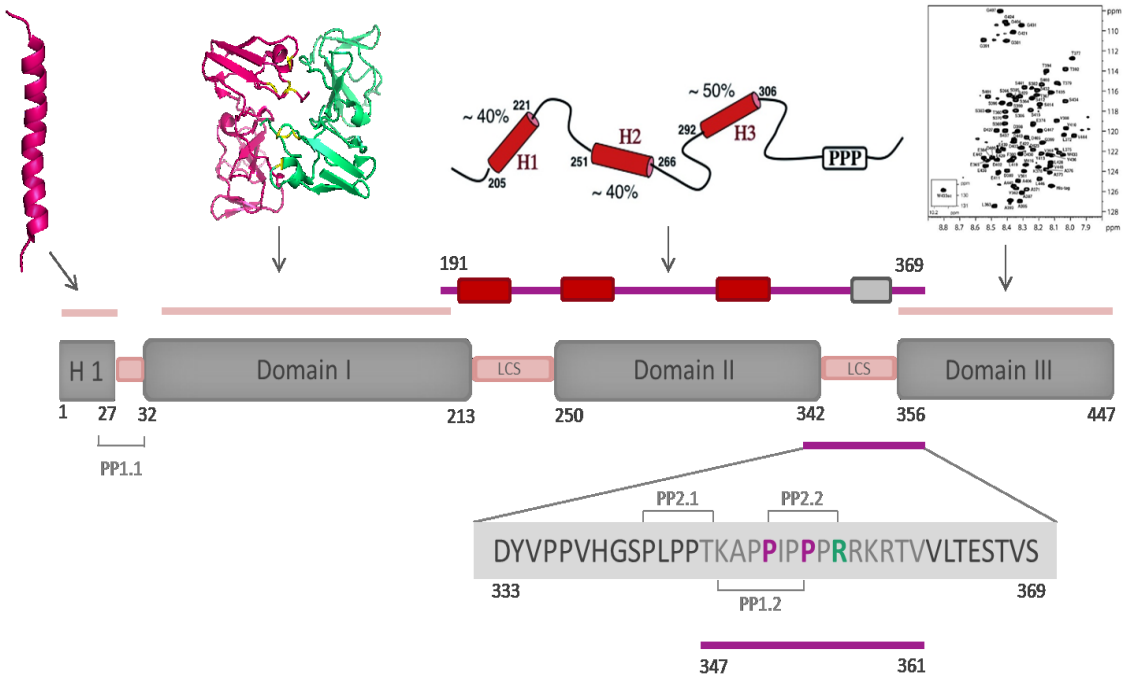

Fig.I.2 NS5A domain organisation. The grey bar describes the domain organisation of NS5A including the "low complexity sequences" (LCS) linkers (pink), and PxxP motives. The corresponding ribbon diagrams of the N–terminal amphipathic helix (Penin et al. 2005; PDB: 1R7C) and the crystal structure of domain 1 (Tellinghuisen et al. 2004; PDB: 1ZH1) are shown on top. The $^{1}H–^{15}N$ HSQC spectrum of domain 3, which is described as intrinsically unstructured (Verdegem et al. 2011), is also shown on top of the respective domain. The fractions of NS5A, which are studied in this work, are highlighted with magenta bars. These are NS5A (191–369), which spans the entire domain II and parts of domain I and III, including the LCS regions as well as the three of four PxxP–motifs. This fragment displays a propensity for three transient α–helices, schematically shown above (chapter VI.5). The helical regions are highlighted in red on the magenta bar. NS5A (333–369), the sequence is highlighted in grey and the corresponding PxxP motives are shown in the above figure denoted as PP1.1, PP1.2, PP2.1 and PP2.2 (MacDonald et al. 2004). Peptide NS5A (347–361) is also highlighted with a magenta bar beneath the sequence, including the main PxxP motif.

Bioinformatics–assisted modeling and proteolysis of NS5A revealed a high plausibility for a three domain organization apart from the N–terminal amphipathic helix. The structure of domain 1 of NS5A was solved by Tellinghuisen et al. 2005 using X–ray crystallography.

NS5A protein exists in multiple phosphorylation states, described as p56 as basal and p58 as hyper, consistent with their migration on sodium dodecyl sulfate polyacrylamide gel electrophoresis SDS PAGE (Kaneko et al. 1994). The phosphorylation of NS5A is a well conserved feature among the different genotypes and *Flaviviridae* family of NS5A proteins. Considerable effort has been put into the characterisation of the phosphorylation sites, which are mainly serine residues and into the identification of the host kinases involved in the phosphorylation (Katze et al.2000), suggesting that NS5A kinase belongs to the CMGC family of kinases (CMGC group: cyclin–dependent kinases (CDKs), mitogen–activated protein kinases (MAP) kinases, glycogen synthase kinases (GSK) and CDK–like kinases), likely to be a proline–directed kinase. The HCV NS protein dependent different phosphorylation patterns, shown for NS5A during HCV replication, affect presumably its interaction and formation of protein complexes with other proteins (Evans et al 2004).

NMR studies on domains 2 and 3 showed that both have no globular structural domain organization, but can be categorized into the family of intrinsically disordered proteins (Verdegem et al. 2011 and Liang et al. 2007)(figure I.2).

I.1.3 HCV nonstructural protein NS5A: interaction with human proteins

One of the possible explanations for HCV persistency in the human liver and the subsequent irreversible liver damages such as cirrhosis or HCC, may be connected to the promiscuous character of NS5A protein. There is an enormous amount of literature describing the intercepting role of NS5A in cellular pathways. These pathways are connected to cell growth, cell cycle control, apoptosis, cell survival and cellular stress response. The focus toward NS5A was catalyzed with investigation of why HCV shows resistance toward IFN. NS5A binds and inhibits directly the IFN–induced kinase, protein kinase R (PKR) (Gale et.al. 1997), thus disrupting the immune response. Furthermore, interacting with growth factor receptor–bound protein 2 (Grb2) (Tan et al. 1999), an adaptor protein involved in growth factor signaling, allows HCV to disturb the mitogen–activated protein kinase (MAPK) mitogenic pathway. The MAPK pathway controls transcription factors which are important for cellular gene expression. Some of the affected genes encode for proteins involved in signal–transducers–and–activators–of–transcription 1 and 3 (STAT1/3) signaling pathway which are part of the IFN dependent genes network (He & Katze 2002). Further, NS5A also modulates the

phosphatidylinositol 3–kinase–protein kinase B (PI3K–AKT) mediated cell survival pathway, contributing to HCV persistence in human cells. Hereby, NS5A interacts directly with the p85 regulatory subunit of PI3K and enhances the phosphotranferase activity of p110, the catalytic subunit of PI3K (Street et al. 2004), disrupting the apoptotic process. In addition to the AKT pathway mediated apoptosis, NS5A also associates with the tumor necrosis factor receptor type 1–associated DEATH domain protein–fas–associated protein with death domain (TRADD–FADD) signaling complex and blocks the tumor necrosis factor (TNF) –dependent apoptosis (Majumder et al. 2002).

NS5A contains a number of polyproline motifs (PxxP) that mediate interaction with a number of cellular proteins including Src–homology–3 (SH3) domains. These domains are involved in various proteins of the cellular signaling and cytoskeletal organization network (Mayer; 2001) and mediate protein–protein interaction by binding to proteins that contain PxxP motifs. The binding to SH3 domains occurs in two possible orientations in which the position of the basic residue designates the binding orientation to the SH3 domain. Therefore, motifs with the consensus sequence K/RxxPxxP are known as class I motifs, whereas class II motifs follow the sequence PxxPxR. NS5A has two class I and two class II motifs which are designated as PP1.1 and PP1.2 for class I and PP2.1 and PP2.2 for class II (MacDonald et al. 2004). Figure I.2 shows the localisation of these protein–protein interaction motifs within the context of the whole NS5A protein. Like HIV Nef NS5A is able to interact via its PxxP motif (PP2.2) with the SH3 domains and modulate the activity of Src–family kinases such as inhibiting Hck, Lyn (interacts with the PP2.1 motif as well), Lck and activating Fyn (MacDonald et al. 2005 and Shelton et al 2008). However, the downstream effects as well, as the physiological role of the NS5A interaction with these kinases remains unclear.

Another interesting human protein which was shown to interact with NS5A through its C–terminal PxxP motif is bridging integrator 1 (Bin1, also known as amphiphysin II) (Zech et al 2003). Substituting the prolines to alanines in the three C–terminal PxxP motifs of NS5A resulted in drastically reduced binding to Bin1 in an *in vitro* pull down assay, but did not completely abolish the interaction. Whereas, a C–terminal deletion (aa 278–447) of NS5A resulted in no Bin1 binding. This specific interaction was also analysed by Nanda et al. 2006, after identifying Bin1 as an NS5A interaction partner in a yeast 2–hybrid screen of 2 human cDNA libraries. The role of NS5A Bin1 interaction in Bin1 induced apoptosis was analysed using an apoptosis assay (TUNEL assay). NS5A successfully inhibited apoptosis in Bin1 transfected HepG cells which are lacking endogenous Bin1. Bin1 alone is not pro–apoptotic in many cell types, but it clearly is linked to Myc controlled death pathways.

Yamaguchi sarcoma viral oncogene homolog (Yes), another Src–family kinase, was identified during the same yeast 2–hybrid screen by the Liang group. The yes kinase plays a role in several signaling pathways one of them being the CD95L/FASLG signaling pathway, triggering AKT–mediated cell

migration and apoptosis. The CD95 death receptor pathway is important for liver apoptosis and regeneration (Reinehr et al. 2012), the main organ affected by HCV infection. One could speculate that interaction of NS5A with Yes kinase is yet another mechanism by which HCV inhibits apoptosis within infected hepatocytes.

I.2 Bridging integrator 1 protein

The human Bin1 gene encodes for various different isoforms, which result from alternative splicing (Wechsler–Reya et al. 1997). The ubiquitously expressed Bin1 gene contains an N–terminal Bin–amphiphysin–Rvs (BAR) domain, a C–terminal SH3 domain and a site for myelocytomatosis (Myc) binding domain (MBD), in between. The middle region is variable among the isoforms. Other splicing isoforms contain other binding sites for Clathrin–AP2 (CLAP) and phosphoinositide binding region (PI) in the middle region as well (figure I.3). Bin1 is a nucleocytoplasmic protein and depending on the isoform also tissue specific.

Fig.I.3 Bin1 domain organisation. Shown is the schematic domain organisation of Bin1 protein, which is expressed ubiquitously. The N–terminal BAR domain, which is important for inducing membrane curvature, is followed by several interaction domains which were named with their specific interaction partners. The phosphoinositide binding region (PI), followed by Clathrin–AP2 binding site (CLAP) and the Myc binding domain MBD. She C–terminal SH3 domain plays

Bin1 is a member of the membrane sculpting BAR protein superfamily. Bin1 is involved in inducing membrane curvature and membrane remodeling via its BAR domain. The function is carried out after hetero–dimerization of two BAR domains which display mainly a highly flexible α–helical fold (Ren et a.l 2006). Beside its function as a membrane remodeling unit, Bin1 is also a Myc interacting adaptor protein with tumor suppressor properties (Sakamuro et al.1996). It is a negative regulator of Myc transcription factor activity. Myc is a key transcription factor, regulating cell proliferation or apoptosis. Loss of Bin1 expression, a mechanism not well understood, yet, leads to malignant transformations as shown for breast carcinoma (Ge et al. 2000). Several research groups investigated the Myc Bin1 interaction. The myc binding domain (MBD) on Bin1 has been first identified as the crucial binding region (Sakamuro et al. 1999). However, NMR experiments and pull–down assays with various Bin1 mutants investigating the Myc Bin1 interaction revealed that the SH3 domain of Bin1

plays a considerable, if not the major role in the interaction (Pineda–Lucena et al. 2005). A conserved class II SH3 binding motif inside the MB1 domain of Myc has been identified as the core determinant for Bin1 Myc interaction. The binding motif on Myc contains two phosphorylation sites at Ser62 and Thr58. Remarkably, only phosphorylation of Ser62 abrogates binding to Bin1 SH3 domain (Pineda Lucena et al. 2005). Thr58 phosphorylation shows no effect on SH3 binding. The two phosphorylation sites are hierarchical and occur in a cell cycle dependent manner (Facchini & Penn, 1998). The Bin1 Myc interaction may be regulated by phosphorylation. Also alternative splicing of Bin1 which results in translation of exon 12, leads to a phenotype which is disabled in Myc interaction. This so called Bin1+12A isoform contains an internal class I SH3 binding motif and has been reported to be the main phenotype in malignant melanoma cells (Ge et al. 1999). It is discussed that the Bin1+12A isoform loses its tumor suppressor ability through intramolecular binding of the intrinsic PxxP from exon 12A motif to the Bin1 SH3 domain, thus blocking Myc interaction (Pineda Lucena et al. 2005). This leads to the conclusion that alternative splicing of Bin1 can be seen as an intrinsic and tissue specific regulating mechanism, by which the accessibility of the SH3 domain plays a key role towards SH3 dependent protein partners. Considering the complex function of the Myc protein in the cells as a driving force in cell cycle and malignant transformation as well as a potent inducer of programmed cell death (Evan et al. 1992), the function and regulation of Bin1 as a tumor suppressor in a Myc context becomes more complicated. The interaction is highly regulated and seems to occur under specific physiological conditions only (Telfer et al. 2005). The interaction of NS5A and Bin1 is likely to have an effect on this sensitive regulatory mechanism. The details are not investigated yet, but remain an interesting challenge in further understanding of HCV infection and HCC development.

I.3 Intrinsically disordered proteins

Intrinsically disordered proteins (IDPs) are highly abundant in nature (Ward et al. 2004) and play a number of crucial roles in living cells. This leads away from the classical idea of protein function connected to a three dimensional fold. In fact, in the last ten years the role of IDPs grew from merely being a rare exception toward a new class of intensely researched proteins (Wright and Dyson, 1999, Tompa 2002). According to DisProt (http://www.disprot.org/), a database for IDPs, currently 645 proteins are registered as IDPs with 1379 disordered regions. IDPs are biologically active and yet fail to form a specific 3D structure. Instead, they exists as dynamic ensembles in which backbone atom positions and Ramachandran angles vary significantly over time with no specific equilibrium values in contrast to well–defined proteins (Uversky et al. 2011). This does not mean that there is an absence

of local order. They exhibit transient order at the level of primary and secondary structure that correlates with their specific functions, allowing a remarkable binding promiscuity. Some IDPS are also able to fold upon binding to their specific interaction partners. IDPs can be classified as 28 distinct categories according to their functions which can be reduced to four functional classes (Dunker et al. 2002). The first class is that of entropic chain in which the function is directly linked to the molecular disorder. The second class is protein modification and the third functional class is molecular recognition. IDPs involved in molecular assembly by coordinating and stabilizing multiprotein complexes are categorized as the fourth functional class. Some protein functional classes do not support disorder and therefore are lacking regions with high disorder contents. Such proteins are involved in enzyme catalytic activities such as amino acid biosynthesis and cell metabolism. A well–defined structure is important for catalytic activity. The other group of proteins consists of transport proteins, which are mostly membrane proteins and therefore are forced to have a certain fold inside the dielectric environment of the membrane (Xie et al. 2007 and Vucetic et al. 2007).

Most of the IDPs are detected and characterisedd using spectroscopic methods such as far UV circular dichroism spectroscopy (Adler et al. 1973) or NMR spectroscopy (Bracken et al. 2004, Dyson and Wright, 2005; De Guzman et al., 2004; Jensen et al. 2010; 2011) just to name two methods. A structural characterisation of IDPs with X–ray crystallography is not suitable. The NMR spectroscopic approach allows analyzing structural propensities, conformational ensembles and local dynamics of the IDPs. The increased backbone dynamics and angular flexibility demand special spectroscopic techniques to capture the events in the NMR time scale. The common approach is utilizing residual dipolar couplings (RDCs) between two pairs of nuclei in partially aligned proteins which is a sensitive tool to characterise structure and dynamics in unfolded proteins as it provides long distance structural information in contrast to the classic nuclear Overhauser effect approach (NOE)(Bernado et al, 2005). Another alternative method to gain long distance information in highly flexible IDPs is paramagnetic relaxation enhancement (PRE) experiments which require the introduction of a nitroxide group to the protein sequence (Phon Wu and Baum, 2010). iHADAMAC, a further NMR approach to cluster amino acids in groups has been introduced recently to gain complementary sequential information on IDPs (Feuerstein et al. 2012).

I.3.1 Amino acid determinants for disorder

There are several determinants for intrinsic disorder in proteins given by the amino acid content. A combination of low hydrophobicity with high net charge is the key determinant for the absence of globular structure in proteins (Uversky et al. 2000)(figure.I.4).

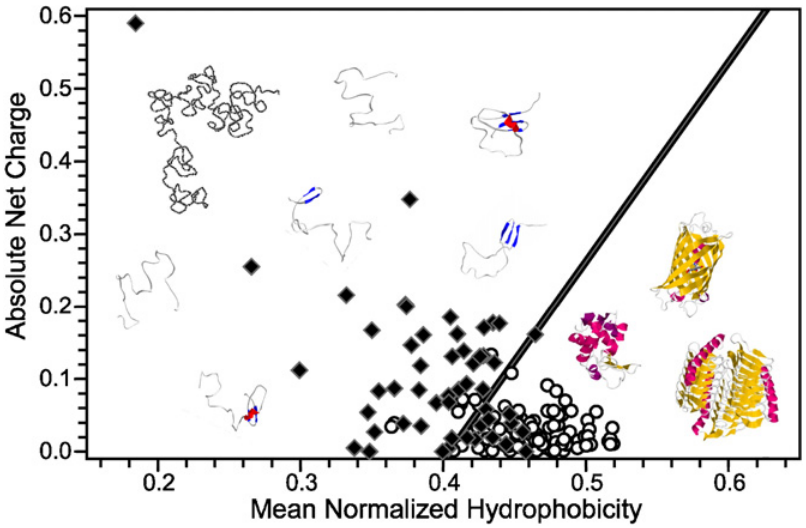

Fig.I.4 Peculiarities of amino acid composition of IDPs. Comparison of the mean net charge and the mean hydrophobicity for a set of 275 folded (open circles) and 91 natively unfolded proteins (black diamonds). The solid line represents the border between extended IDPs and compact globular proteins. Illustrative examples of extended IDPs (native coils and native pre–molten globules) and some ordered globular proteins are shown. (taken from Uversky, 2011)

Amino acids can be categorized into two classes with respect to their ability to promote order within a protein. These so called order promoting amino acids are Ile, Leu, Val, Trp, Tyr, Phe, Cys and Asn, whereas Ala, Arg, Gly, Gln, Ser, Glu, Lys and Pro are the disorder promoting amino acids (Williams et al. 2001). These common sequence features shared by IDPs are the basis for several bioinformatical approaches to define algorithms to predict disorder which is encoded in the primary sequence of a protein (He et al. 2009). High proline content is also in disfavour of rigid secondary structure, but in favour of the conformational open left handed polyproline helix (PPII).

I.3.2 IDPs: Proteins with a complex binding mechanism?

The binding mechanisms and in particular the binding promiscuity of IDPs is one of the unique functional characteristics which is subject to intensive research. Proteins with the ability to bind multiple partners are known as hub proteins (Han et al. 2004). Several models were proposed to describe the ability to bind multiple partners, not fitting the classical molecular recognition mechanism. Neither the “lock to key”, nor the “induced–fit” models deliver satisfactory explanations

for how one protein can bind multiple partners. In contrary experimental data proposed that IDPs can be considered as plastic and can adopt specific structures upon binding to different partners (Kriwacki et al. 1996). This comes along with high specificity, but low affinity toward the different partners in the respective environment. Thereby, these observations suggest molecular recognition via disorder–to–order transition as a reasonable mechanism for protein–protein interactions. Disorder is also linked to kinetic advantages during the binding event. The flexibility to search throughout the space without conformational restrictions increases the capture radius leading to faster binding kinetics, which is the idea behind the "fly casting–mechanism" (Shoemaker et al. 2000). It is a two–step mechanism in which the unfolded polypeptide first binds weakly over a distant space to its interaction partner and folds while approaching the binding site. In contrast to the "fly–casting–model", comparison of experimental binding kinetics data available for IDPs showed that IDPs bind in general faster than ordered proteins and molecular dynamics experiments on IDP complexes were performed to show that they follow high on– and off–rates, resulting from the lower free energy barrier. In contrast, the capture rates of IDPs and ordered proteins were similar, proposing that the low energy barrier is the major kinetic advantage of IDPs (Huang and Liu, 2009).

I.3.3 IDPs involved in diseases

Playing a key role in many regulatory cellular processes, there is an increasing number of diseases connected to IDPs ranging from neurodegenerative diseases to cancer. Protein conformational diseases may not only result from protein misfolding but also from missignaling or misidentification through IDPs (Uversky et al. 2008) emphasizing the importance of research toward IDPs as drug targets. Also pathogenic microbes and viruses have a set of proteins which display intrinsically disordered domains or regions. IDPs have been recently described and discussed for measle virus nucleocapsid protein (Jensen et al. 2011), for matrix proteins of Human Immuno Deficiency Virus (HIV) related proteins (Goh et al. 2008), Influenza viruses (Goh et al. 2009) and for HCV NS5A (Liang et al. 2007). Long disordered regions in proteins are poorly immunogenic and induce only a weak immune response, thus are a tool for viruses to escape host immune response. It is speculated for highly flexible disordered regions in viral proteins with a small antibody binding site, that antibody binding is energetically not favourable. On the other hand, binding to the larger host receptor provides enough energy to overcome the flexibility barrier and induce binding through disorder–to–order transition (see chapter I.3.2) (Goh et al. 2008).

I.4 Aim of the work

Since NS5A plays a key role in many viral processes, including viral replication as well as intercepting in host cell pathways, studies describing the character and mode of NS5A interaction, are highly in focus. The objective of this present work is to characterise the interaction of hepatitis C virus NS5A fragments with different SH3 domains, which were described in literature as physiological binding partners and are significant for cellular signaling pathways. Several fragments which ranged from $NS5A_{191–369}$ to $NS5A_{333–369}$ and the shorter 15–mer fragment comprising the residues (347–361) of NS5A will be used in surface plasmon resonance spectroscopy (SPR) and nuclear magnetic resonance spectroscopy (NMR) studies with the respective SH3 domains. The results of the present work should deliver information about the interaction in a quantitative and qualitative way, allowing elucidating the binding determinants of NS5A, which is able to interact and intervene with many cellular factors in atomic resolution level. In this context protocols for expression and purification of recombinant $NS5A_{191–369}$ and $NS5A_{333–369}$ proteins were to be developed for future structural and interaction studies with the SH3 domains. Expression and purification protocols for the SH3 domains of Yes and Bin1 were also to be optimised in the same manner meeting the requirements of the spectroscopic methods used in this work. Furthermore the structural properties of $NS5A_{191–369}$ should be studied using NMR spectroscopy.

I. Material and Methods

II.1 Materials

II.1.1 Bacterial strains

In this work only the following *Escherichia coli* (E. *coli*) strains were used (table II.1.2).

Table.II.1.1 Strain, genotype and reference

Strain	Genotype	Reference
E. coli BL21(DE3)	F^-, *omp*T, *hsdS*B, (rB^-, mB^-), *dcm*, *gal*, λ(DE3)	(Grodberg & Dunn, 1988)
E. coli Rosetta(DE3)	F^-, *omp*T, *hsdS*B, (rB^-, mB^-), *dcm*, *gal*, *lacY1; pRARE;* λ(DE3); Cm^R	Novagen, Darmstadt
E.coli Rosetta(DE3) $T1^R$	F^-, *omp*T, *hsdS*B, (rB^-, mB^-), *dcm*, *gal*, *lacY1; pRARE;* λ(DE3); *recA* , *endA-* , *lacI q* ; *tonA*;Cm^R	Novagen, Darmstadt
E. coli BL21(DE3) $T1^R$	F^-, *omp*T, *hsdS*B, (rB^-, mB^-), *dcm*, *gal*, λ(DE3); *recA* , *endA-* , *lacI q* ; *tonA*	Novagen Darmstadt
E.coli Mach 1	F´{*lac*I^q Tn10(Tet^R)};*mcr*A; Δ(*mrr-hsd*RMS-*mcr*BC); Φ80*lac*ZΔM15; Δ*lac*X74; *deo*R; *rec*A1; *ara*D139; Δ(*ara-leu*)7697;*gal*U; *gal*K; *rps*L; *end*A1; *nup*G	

II.1.2 Oligonucleotides

The oligonucleotides which were used to amplify the SH3 domains of Bin1 and Yes and to generate $NS5A_{191-369}$ deletion mutant were purchased from BioTez, Berlin and are listed in the table below together with other oligonucleotides used in this work.

Tab.II.1.2. Name and sequence of the oligonucleotides

Name	DNA sequence
Bin1 SH3	$^{5'}$CAT AGC TGG TAT CCG GTG CCG ATT CCG CCG AGC AGC TAA GC$^{3'}$ $^{3'}$GTA TCG ACC ATA GGC CAC GGC TAA GGC GGC TCG TCG ATT CGC CGG$^{5'}$
Yes SH3	$^{5'}$GGA GGA GGA TCC GGT TTA ACA GGT GGT GTT ACT ATA TTT GTG G$^{3'}$ $^{3'}$GGA GGA CTC GAG TTA TGC CTG AAT GGA ATC TGC AGG TAC GAC TCA CTA TAG GG$^{5'}$
NS5A$_{191-349}$	$^{5'}$GGA TCC CTC CGC GGC GGT GAA CCG GAA CC$^{3'}$ $^{3'}$GAT TAT GTG CCG CCG GTG GTG CAT TAA GCG GCC GC$^{5'}$
T7 Terminator	$^{5'}$GCT AGT TAT TGC TCA GCG G$^{3'}$

II.1.3 Plasmids

All the plasmids used in the present work are summarized in table II.1.3

Tab.II.1.3 List of vectors

Name	Resistance	Property	Source
pGEX-6P–2	Ampicillin	Expression vector	Amersham Biosciences, Freiburg
pTTK19xUb	Kanamycin	Expression vector	Kohno et al. 1998
pDsRed–N1	Kanamycin	Eucaryotic expression vector	Clontech
pCFP–N1	Kanamycin	Eucaryotic expression vector	Clontech

II.1.4 Molecular Weight Marker

The markers used to estimate the molecular weight of protein or of DNA during the progress of an electrophoresis run are displayed in table II.1.4.

Tab.II.1.4 Name and company of the used Markers

Name	Company
PageRuler Prestained Protein Ladder	MBI Fermentas, St.Leon–Rot
Prestained Protein Marker, Broad Range	New England BioLabs, Frankfurt am Main
DNA standard 5000bp – 5 kb	Biozym, Hessisch Oldendorf

GeneRuler 100bp DNA Ladder	MBI Fermentas, St. Leon–Rot

II.1.5 Proteins and peptides

All the protein and peptide sequence used in this work are listed below in table II.1.5

Tab.II.1.5 Name and amino acid sequence of used proteins and peptides. The N–terminal GPLGS peptide overhang caused by HRV 3C digestion is highlighted in grey.

Name	Sequence
Bin1 SH3	GPLGSLPPGFMFKVQAQHDYTATDTDELQLKAGDVVLVIPFQNPEEQDEGWLMGVKESD WNQHKELEKCRGVFPENFTERVP
Yes SH3	GPLGSGLTGGVTIFVALYDYEARTTEDLSFKKGERFQIINNTEGDWWEARSIATGKNGYIPS NYVAPADSIQALE
Lyn SH3	GPLGSPEEQGDIVVALYPYDGHIPDDLSFKKGEKMKVLEEHGEWWKAKSLLTKKEGFIPSN YVAKLNT
Fyn SH3	GPLGSGGTGVTLFVALYDYEARTEDDLSFHKGEKFQILNSSEGDWWEARSLTTGETGYIPS NYVAPVDSIQA
NS5A (191–369)	GPLGSGTGSLRGGEPEPDVTVLTSMLTDPSHITAETAKRRLARGSPPSLASSSASQLSAPSLK ATCTTHHDSPDADLIEANLLWRQEMGGNITRVESENKVVILDSFEPLHADGDEREISVAAEI LRKSRKFPSALPIWARPDYNPPLLESWKDPDYVPPVVHGCPLPPTKAPPIPPPRRKRTVVLT ESNVS
NS5A (191–340)	GPLGSLRGGEPEPDVTVLTSMLTDPSHITAETAKRRLARGSPPSLASSSASQLSAPSLKATCT THHDSPDADLIEANLLWRQEMGGNITRVESENKVVILDSFEPLHADGDEREISVAAEILRKS RKFPSALPIWARPDYNPPLLESWKDPDYVPPVVH
NS5A (333–369)	DYVPPVVHGSPLPPTKAPPIPPPRRKRTVVLTESTVS
NS5A (347–361)	TKAPPIPPPRRKRTV

II.1.6.Enzyme

Listed in table II.1.6 are all the relevant enzymes used in the present work

Tab.II.1.6 List of enzymes used in this work

Enzym	Comapany
*Bam*H1 *Not*I; *XHo*I	MBI Fermentas, Leon–Rot
Vent–polymerase	New EnglAnd Biolabs, Frankfurt am Main
Shrimp alkaline phosphatase (SAP)	MBI Fermentas, Leon–Rot
T4–DNA–ligase	MBI Fermentas, Leon–Rot
Lysozym	AppliChem, Darmstadt

DNAse A	AppliChem, Darmstadt
T4–DNA–Polymerase	MBI Fermentas, Leon Rot
YUH–Protease	Expressed and purified in this laboratory; plasmid kindly provided by Kohno group, Japan
Anti–M13–HRP–conjugated	Amersham Bioscience
HRV 3 C protease (PreScission)	Expressed and purified in this laboratory

II.1.7 *E. coli* cell culture medium

All the solutions components used for cultivation of *E. coli* cells are summarized below. The culture media utilized in the expression of various proteins were sterilized by autoclaving. Prior to usage the desired concentration of the respective antibiotic was added to the medium. Minimal medium 9 (M9) is described in methods

LB medium (Luria Bertani)

10 g Tryptone

5 g Yeast

19 g NaCl

ad 1000 ml H_2O bidest

II.1.8 Solutions and buffers

Solutions and buffers which are not listed below will be described in the respective section of the methods part

Ampicillin solution	200 mg/ml Ampicillin in H2O bidest., sterile filtered
Anode buffer (Tricine gels):	0.2 M Tris/HCl, pH 8.9
APS:	10 % (w/v) Ammoniumperoxodisulfat in H2O bidest.

Lysis buffer:	PBS with 10 mM β–Mercaptoethanol, 1 mM EDTA, 0.1% (w/v) 2 µg/ml Lysozym, DNase, complete protease inhibiting tablet
Fluorescence titration buffer:	1x PBS, 1 mM DTT
Hydrolase buffer:	50 mM Tris HCl pH 8.0 100 mM NaCl 1 mM 2–mercaptoethanol
Kanamycin–solution:	100 mg/ml Kanamycin in H_2O bidest., steril filtrated
Kathode buffer (Tricine gels):	0.1 M Tris/HCl, 0.1 M Tricin, pH 8.25, 0.1% (w/v) SDS
Laemmli loading buffer:	40 % (w/v) Saccharose, 3 % (w/v) SDS, 4% (v/v) 2–mercaptoethanol, 0.075 % (w/v) Bromphenolblue
NMR–sample bufferr:	50 mM KPi, 20 mM NaCl
PBS:	140 mM NaCl, 2,7 mM KCl, 10 mM Na2HPO4, 1,8 mM KH2PO4, pH 7.3
Protein dying reagent:	0.05 % (w/v) Coomassie Brilliant Blue R–250, 45% (v/v) Methanol, 9.2 % acetic acid

II.1.9 Chemicals and Kits

Acrylamide 4 K solution (30%) (Mix 29:1)	AppliChem, Darmstadt
Agarose SeaKem	Fluka, Neu–Ulm
Ammoniumchlorid [^{15}N]	Euriso–top, Saint–Aubin, France
Bis–Tris	Roth, Karlsruhe
Complete–Protease–Inhibiting tablet	Roth, Karlsruhe
dNTPs (desoxy–Nukleosid–Triphosphate)	MBI Fermentas, St. Leon Rot
Formamid	Sigma, München
Glukose [^{13}C]	Euriso–top, Saint–Aubin, France
Glutathion, reduced	Sigma, München
Glutathion–Sepharose 4B	Amersham Biosciences,
DEAE Sepharose	GE Healthcare, Munich

NTA Sepaharose	Amersham Biosciences,
Isopropyl–β–D–Thiogalactosid (IPTG)	Boehringer, Mannheim
2–mercaptoethanol	Roth, Karlsruhe
Midi Nucleobond AX 20und AX100 Kit	Machery–Nagel, Düren
Nucleo Spin Kit	Machery–Nagel, Düren
Phosphat–Citrat–buffer with Sodium–Perborat	Sigma, München

II.1.10 Other materials

Spectra/Por dialysis membrane (MWCO: 1000 und 3500 Da)	Roth, Karlsruhe
Minisart sterile filter (0,22 µm)	Sartorius, Göttingen
Microtiter plates Polysorp 96F	Nunc, Wiesbaden
Ultrafiltrations concentratoren (MWCO: 3000 Da)	Amicon, Beverly,USA
Biacore sensorchip: CM5; CM 5 S	GE Healthcare, Munich
NMR Tubes: Shigemi NMR tube 5 mm	Shigemi Corp., Tokyo Japan

Remaining materials were purchased from VWR–International (Darmstadt); Eppendorf (Wesseling–Berzdorf) and Sartorius (Göttingen).

II.1.11 Equipment

Tab.II.1.11 Equipment

Equipment	**Company**
BIAcore X; BIAcore T100; BiaCore T200	GE Healthcare, Munich
DNA –horizontalelektrophoresis	Amersham Biosciences
Fluorescence spektrometer: Perkin–Elmer LS 55	Perkin Elmer, Boston, USA
GelDoc2000	Bio–Rad, München
Lyophilizer Alpha 1–4	Christ, Osterode am Harz
NMR Spectrometer: Varian Unity INOVA, 600MHz, 800MHz and 900 MHz	Varian, Palo Alto, USA
SDS–PAGE: Mighty Small II	Hoefer/ Amersham Bioscience, Freiburg
PCR : Thermocycler PTC 200	Biozym, Oldendorf
Incubator	Unitron, Infors–HT, Einsbach
Ultrasonicator	Branson Sonifier 250, Branson Ultrasonics Corp., Danbury, USA

Centrifuge	Centrifuge 5810, Eppendorf Beckman – Coulter Avanti J–20 and J–301
CD	Jasco J810 CD–spectropolarimeter, Jasco, Gross–Umstadt
DLS	DynaPro DLS, Wyatt Technology Corporation, Santa Barabara, USA
UV	UV/VIS Spectrometer, Lambda 25, PerkinElmer, Skelton, MA, USA
FPLC	HiPrep 26/10 Desalting Column, HiLoad 26/60 Superdex 75 pg column, Amersham BioSciences, Freiburg
HPLC	Äkta purifier system, Amersham BioSciences, Freiburg

II.1.12 Data banks, internet based tools and other software used

The internet data banks SwissProt (http://expasy.org/)and TrEMBL (http://expasy.ch/sprot/) provided information for DNA and protein sequences. Through the protein data bank (PDB) (http://www.rcsb.org/pdb/home/home.do), information on experimentally determined structures of protein was obtained. Primer design and analysis of DNA sequencing was carried out using BCM Search Launcher (http://searchlauncher.bcm.tmc.edu/). Various physical and chemical parameters for a given protein sequence were computed using ProtParam (http://web.expasy.org/protparam/). For NMR spectra processing, VNMRJ (Version 1.1D, Varian, Palo Alto, USA) and NMRPipe (version 2.3; Delaglio et al. 1995). For spectra visualization, NMRDraw (version 5.0; Delaglio et al. 1995) and CARA (version 1.8.4; Keller, 2004) were utilized. PyMol (DeLano, 2002) was used to visualize various protein structures. Software tools not mentioned here will be described in the respective section in methods.

II.2 Methods

II.2.1 Cloning

The SH3 domains of Bin1 and Yes were cloned into the pGEX–6P–2 vectors (GE Healthcare) using RZPD clones. The primers used for this cloning are listed in the table II.1.2. The I.M.A.G.E clone with the ID: IRAUp96950629D6 for Bin1 and the clone IRAKp961712106Q2 for Yes form Source Lifesciences Biosciences (Berlin) were used.

II.2.1.1 DNA–Digestion

Plasmids were digested with restriction endonucleases for linearization. The respective insert was digested with the same endonucleases to facilitate matching sticky ends between plasmid and insert. The commercially available enzymes and the buffers were used according to the manufacturer's instructions. 1 U enzyme was used to digest 1 µg DNA. 1–10 µg of DNA in a volume between 20–50 µl was incubated for 1–3 hours at 37 °C for digestion. The success of the reaction was probed via gel–electrophoresis, adding DNA–ladder to distinguish between the resulting fragments.

II.2.1.2 Dephosphorylation

Dephosphorylation of linearized plasmids is a method employed to prevent the majority of plasmids simply recircularising during the ligation step when cloning your DNA of interest. Thus shrimp alkaline phosphatase [SAP] will catalyze the removal of 5' phosphates from nucleic acid templates. 1 µg of DNA was incubated with 1 Unit of SAP for 1 hour at 37 °C. Inactivation of SAP by the end of the incubation period was performed heating the sample up to 65 °C for minimum 20 minutes. The product is ready to use in the Ligation step.

II.2.1.3 Ligation

T4 DNA Ligase was used to insert the DNA fragment of desire into a linearized plasmid. Around 100 ng of plasmid DNA was incubated with a two to ten times excess of insert DNA with 1 mM ATP and 1 U T4 DNA–Ligase for 1 hour at room temperature. E. *coli* Mach 1 cells were transformed with 2 µl of the ligation sample, subsequently.

II.2.1.4 Transformation of E. *coli*

Competent E. *coli* cells stored at -80 °C were thawed on ice for 5 minutes before adding the ligation–mix or 100 ng plasmid DNA for transformation. The DNA– *E. coli* mixture rested on ice for 30 minutes. A heat activation step for 45 s at 42 °C follows this. Afterwards 800 µl of Luria Bertani (LB) medium were added to the mixture and incubated at 37 °C for 1 hour , shaking. Plate out the suspension on a LB agar plate containing the appropriate antibiotic, incubate over night at 37° C. Only bacteria with the antibiotic resistance on the plasmid with insert.

II.2.1.5 Isolation of plasmid DNA

Based on the method of alkaline lysis in accordance with Ish–Horowitz & Burke (1982), DNA was isolated and purified using Macherey and Nagel AX column kits following manufacturer`s instructions

II.2.1.6 PCR Reaction

Total recombinant DNA was amplified in vitro using specific primers and Vent polymerase as described by Mullis & Faloona 1987. The polymerase chain reaction allows the selective amplification of DNA sequences. With this technique it is possible to amplify a template by the factor of 106 – 108 within a short time period. A typical PCR mixture consists of a DNA template, specific forward and reverse primers with sequences complementary to the flanking regions of the DNA template, dNTPs, a thermostable DNA polymerase with suitable buffer components and magnesium ions as cofactors for the polymerase. Each reaction cycle comprises a DNA denaturation, primer hybridization and an elongation step. Therefore, under optimal conditions the amount of DNA templates nearly doubles after each reaction cycle and provokes an exponential increase. For amplification of genes for further cloning steps, PCR mixtures of volumes between 25 and 100 l were prepared including a PCR buffer solution suitable for the corresponding polymerase. Primers, dNTPs, and polymerase were added to final concentrations of 1 M, 0.25 mM and 1 U/50 l, respectively. About 1 ng of pure template DNA was added per l of reaction mixture. If Vent polymerase was used, magnesium sulfate was added to a final concentration of 2 mM. In case of Taq polymerase magnesium chloride was supplemented to a final concentration of 2 mM. The different cycles of the PCR were specifically adapted to the melting temperatures of the applied primers and to the overall length of the amplified DNA sequences. After an initial denaturation step at 95 ℃ for 5 minutes a variable program with 25 cycles (denaturation at 95 ℃ for 30 s, primer annealing at the theoretically calculated annealing temperature for 30 seconds and elongation at 72 ℃ for 1 min/kb of target gene) was followed by a final elongation step for 2 minutes at 72 ℃. Positive *E. coli* clones carrying vectors with correct inserts after transformation with ligation reaction mixtures were identified by colony PCR. The advantage of this procedure is the omission of amplification and isolation of putative negative clones.

II.2.1.7 Agarose gel electrophoresis

Electrophoresis is the movement of charged particles in an electric field. Difference in charge and mass, result in difference in movement of the particles. Here agarose gel electrophoresis was used to resolve DNA fragments produced by polymerase chain reaction or restriction enzyme digestion. The native gels were produced dissolving and heating the agarose polymer powder in 1x TAE buffer and cooling down. Adding 1 mg/l ethidiumbromide before the polymerization starts. DNA samples were mixed with 1x loading dye before being loaded into the wells of the gel. Gels were run horizontally between 80 V and 100 V in 1x TAE buffer. On completion of electrophoresis, DNA was visualized using transmitting UV light. A BioRad Gel Doc 2000 imager using Quantity One 5.0.1 software was used for analysis.

TAE Buffer

40 mM Tris acetate, pH 8.0

1 mM EDTA

II.2.1.8 DNA extraction from agarose gel

After preparative DNA gel electrophoresis desired DNA fragments were excised from gels with a scalpel and DNA was subsequently extracted with the NucleoSpin Extract Kit according to the user manual. Elution of DNA was performed with double distilled water instead of elution buffer.

II.2.2 Concentration determination via UV/Vis spectroscopy

Concentration of proteins, peptides and DNA was calculated through the absorption of the molecules in the UV/Vis spectrometer following the Lambert–Beer–law. The absorption for proteins and peptides was measured at 280 nm for nucleic acids the absorption was measured at 260 nm. If necessary the samples were diluted to 1:20, 1:50 or 1:100 using 100 µl cuvettes.

Lambert–Beer– law:

$A = \varepsilon \bullet c \bullet d$

A is the absorption at 280 or 260 nm, *c* is the concentration in mol/l and *ε* is the molar extinction coefficient in $cm^{-1}mol^{-1}l$. *d* represents the cuvette width which the beam of light has to travel through.

Theoretical molar extinction coefficients for each protein in random coil state can be calculated based on the extinction of its aromatic residues with P*rot*P*aram*–Tool

(http://web.expasy.org/protparam/).

II.2.3 Protein preparation techniques

II.2.3.1 SDS–PAGE according to Laemmli

Separation of the proteins according to their molecular weight is achieved with the anionic detergent sodium dodecyl sulfate (SDS). SDS has a denaturing effect on the protein structure via its aliphatic residues. A full denaturing effect is reached with adding 2–mercaptoethanol to the mixture which reduces the disulfide bonds. SDS makes sure that the overall charge of the denatured protein is negative and allows thus fractionation by approximate size during electrophoresis through the poly acryl amid–matrix. In this work DISK–electrophoresis was used to analyse the protein samples or western blots (SDS–PAGE, Laemmli, 1970). It combines two gel matrices with different pore sizes, facilitating a sharpening of the protein bands and avoiding aggregation of the proteins.

Hoefer Mighty Small SE 260 gel electrophoresis chambers (Hoefer Scientific Instruments, San Fransisco USA) utilizing 10 x 10.5 cm² plates were used for sodium dodecyl sulfate polyacrylamide gel electrophoresis (SDS PAGE) in this work. To estimate the molecular weight of the protein samples, 6 µl of Protein Molecular Weight Marker (MBI Fermentas, St. Leon–Rot) was applied into one of the gel slots. 1 x Laemmli buffer was added to the protein samples before boiling for 5 minutes at 95° C for further denaturation. 10 µl of each sample were applied into the remaining slots on the gel. The run was carried out using a constant electric current of 40 mA / gel. After electrophoresis the gel was stained with 100 ml Coomassie Brilliant blue R 250 for 3 minutes in the micro wave. The blue gels were destained with boiling water allowing visualization of the separated proteins. Documentation was undertaken in Gel Doc 200 unit (Bio–Rad, Munich).

Following buffers and solutions were used for SDS PAGE:

5% Gels	**15% Gels**
4.85 % (w/v) acrylamide	14.55% (w/v) acrylamide
0.15% (w/v) *N*,*N*'–Methylenebisacrylamide	0.45% (w/v) *N*,*N*'–Methylenebisacrylamide
125 mM Tris/HCl, pH 6.8	375 mM Tris/HCl, pH 8.8
0.1% (w/v)SDS	0.1% (w/v)SDS
0.1% (w/v)APS	0.1% (w/v)APS
0.1% (v/v) TEMED	0.1% (v/v) TEMED

SDS running buffer	**Coomassie Stain**
50 mM Tris/HCl, pH 8.3	25% Isoproponol
385 mM Glycin	10% acetic acid
0.1% (w/v) SDS	0.5 g/l Cooomassie Brilliant Blue R250

II.2.3.2 Expression of recombinant proteins and peptides

After validation of the DNA sequence E. *coli* cells were transformed with the respective plasmids. A pre–culture with the correct antibiotics in the right concentration served to inoculate the main culture the following day. Incubation was done shaking the flasks at 200 rpm at 37 °C for all cultures. Gene–expression was induced between 0.6–0.8 bacterial optical density of the medium at 600 nm. A concentration between 0.5–1 mM IPTG was chosen to induce protein expression and the *E. coli* system was incubated for another 4–5 hours without change of conditions. Afterwards the bacteria were harvested upon centrifugation at 6000 g for 20 minutes. The bacterial pellets were washed with 1x PBS buffer and stored at –20 °C. Protein expression was surveyed taking samples for SDS PAGE analysis before inducing gene expression and afterwards at different time points before harvesting.

II.2.3.3 Expression in LB Medium

Proteins for molecular biological experiments which did not require isotopic labeling were expressed in LB Medium as stated in chapter (II.1.7).

II.2.3.4 Expression in M9 medium

Proteins subjected for NMR experiments and further structure biological experiments involving NMR were expressed in isotopic labeled M9 medium

M9 Medium

9,1 g/l $NaH_2PO4 \cdot 2\ H_2O$

3 g/l $KH_2PO_4 \cdot 2\ H_2O$

0.5 g/l NaCl

0.5 g/l NH_4Cl or $[^{15}N]\ NH_4Cl$ (Cambridge isotopes, Andover, USA)

100 µM $CaCl_2$

2 mM $MgSO_4$

5 mg/l Thiaminhydrochloride

0.2% (v/v) TS2 (trace elements)

0.1% (v/v) Vitaminecocktail

4 g/l Glucose or 2 g/l [^{13}C] Glucose (Cambridge isotopes, Andover, USA)

10 µM Fe(III)–citrate

TS2– Solution

30 mg /l $MnCl_2 \cdot 4\ H_2O$

100 mg/l $ZnSO_4 \cdot 7\ H_2O$

300 mg /l H_3BO_3

200 mg/l $CoCl_2 \cdot 6\ H_2O$

20 mg/l $NiCl_2 \cdot 2\ H_2O$

10 mg/l $CuCl_2 \cdot 2\ H_2O$

900 mg/l $Na_2MoO_4 \cdot 2\ H_2O$

20 mg/l Na_2SeO_3

Vitamine cocktail

1 g/l Biotine

1 g/l Choline chloride

1 g/l Folic acid

1 g/l Nicotine amide

1 g/l Sodium–D–panthothenate

1 g/l Pyridoxal hydrochloride

II.2.3.5 Bacterial cell lysis

For suspending one gram cell pellet 5 ml of lysis buffer was used. The bacterial suspension was sonicated three times for 60 s on ice to disrupt the cells (Branson Sonifier 250, Branson Ultrasonics Corp., Danbury, USA). To separate the soluble fractions from the insoluble cellular contents, the lysate was centrifuged for 45 minutes at 45000 x g at 10 °C. For further purification steps for soluble proteins or peptides the supernatant only was processed or the pellet if proteins or peptides of interest were insoluble.

II.2.3.6 Purification of SH3 Domains

Following buffers were employed for SH3 domain protein purification:

10 x PBS buffer

1.4 M NaCl

27 mM KCl

Lysis buffer

1 x PBS, pH 7.3

2 mM DTT

100 mM Na2HPO4

18 mM KH2PO4

pH 7.3

1 Complete protease inhibitor cocktail tablet

20 µg/ml DNase A

20 µg/ml Lysozym

SH3 washing/equilibrium buffer

1 x PBS, pH 7.3

2 mM DTT

SH3 elution buffer

50 mM Tris/HCl, pH 8.0

10 mM Gluthatione $_{red}$

2 mM DTT

II.2.3.6.1 Affinity chromatography

First purification step of the Gluthatione–S–transferase (GST) fusion SH3 domain follows the principles of affinity chromatography using Gluthatione Sepharose 4B (GE Healthcare, Munich). GST simply binds to its ligand gluthatione which is covalently coupled to the sepharose. Elution is achieved upon addition of reduced gluthatione to the complex. Purification was performed by packing a chromatography column with 0.5 ml GSH sepharose for each gram bacterial cell pellet which was lysed. Firstly the sepharose was washed with H_2O bidest and equilibrated with the respective buffer using 10 x the column volume. Next the cell free cytoplasmic supernatant from chapter II.2.3.5 was loaded on the column and washed with 10 x the column volume with washing buffer. Elution of the fusion protein was carried out adding 5 x the column volume elution buffer to the loaded sepharose. All purification steps were subjected to SDS PAGE analysis.

II.2.3.6.2 Cleaving the GST–tag from GST–SH3 fusion protein with HRV 3C protease

The following buffer was used:

50 mM Tris/HCl, pH 7.0

150 mM NaCl

1 mM DTT

1 mM EDTA

Digestion of the eluted GST–SH3 fusion protein was performed during the process of dialysis in the above mentioned buffer at 4 °C. After determining the protein concentration in the elution fractions, 5 Units of HRV GST–3C– protease were employed for each mg fusion protein. Cleavage of the tag was almost 100% after 2 hours of incubation. The success of the digestion was analysed via SDS PAGE.

II.2.3.6.3 Size Exclusion Chromatography (SEC)

For the final purification step size exclusion chromatography employing a Superdex75–column, GE Healthcare (HiLoad 26/70 Superdex 75 pg) was elaborated. Size exclusion is based on the different permeation properties of the analytes in a porous stationary phase. Pore size of the stationary phase is given. Higher molecular proteins will escape the pores and elute in an earlier time whereas smaller molecular proteins will be captured within the pores and elute in a later period of time. The protein sample volume was concentrated down to 5 ml using ultrafiltration. The column was washed with H2O bidest before equilibrating it with the low salt potassium phosphate buffer at pH 6.4. After the protein sample was loaded to the column the chromatography was run at 4 °C at a 1.5 ml/min flow rate. Each elution fraction containing 4.5 ml was analysed via SDS PAGE to determine the fractions with the clean SH3 domain. Fractions with similar purity were merged and concentrated for further experiments.

Low salt buffer:

50 mM $KaPO_4$

20 mM NaCl

2 mM DTT

pH 6.4

II.2.3.7 Purification of $NS5A_{191–369}$

II.2.3.7.1 Affinity Chromatography and on column tag cleavage

The initial purification steps are described already in chapter (II.2.3.6.1). After washing the loaded column with five times the column material volume with equilibrium buffer and 5 x times with HRV 3C protease buffer as noted in chapter (II.2.3.6.2). The loaded column material was suspended in six times the column volume HRV 3C protease buffer into a protein–sepahrose–slurry. Add about 30 U of HRV GST–3C– protease to the slurry and incubate on a shaker at 4 °C over–night. Load the

protein–sepahrose–slurry again on a column fractionate the flow through. The outcome of the on column digestion was analysed on SDS PAGE.

II.2.3.7.2 Anion Exchange Chromatography

Ion exchange is based on the exchange of ions between two molecules. The net charge of a protein depends on its amino acid composition. Thus the overall charge of a protein depends on the pH of the buffer it is solved in. Theoretically it will be charged positively if the pH of the buffer is below the isoelectric point (pI) which is the theoretical pH the protein has a net charge of zero. If the pH is above the pI value the charge will be negative. Knowing the amino acid composition and the pH of the buffer one can calculate the theoretical net charge of the protein and use this for Ion exchange chromatography. $NS5A_{191–369}$ has a theoretical pI of 5.6 and is negatively charged at pH 7. The protein was dialysed against 10 mM sodium phosphate buffer, pH 7.0 so it is negatively charged. 5 ml of DEAE anion exchange resin (GE Healthcare, Munich) was loaded on a column and equilibrated with 50 ml of the 10 mM sodium phosphate buffer, pH 7.0. The $NS5A_{191–369}$ anion was loaded to the column and eluted using an increasing Na^+ Cl^- salt gradient in the sodium phosphate buffer as described in the table II.2.1 to exchange anions. All fractions were analysed with SDS PAGE to determine the fraction with the pure $NS5A_{191–369}$.

Table II.2.1 The salt gradient concentration, steps and the column volume (CV) used

NaCl [mM]	Column volume
50	3 x 1 CV
100	2 x 1 CV
150	2 x 1 CV
200	2 x 1 CV
300	1 x 2 CV
400	1 x 2 CV
500	1 x 2 CV
1000	1 x 1 CV

The fractions containing the pure protein were merged and concentrated for further experiments or even dialysed. The protein was stored at –80 °C with 1 complete protease inhibitor cocktail tablet per 50 ml sample.

II.2.3.8 Purification of $NS5A_{333–367}$

II.2.3.8.1 Affinity Chromatography Using IMAC

Proteins with histidine tags can be purified using Ni–NTA sepharose. Two histidine molecules form a complex with the nickel ions. The overall protein fold of the fusion partner is not important for complex formation and binding of the fusion protein to the column. Just the number of accessible histidines is relevant for column binding. The protein is eluted with adding a high affinity nickel complex partner, imidazole to replace the protein nickel complex. The purification conditions are usually optimisedialysedd with adjusting the concentration of the new partner. IMAC purification can be carried out either under native or denaturing conditions. The $NS5A_{333–367}$ peptide used in this work was purified natively.

Following buffers were used for the IMAC steps:

Lysis buffer	Washing buffer	Elution buffer
	50 mM NaH_2PO_4	
	300 mM NaCl	
10 mM Imidazole	20 mM Imidazole	250 mM Imidazole
	pH 8.0 (adjust with NaOH)	

1 ml Ni–NTA sepharose, Qiagen (Hilden) was used per gram bacterial cell pellet which was lysed for the purification. The column was washed with two times column volume H_2O and equilibrated afterwards with ten times column volume with lysis buffer. The lysed bacterial cell extract is loaded two times on the Ni–NTA column after catching the flow through and reloading it. Following this step the loaded column was washed ten times the column volume with washing buffer. Afterwards the fusions protein was eluted with five times the column volume elution buffer. All purification steps are fractioned and analysed on SDS PAGE. The protein fractions of interest were subjected to hydrolytic digestion of the deca–his–tag.

II.2.3.8.2 Cleavage of the deca–his–tag with Yeast Ubiquitin Hydrolase from the fusion peptide

The His10–Ubiquitine–NS5A$_{333–367}$ protein coded in the pTKK19ubi–vector contains a yeast ubiquitin hydrolase recognition motif. The denoted vector was especially designed for isotope labeled biosynthesis of peptides (Kohno et al. 1998). The hydrolase cleaves directly between the His10–Ubiquitin–tag and the peptide without causing amino acid overhangs or blocked ends.

Hydrolase buffer
50 mM Tris/HCl pH 8.0
100 mM NaCl
1 mM 2–mercaptoethanol

The fusion protein was dialysed against the above buffer in a dialysing membrane with a molecular cut off of 3500 Da at 4 °C over–night. The buffer was changed once after 2 hours of dialyzing. Afterwards the cleavage took place at 37 °C on a shaker over night by adding 1/7 the of the fusion protein concentration YUH. The success of the reaction was analysed on SDS PAGE. The cleaved products were separated with reversed phase chromatography afterwards.

II.2.3.8.3 Reversed Phase Chromatography

The basic principle behind the separation of reversed phase chromatography lies within the hydrophobic interaction of the biomolecules with the n–alkyl hydrocarbons immobilised on the matrix. The proteins get adsorbed by the matrix. The hydrophobic character of each protein is given by its hydrophobic amino acid content and thus is the basis for separation upon elution with an organic solvent gradient. The separation was performed on a RPC 3 ml resource column, GE Healthcare (Munich) on Aekta systems, GE Healthcare (Munich). The Cleavage was loaded on the column and separated employing a step gradient between 0% and 80% Acetonitrile and 0.1% TFA. The RPC run was detected measuring the absorption at 280 nm and 215 nm. All the fractions were collected; the fractions with protein or peptide content were lyophilized and analysed as described earlier with SDS PAGE, based on the Tris–Tricine system.

Buffer A	**Buffer B**
0.01% TFA	80% Acetonitrile
100% H_2O	0.01% TFA

II.2.3.9 Conserving Proteins and Peptides

The pure proteins and peptides were lyophilised for further storage at -20 °C.

II.2.4 Circular Dichroism (CD) Spectroscopy

Circular Dichroism (CD) is a spectroscopic method to measure secondary structure elements in proteins. CD spectroscopy does not need extra labeling of the samples. It operates in the UV–VIS range of the spectral field which lies between 180 nm and 250 nm. The CD effect is observed when optically active matter absorbs left and right hand circular polarized light slightly differently. Protein solutions are optically active due to chirality of the protein backbone and aromatic amino acids. According to the secondary structure composition of a protein the absorption profile in CD spectroscopy of each protein will differ. Random coils, beta sheets and alpha–helices have characteristic absorption minima in the spectrum which provides secondary structural information for a protein.

The measurement was carried out on a Jasco–J810 CD spectrometer (Jasco, Groß–Umstadt) at 21°C using quartz cuvettes (Hellma, Mülheim) with 0.2 cm width. The concentration of the $NS5A_{333–367}$ was 12.5 µM in Potassiumphosphate buffer, pH 6.5. The measured wavelength ranged from 188 nm to 250 nm. The data was recorded at 10 nm per minute with 1 nm resolution. The sensitivity of the spectrometer was set to 100 mGrad. The spectrum was accumulated three times. The buffer spectrum was subtracted from the peptide spectrum for further processing. In order to obtain mean molar ellipticity per amino acid residue ($[\theta]_{MRW}$) the following function was used on the recorded spectrum.

$$[\theta]MRW = \frac{\theta \cdot 100}{N \cdot d \cdot c}$$

$[\theta]_{MRW}$= mean molar ellipticity per amino acid residue [degree • cm² • $dmol^{-1}$]

θ = measured ellipticity [mdegree] d = cuvette width

N = Number of amino acid c = protein/peptide concentration [M]

II.2.5 Dynamic Light Scattering (DLS)

DLS is a method to examine the hydrodynamic radius of particles in solution or suspension. The evaluated diffusion rate of the scattering particles in a sample gives information about size and

distribution. The detected photon signals are subjected to an autocorrelation to calculate the diffusion coefficient. The diffusion coefficient is according to the Stokes–Einstein–function directly related to the hydrodynamic radius.

Stokes Einstein function:

$$d(H) = \frac{\kappa_B T}{6 \pi \mu R}$$

d (H) = hydrodynamic radius

κ_B = *Boltzmann constant*

T = temperature

μ = viscosity

R = particle radius

The DLS experiments were performed at DynaPro DLS system (Proteinsolutions, Lakewood) at 25 °C, at a fixed 90° angle and a cuvette width of 3 mm. Bin1 SH3 samples with concentrations between 20 µM to 1000 µM were filtered through 0.02 µm Anatop filters (Whatman) before measurement was taken. Data acquisitions were averaged and analysed with Dynamics V6 software. Using this software autocorrelation functions were calculated and regularization fit was performed in order to obtain the size distribution histogram for each protein concentration.

II.2.6 Surface Plasmon Resonance Spectroscopy

The surface plasmon resonance (SPR) spectroscopy is a powerful method to measure bio molecular interactions in real time without the need of further labeling. One of the interactants the protein of interest is immobilised to the gold sensor surface and the other interactant, the analyte is in solution and passed over the sensor surface. The sensor surface is covered with a thin gold layer which is crucial for the optical principle of the SPR spectroscopy. The resonance process occurs when plane polarized light hits the surface of the gold film and causes a total internal reflection. The combination of the gold layer and a half circular prism creates an electric field which interacts with the free electrons of the gold layer, turning them under certain conditions into surface plasmons. Molecules immobilised on the gold film and other molecules binding to them can change the angle of the above mentioned internal reflection. Thus an interaction between the two molecules changes the mass on the sensor surface, and is therefore detected as a change of angle. This angle is called SPR angle and the detected change is called the *response* in a sensogram which is a function of the local molecule concentration.

The SPR interaction analysis can be used to identify a binding reaction, determine the affinity and ideally calculate the association and dissociation rates of the binding situation. Depending on the

interaction the dissociation constant K_D can be also determined using the steady state kinetics as a function of the injected analyte concentration.

Function 1:

$$K_D = \frac{1}{K_A}$$

$$R_{eq} = \frac{K_A \cdot [A] \cdot R_{max}}{K_A \cdot [A] + 1}$$

R_{eq}: Response in Steady state

K_A: Association constant

[A]: Concentration of analyte

$_{max}$= Maximum response

Function 2:

For measuring "two site saturation" kinetics with two binding events the following function in Sigmaplot 11.0 was used to measure the K_D values from the steady state kinetics.

$$f = \frac{R_{max}1 \cdot [A]}{K_D 1 \cdot [A]} + \frac{R_{max}2 \cdot [A]}{K_D 2 \cdot [A]}$$

K_D: Dissociation constant

The SPR experiments were carried out on Biacore X and Biacore T200 with Biacore Control X and Biacore control T200 software (GE Healthcare, Munich). The data was recorded at rate of one to five Hz at 25 °C. After system equilibration to the new conditions and baseline stabilization, all immobilizing reactions and binding studies were performed. The "double–bubble" technique was chosen for sample injection, meaning 5 µl of air and 5 µl of sample are injected following the sample injection. This prevents diffusion of the sample into the running buffer.

II.2.6.1 Ligand immobilization

CM5 chips for the experiments at Biosensor Biacore X and CM5 S series chips at the Biosensor Biacore T200 were used in this work. These chips have a carboxy–methyl dextran layer which is associated to the gold surface over a linker. Thus ligands are immobilised covalently via amine coupling. For this purpose the carboxyl groups on the dextran matrix were activated by conversion into N–hydroxysuccinimid ester applying 1–ethyl–3–dimethylaminopropyl–carbodiimid (EDC) and N–hydroxysuccinimid (NHS) on the surface. Ligands with free primary amine groups form with the N–hydroxysuccinimid ester amide bonds. Remaining free reactive groups are deactivated with ethanolamine afterwards. In this work the ligands were immobilised using 10 µl/ min flow rate at 25 °C. Proteins must be positively charged for the coupling reaction. They were dialysed against 10 mM sodium acetate buffer pH 4.0 or 4.5.

Following buffers were used for the SPR experiments:

Surface activation solutions

50 mM EDC

200 mM NHS

Surface deactivation solution

1 M ethanolamine

SH3 coupling buffer

10 mM Na–acetate, pH 4.0

$NS5A_{191–369}$ coupling buffer

10 mM Na–acetate, pH 4.0 and 4.5

SPR running buffer

10 mM HEPES, pH 7.4

150 mM NaCl

3 mM EDTA

0.005 % Surfactant P20 (SP 20)

1 mM 2–mercaptoethanol

All buffers were degased and filtered using a cellulose membrane with 0.2 µm molecular cut off.

II.2.6.2 Immobilization of $NS5A_{191–369}$

The $NS5A_{191–369}$ was expressed and purified in this work. The protein was dialysed against 10 mM sodium acetate buffer pH 4.5. The Flow cells were activated as described in chapter II.2.6.1 as a constant flow rate of 10 µl/ min for 360 seconds. $NS5A_{191–369}$ was injected with the same flow rate. The active cell was blocked afterwards with 1 M of ethanolamine HCl pH 8.5 injection, maintaining the same flow rate for 360 seconds. The procedure was performed for the reference cells with 10 mM sodium acetate buffer injection instead of $NS5A_{191–369}$.

II.2.6.3 Evaluation of SPR data

Biacore data were evaluated using BiaEvaluation 4.1 (GE Healthcare) and Sigmaplot 11.0. All obtained binding data were double referenced. This was achieved by collecting the data in dual–channel mode with a reference flow cell (termed FC–A) connected upstream of the flow cell with immobilised ligand (termed FC–B) and the subtraction of the obtained binding responses with a blank buffer injection. A twofold referencing was performed with the binding data of the interaction between analyte and immobilised ligand. To obtain a single set of parameters for the interaction analysis performed on different surfaces activities a global fit was performed using a 1:1 interaction model that included a mass transport step. The model was adapted from Karlsson et al. (2006). The parameter R*I* correcting for slight differences in the refractive index of different analyte concentrations was set to zero because at least double referencing was performed.

II.2.7 Nuclear Magnetic Resonance Spectroscopy (NMR)

NMR is beside X–ray crystallography the standard method to determine the atomic high resolution protein structure in solution. In contrast to crystallography NMR probes proteins in solution thus mimicking the physiological conditions more accurately. Examining dynamic properties of molecules or protein domains, monitoring intermolecular interactions, as well fast identification of interaction partners as in SAR and STD NMR experiments (Wang et al. 2004) can be probed all with NMR spectroscopy. A big step in bio molecular NMR spectroscopy was the use of *U*–$^{13}C/^{15}N$ isotope labeled bio molecules for over expression in bacteria (Lemaster 1994) which lead to development of higher dimensional NMR spectroscopy in order to meet the need for the structural elucidation of proteins and other bio molecular structures.

The 2D and 3D NMR experiments performed in this work to calculate the complex structure between Bin1 SH3: $NS5A_{333–369}$, are listed in table II.2.7.1.

II.2.7.1 General measuring conditions

The NMR experiments were acquired on NMR Varian Unity INOVA and respectively VNMRS spectrometers run at 600 MHz, 800 MHz and 900 MHZ proton frequency (Varian, Palo Alto, USA). Either cryogenic cooled 5 mm Z–PFG–^{1}H[^{13}C,^{15}N]– probe heads or room temperature run XYZ–PFG–^{1}H[^{13}C,^{15}N]–probe (Varian, Palo Alto, USA) heads were used. All experiments were recorded between 25 °C and 30 °C. The samples were measured in 5 mm Shigemi NMR tubes (BMS–005V, Shigemi, and Tokyo, Japan). The processing of the spectra was done with VNMR and NMRpipe (Delaglio et al. 1995) as well with NMRView (Johnson et al. 2004). For analysis, assignment and visualizing of the spectra CARA was used.

Tab.II.2.7.1.Acquisition and processing parameters of the used NMR experiments for the Bin1 SH3:NS5A$_{333–369}$ complex. sw$_1$–sw$_3$: spectral width of the respective dimensions, t1–t3: number of complex points in the respective dimensions; nt: number of scans for each experiment; d1: delay time between two experiments; mix: mixing time. (Bodenhausen et al.1980; Kay et al. 1990a; Wittekind & Mueller 1993; Kay et al. 1990b; Ikura et al. 1991; Bax et al. 1990; Olejniczak et al. 1992;Zuiderweg et al. 1989; Norwood et al, 1990; Grzesiek et al. 1993; Montelione et al. 1992; Sattler et al. 1999)

Experiment	sw$_1$ [ppm]	t1 [points]	sw$_2$ [ppm]	t2 [points]	sw$_3$ [ppm]	t3 [points]	d1 [s]	nt	Mix [ms]
2D (^{1}H^{15}N)HSQC	14.0	2048	24.2.0	200	–	–	1.25	8	–
2D (^{1}H^{13}C)HSQC aliphatic	16.4	1536	64.2	456	–	–	1.5	16	–
2D (^{1}H^{13}C)HSQC aromatic	16.4	2048	26.0	400	–	–	1.5	32	–
3D HNCO	11.5	1536	12.3	128	27.4	75	1.25	8	–
3D HNCACB	16	1536	57.8	128	27.4	75	1.4	16	–
3D HCCH–COSY	12	1536	10.5	180	56.3	128	1.4	8	–
3D HCCH–TOCSY	12	1536	10.5	192	56.3	128	1.4	8	–
3D HCC(CO)NH	16	1190	66.3	200	27.4	80	1.5	16	–
3D CC(CO)NH	16	1190	76.7	200	27.4	76	1.5	16	–
3D(^{1}H^{1}H^{15}N)–HSQC–NOESY	14.3	2048	10.3	128	27.4		1.25	8	120
3D (^{1}H^{13}C^{1}H)–HSQC–NOESY (aliphatic)	14.3	1536	5.2	140	52.4	150	1.4	16	100
3D (^{1}H^{13}C^{1}H)–HSQC–NOESY (aromatic)	14.3	1536	2.6	180	24.5	190	1.6	16	150

II.2.7.2 Sample Preparation

For protein–protein interaction studies, the SH3 domains of Yes, Fyn and Bin1 were diluted to a concentration of 100 µM in low salt NMR buffer. The respective buffers are listed below. The synthetic peptides NS5A$_{347–361}$ and Myc$_{55–68}$ were solved in water to get rid of TFA artifacts and

lyophilized. This washing step was repeated and the peptides were dissolved in the low salt NMR buffers as denoted below. The peptide concentration was 10 mM.

SH3 NMR buffer

50 mM $KaPO_4$, pH 6.4

20 mM NaCl

2 mM DTT

7 % (v/v) D_2O

$NS5A_{191–369}$ NMR buffer

100 mM $NaPO_4$, pH 6.5

2 mM DTT

7 % (v/v) D_2O

$NS5A_{333–367}$ /$NS5A_{347–361}$ /$Myc_{55–68}$ NMR buffer

50 mM $KaPO_4$, pH 6.4

20 mM NaCl

2 mM DTT

7 % (v/v) D_2O

II.2.7.3 SH3 domain interaction studies with NS5A peptides

Chemical shift perturbance (CSP) experiments are a simple tool to probe the interaction between a protein and its ligands. Therefore a set of [^{15}N–^{1}H]–HSQC experiments is run by gradually adding the ligand to the free protein. It monitors the change of chemical shift of the amide correlations of each amino acid of the protein upon ligand binding in the spectra. Thus the dynamics of an interaction can be monitored by gradually increasing the ligand concentration. Superposition of the recorded set of spectra reveals information about the “exchange” rates between protein and ligand.

II.2.7.3.1 Bin1 SH3 domain interaction studies with $NS5A_{347–361}$ and $Myc_{55–68}$

100 µM of [*U*–^{15}N]–Bin1 SH3 was used for the interaction studies. The peptides $NS5A_{347–361}$ and $Myc_{55–68}$ were added in six steps to the ^{15}N–labeled SH3 domain till equimolarity (90 µM) between peptide and SH3 domain was reached. [^{15}N–^{1}H]–HSQC experiments were run for each titration step and for each peptide separately. The spectra were superposed to display the interaction between ^{15}N labeled Bin1 SH3 and the peptides. The chemical changes for the free–state amide signals of the SH3 domain upon ligand binding can be used to map the binding region on the molecular surface of the protein, if 3D structure is already present. The following functions were elaborated to map the binding regions of the NS5A and Myc peptides on the Bin1 SH3 surface as a function of the chemical shift change.

Function 3:

$$\Delta\delta_{norm}{}^{1}H = \frac{\Delta\delta^{1}H}{\Delta\delta_{\max}{}^{1}H}$$

Function 4:

$$\Delta\delta_{norm}{}^{15}N = \frac{\Delta\delta^{15}N}{\Delta\delta_{\max}{}^{15}N}$$

Function 5:

$\Delta\delta\ {}^{1}H^{15}N = [(\Delta\delta_{norm}{}^{15}N^{2}/5) + (\Delta\delta_{norm}{}^{1}H)\ {}^{1/2}]$

$\Delta\delta^{1}H$= *chemical shift difference for* ${}^{1}H$ *[Hz]*

$\Delta\delta_{max}{}^{1}H$= *maximal observed chemical shift difference in* ${}^{1}H$ *[Hz]*

$\Delta\delta^{15}N$=*chemical shift difference for* ${}^{15}N$ *[Hz]*

$\Delta\delta_{max}{}^{15}N$=*maximal observed chemical shift difference in* ${}^{15}N$ *[Hz]*

$\Delta\delta_{norm}{}^{15}N$= *normalized chemical shift difference for* ${}^{15}N$ *[Hz]*

$\Delta\delta_{norm}{}^{1}H$= *normalized chemical shift difference for* ${}^{1}H$ *[Hz]*

II.2.7.4 Torsion Angle Likelihood Obtained from Shift and sequence similarity (TALOS)

The restrictions for the torsion angles were obtained using the software TALOS^{+} (Cornilescu et. al., 1999; Shen et al. 2009). Talos uses an empirical database of backbone chemical shift information to predict the Ψ and Φ dihedral angles. It combines the empirical data from the backbone resonance assignment for H^{α}, C^{α}, C^{β} C' and N atoms for a given protein sequence correlating the secondary chemical shifts with the secondary structure for a protein.

II.2.8 Fluorescence Spectroscopy

Fluorescence spectroscopy can be used to measure protein–protein interaction using the intrinsic fluorescence of the amino acid tryptophan. During the recording of the spectrum the aromatic residues (tryptophan) are excited with a 280 nm beam and the emission is measured subsequently between 300 and 350 nm (Lottspeich et al. 1998). The binding pocket of SH3 domains contains for most cases two conserved tryptophans. Upon ligand adding and binding, the chemical environment of the tryptophanes change, this can be measured as a change of fluorescence. A gradual titration of the ligand will lead to a stepwise change of fluorescence, which can be plotted as a function of ligand concentration.

The binding affinity of $NS5A_{347–361}$ to Yes SH3 domain was measured recording fluorescence spectra at a Perkin–Elmer LS 55 fluorescence spectrometer (Perkin–Elmer, Boston, USA). 1.6 ml of a 0.5 µM free SH3 protein solution in PBS buffer with 1 mM DTT was measured in 2 ml quartz cuvette (Hella, Müllheim) at 21.5 °C. The peptide was dissolved in the same buffer and titrated to the SH3 domain in the cuvette gradually after 1 minute mixing time between each concentration step. The titration was stopped after no significant change of fluorescence intensity when the system reached saturation. The titration was performed three times. To take the dilution effect of the intrinsic fluorescence caused by adding the peptide into account a control experiment was run with the same titration steps with just adding buffer in the respective volume. Excitation wavelength was 290 nm, and the emission wave length was measured at 345 nm. The measeuring slit was 6 nm. The emission for each titration step was recorded for 30 s with 300 data points.

The interaction between SH3 and the peptide follows the equation below:

$$K_D = \frac{[P]\times[L]}{[PL]}$$

[P]= free protein concentration (SH3 domain)

[L]= ligand concentration ($NS5A_{347–361}$)

[PL]= concentration of protein:ligand complex

To calculate the K_D values for the Yes SH3 interaction with $NS5A_{347–361}$ from the fluorescence emission data a non–linear regression in Sigmaplot 11.0 was employed following the function below.

Function 6:

$$F = F_{min} + \left(\frac{[P]+[L]+K_D}{2} - \sqrt{\frac{([P]+[L]+K_D)^2}{4} - [P]\times[L]} \right) \times \frac{(Fmax - Fmin)}{P}$$

F= Intensity of fluorescence at the respective ligand concentration

P= protein concentration [µM]

L= ligand concentration [µM]

F_{min}= Fluorescence intensity of the protein prior to titration

F_{max}= Fluorescence intensity of the protein at peptide saturation point

K_D= Dissociation constant [µM]

II. Results

Three HCV protein NS5A fragments were used in this work to characterise the interaction to a set of SH3 domains. The $NS5A_{191–369}$ protein fragment was sub–cloned from an E. coli codon optimised synthetic gene purchased from Geneart (Regensburg). A two–step purification protocol for this 188 amino acid protein was established in this work. $NS5A_{333–369}$ was cloned by T. Tran. Optimising purification of the 37–mer peptide was part of this work. The SH3 domains of Fyn, and Lyn investigated with NS5A fragments in this work were purified following existing protocols. The SH3 domains of Bin1 and Yes were cloned with PCR amplification technique using an IMAGE–c–DNA clone. Establishing expression and purification protocols were part of this work.

III.1.1. Cloning of the SH3 domains of Bin1 and Yes

To isolate and amplify the SH3 domain encoding DNA of human Bin1 and Yes PCR technique was employed. The corresponding IMAGE–cDNA clones (chapter II.2.1) served as template for the PCR. The PCR products were purified and isolated by gel electrophoresis (chapter II.2.1.6) and gel extraction (chapter II.2.1.8). The amplified products were successfully cloned using BamH1 and Not1 restriction sites into the pGEX–6P–2 E. *coli* expression vectors (GE Healthcare, Munich). The clones were verified through sequencing by Seq–Lab (Göttingen).

Tab.III.1.1.1. Amino acid sequences of the cloned human Bin1 and Yes SH3 domains. The N–terminal GPLGS peptide overhang caused by HRV 3C digestion is highlighted in red.

Bin1 SH3	**GPLGS**LPPGFMFKVQAQHDYTATDTDELQLKAGDVVLVIPFQNPEEQDEGWLMGVKESDWNQH KELEKCRGVFPENFTERVP
Yes SH3	**GPLGS**GLTGGVTIFVALYDYEARTTEDLSFKKGERFQIINNTEGDWWEARSIATGKNGYIPSNYVAPA DSIQALE

III.1.2. Expression and purification of the SH3 domains

The SH3 domains were over expressed in M9 minimal medium for NMR experiments. In case only ^{15}N labeling was needed ^{15}N–ammonium chloride was added to the medium as sole nitrogen source. ^{13}C–glucose was added to the medium additionally as carbon source when [*U*–^{13}C/^{15}N] labeled

proteins were required for NMR experiments. For all other experiments protein was over expressed in LB medium.

SH3 domains were either over expressed in E. *coli BL21 (DE3) T1*^{R} or *E. coli Rosetta T1*^{R} bacterial strains. Both strains have a resistance against bacteriophage T1. The expression of the GST–SH3 fusion protein was induced after the optical cell density at 600 nm (OD_{600}) reached 0.6 by adding 0.5 mM IPTG to the culture. The cells were harvested after 4–5 hours of incubation. The bacterial yield was between 2 and 3 g bacterial cell pellet for each litre culture. The pellets were stored at -20 °C until further processing. The pellets were disrupted by sonication after suspending in lysis buffer as described in chapter II.2.3.5. Insoluble particles and whole cells were separated from the soluble part with centrifugation. The supernatant was used for the purification step on the GSH sepharose, adjacently. Figure III.1.2.1 shows on two SDS PAGEs the GSH sepharose affinity chromatography purification step for the GST–Bin1 SH3 representative for all GST–SH3 domain purifications in this work.

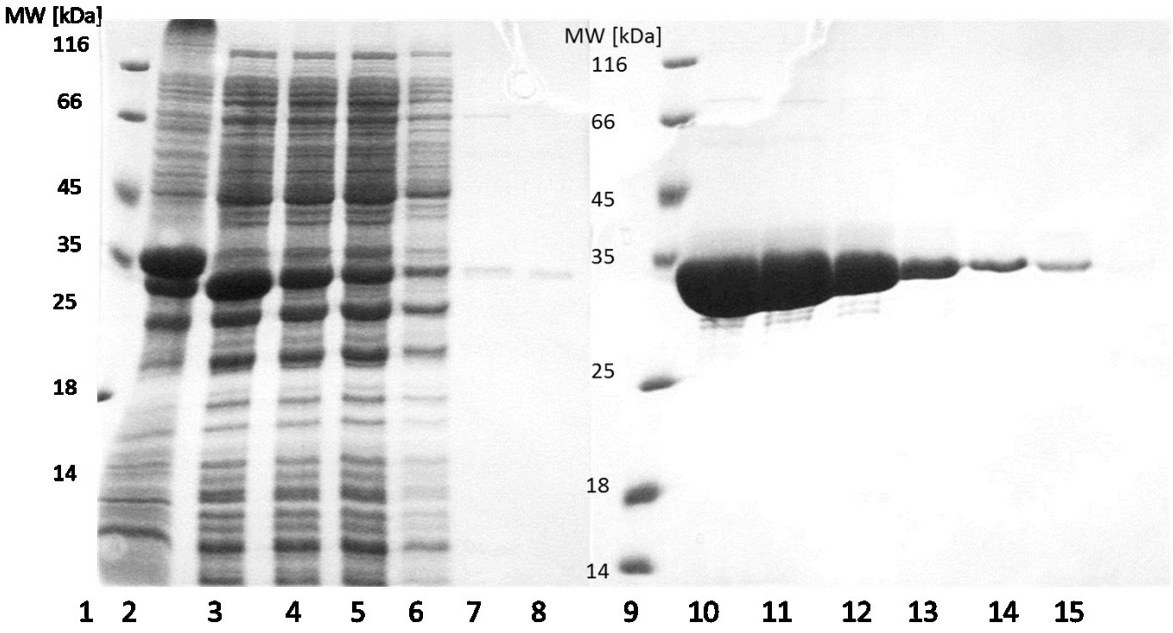

Figure III.1.2.1 GST–Bin1 SH3 affinity chromatography step of GSH sepharose. Lanes 1 and 9 display the molecular weight marker (Fermentas). Lane 2 shows the pellet after cell lysis and centrifugation, lane 3 is the supernatant with the GST–Bin1 SH3 domain making a dominant band around 35 kDa. Lanes 4 and 5 are the respective flow through fractions. Lanes 6–8 summarize the wash fractions. Lanes 10–14 depict the 5 elution fractions with the GST–Bin1 SH3 domain (35 kDa). Lane 15 represents column material after elution.

The flow through was loaded a second time on the GSH column, because it contained still unbound GST–SH3 domain. Most of the E. *coli* proteins could washed away during the washing step with 1x PBS from the column. Most of the protein was eluted in the fractions 1–3 (lanes 10–12 in figure

III.1.2.1). The fractions 4 and 5 (lanes 13 and 14 in figure III.1.2.1) also contained enough protein so that all fractions were pooled and dialysed against HRV 3C protease buffer overnight at 4° C. The Protease was added while the dialysis was on going. The cleavage was analysed on a SDS PAGE. The cleavage of the SH3 domain from the GST tag was almost 95%. The cleaved sample was subsequently concentrated down to 5–7 ml using an ultrafiltration tube and the products of the cleavage step were separated employing size exclusion chromatography. The elution profile in figure III.1.2.2 below of Bin1 SH3 is representative for all SH3 domains. The fractions 12 to 19 contained the GST tag (figure III 1.2.2 (A)) whereas the fractions 25 to 31 contained the Bin1 SH3 domain (figure III 1.2.2 (B)).

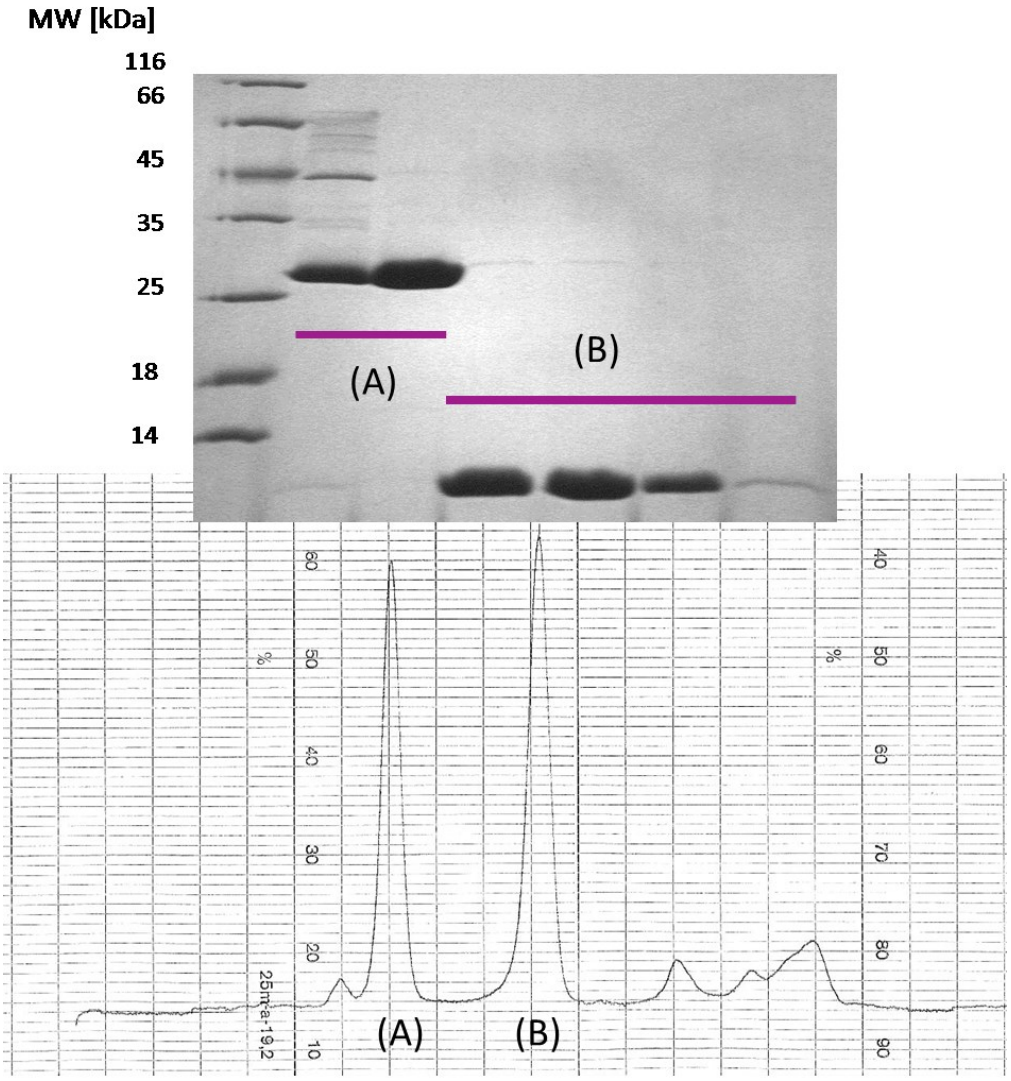

Fig III.1.2.2: 16% SDS PAGE of Bin1 SH3 after the Size exclusion chromatography (SEC) with the elution profile below. The different fractions of the SEC run, here grouped into (A) and (B), are applied on the gel as depicted. The fractions in (A) contain the GST tag as seen on the SDS PAGE above. The GST tag runs around 26 kDa. The fractions in in (B) contain the pure Bin1 SH3 domain as seen on the SDS PAGE above. Bin1 SH3 is 8 kDa big.

The overall yield of the Bin1 SH3 was 5 mg/litre LB expression culture and was calculated using the extinction coefficient of the tryptophan and tyrosine at 280 nm as described in chapter II.2.2. Respectively the SH3 domains of Yes, PI3K and Lyn were purified accordingly and yielded in similar quantities of protein.

III.1.3. Expression and purification of $NS5A_{333–369}$

The His_{10}–ubiquitin–$NS5A_{333–369}$ construct was expressed in 2 x 1l LB medium for experiments which did not require isotope labeling. The expression was induced with adding 1 mM IPTG after the bacterial cells growth reached an optical density of OD_{600} 0.6. The cells were harvested 5 hours after induction with IPTG. The cells were disrupted by sonicating the suspended pellets as described previously. The soluble fractions were separated from the insoluble cell fractions with centrifugation. The supernatant with the His_{10}–ubiquitin–$NS5A_{333–369}$ was incubated on a column with pre–loaded 10 ml Ni–NTA sepharose. Washing and elution steps followed the protocol as described in the methods chapter II.2.3.8.1 earlier via affinity chromatography (figure III.1.3.1).

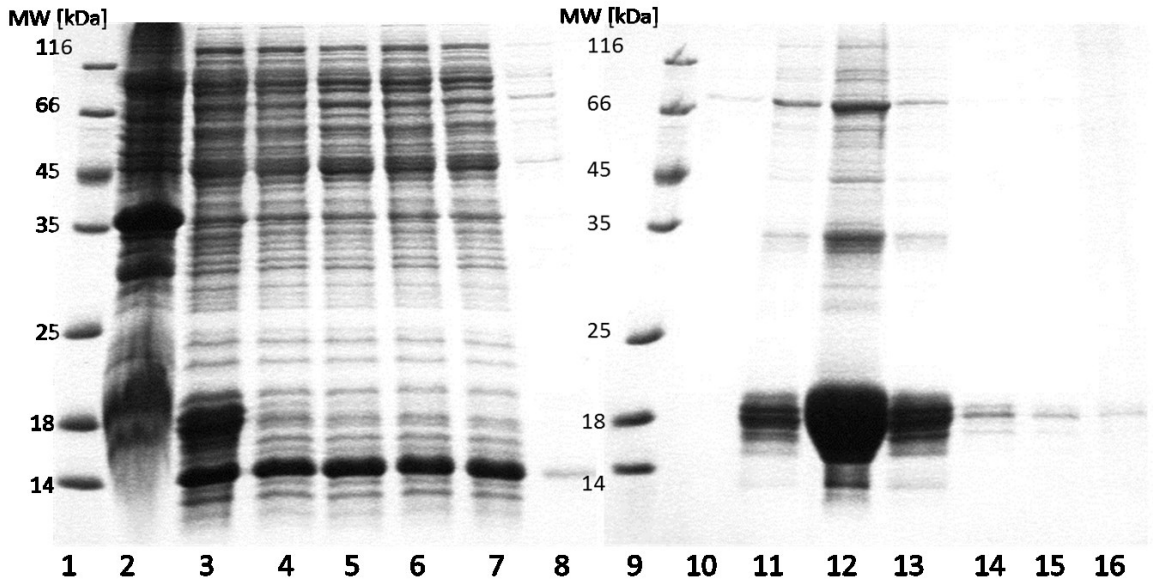

Fig. III.1.3.1 His_{10}–ubiquitin–$NS5A_{333–369}$ Ni–NTA affinity chromatography step. Lanes 1 and 9 display the molecular weight marker (Fermentas). Lane 2 shows the pellet after cell lysis and centrifugation, lane 3 is the supernatant with the His_{10}–ubiquitin–$NS5A_{333–369}$ domain making a dominant band around 14 kDa. Lanes 4 and 5 are the respective flow through fractions. Lanes 6–8 summarize the wash fractions. The wash fractions contain His_{10}–ubiquitin–$NS5A_{333–369,}$ which did not bind to the Ni–NTA. Lanes 10–15 depict the 6 elution fractions with the His_{10}–ubiquitin–$NS5A_{333–369}$ (14 kDa). Lane 16 represents column material after elution, which shows traces of His_{10}–ubiquitin–$NS5A_{333–369.}$

Fusion protein was dialysed against 50 mM Tris/HCl pH 8.0, 100 mM NaCl and 1 mM 2–mercaptoethanol and the His–tag was cleaved by adding Yeast Ubiquitin Hydrolase (YUH) over night. To check the success of cleavage reaction samples were analysed by SDS PAGE (fig.III.1.3.2).

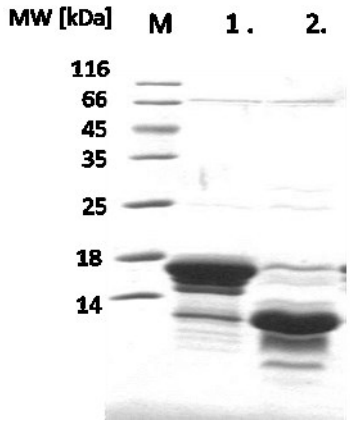

Fig.III.1.3.2: His_{10}–ubiquitin–$NS5A_{333–369}$ YUH digestion on 16% SDS PAGE. Not all products of the overnight digestion can be seen on the 16% SDS PAGE. The 4 kDa small $NS5A_{333–369}$ cannot be seen on this PAGE. The success of the reaction is estimated monitoring the molecular weight change of the His_{10}–uiquitin–peptide (lane1) to His_{10}–uiquitin (lane2), indicating that the $NS5A_{333–369}$ was digested.

Digestion with YUH over night of the His_{10}–ubiquitin–$NS5A_{333–369}$ protein construct was nearly complete as shown in figure III.1.3.2. The almost 15 kDa fusion protein (lane 1), slightly running at higher molecular weight was cleaved with the hydrolase into His_{10}–ubiquitin 11.3 kDa and the $NS5A_{333–369}$ peptide (lane 2). The almost 4 kDa peptide cannot be detected on SDS PAGE. The different components of the digestion were separated from each other by reversed phase chromatography (chapter II.2.3.8.3). 2 ml sample were loaded on the 3 ml RPC resource column to avoid over loading of the column. The different components could be separated with increasing acetonitrile concentration by running a two–step gradient. The $NS5A_{333–369}$ peptide was eluted from the column at acetonitrile concentrations between 18% and 20%. The fractions with the peptide were lyophilized and probed on SDS PAGE using the Tris/Tricine system for low molecular peptides (figure III.1.3.3). The purified $NS5A_{333–369}$ can be seen in the lanes 1 and 2. Both lanes show a further band running lower than the assumed $NS5A_{333–369}$ band around 4 kDa.

The fractions with the $NS5A_{333–369}$ from all runs were pooled together and lyophilized. Around 100 µg of the peptide powder was subjected to LC–MS mass spectroscopy (ZCH, Forschungszentrum Jülich). The results of the mass spectroscopy analysis show that the mass of the main component of these fractions is 3987 Da (main peak in figure III.1.3.4) which matches the mass of $NS5A_{333–369}$. There is a second peak with five times less intensity counts per second at 3610 Da, which might correspond to the second band on the gel analysis. The overall yield of the $NS5A_{333–369}$ peptide was 10 mg/ litre LB expression culture and was calculated using the extinction coefficient of the tyrosine at 280 nm as described in chapter II.2.2.

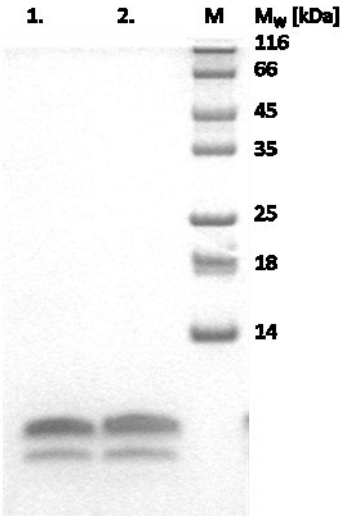

Fig III.1.3.3: 16% Tris/Tricine SDS Page of the $NS5A_{333–369}$ fractions from the RPC run. Lane 1 and 2 show the fractions which eluted between 18 and 20% acetonitrile concentration. M is the MBI marker (Fermentas.) The protein bands in the lanes 1 and 2 are the pure $NS5A_{333–369}$

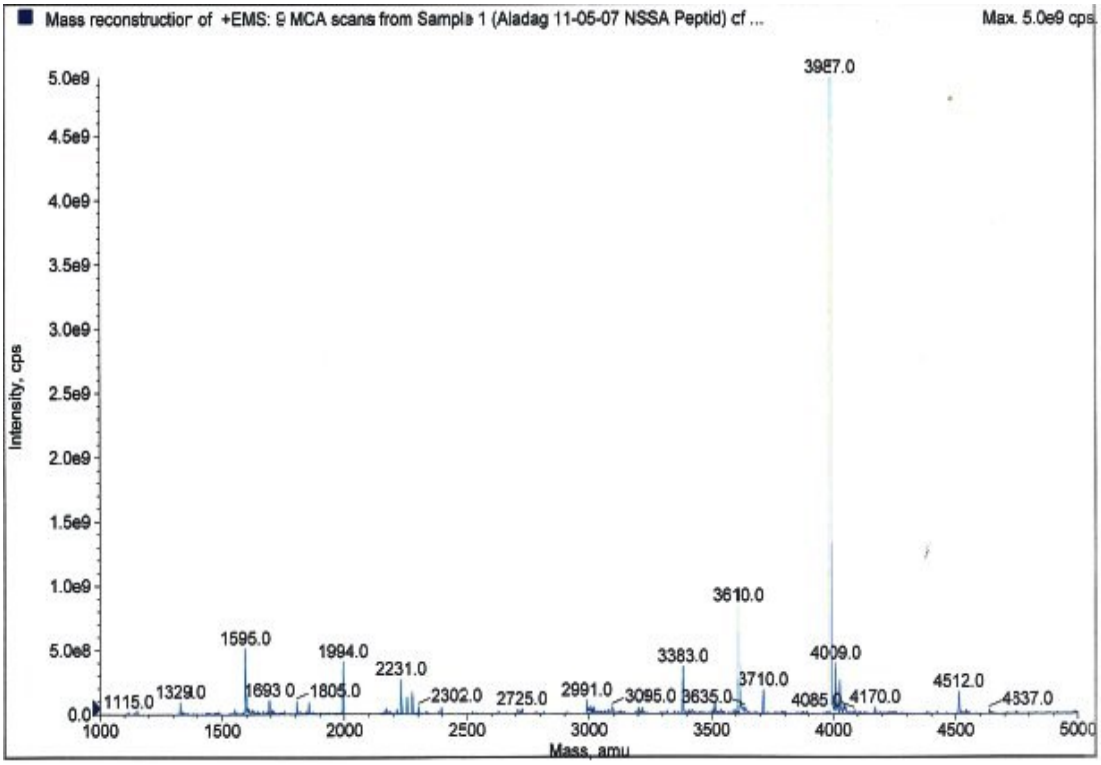

Fig. III.1.3.4: LC–MS mass spectroscopy of $NS5A_{333–369}$. The main intensity peak arises at 3987 Da which is consistent with the mass of $NS5A_{333–369}$. The other significant intensity peak comes at 3610 Da.

III.1.4. Sub–cloning of the NS5A $_{191–369}$ fragment into pGEX–6P–2 vector

The NS5A fragment comprising residues 191–369 from genotype 1b (strain HC–J4), used in this work, was commercially bought from Geneart (Regensburg). The initial synthetic gene was incorporated into a pOTB7 vector with the restriction sites for the enzyme BamH1 at 5' and NotI 3' end of the gene. The gene of interest was sub cloned into the multiple cloning site of the target vector pGEX–6P–2 elaborating the denoted enzymes BamHI and NotI (Fermentas). Both target vector and insert were digested by BamHI and NotI. The DNA was purified by gel electrophoresis and gel extraction before ligation of the NS5A$_{191–369}$ coding DNA into the pGEX–6P–3 vector. E*. coli Top 10* strains were transformed with part of the ligation samples. Prospective positive clones were further screened with a PCR step. Candidates showing the correct base pair size for vector with the NS5A insert, were send for sequencing for further confirmation. (Seqlab, Göttingen). Subsequently the expression strain E*. coli BL21 Rosetta T1*^{R} was transformed with the vector pGEX–6P–2_NS5A$_{191–369.}$

Tab. III.1.5 Amino acid sequence of NS5A$_{191–360.}$ The N–terminal GPLGS peptide overhang caused by HRV 3C digestion is highlighted in red.

NS5A$_{191–369}$	**GPLGS**GTGSLRGGEPEPDVTVLTSMLTDPSHITAETAKRRLARGSPPSLASSSASQLSAPSLKATCTT HHDSPDADLIEANLLWRQEMGGNITRVESENKVVILDSFEPLHADGDEREISVAAEILRKSRKFPS ALPIWARPDYNPPLLESWKDPDYVPPVVHGCPLPPTKAPPIPPPRRKRTVVLTESNVS*

III.1.5. Expression and purification of NS5A$_{191–369}$

For NMR $^{1}H^{15}N$–HSQC experiments [*U*–^{15}N]–NS5A$_{191–369}$ was expressed in M9 minimal medium with [^{15}N] ammonium chloride as sole nitrogen source. For SPR and other experiments NS5A$_{191–369}$ was expressed in LB medium. After transforming E*. coli BL21 Rosetta T1*^{R} with pGEX–6P–2_NS5A$_{191–369}$ expression took place in 4x 1 litre medium. After bacterial cells growth reaching an optical density of OD_{600}= 0.8, 0.5 mM IPTG was added to induce expression of recombinant GST–NS5A$_{191–369}$. Bacterial cells were harvested after 5 hours of incubation time. The expression was screened by SDS PAGE (fig. III.1.5.1). The screen shows clearly an increasing expression band around 45 kDa in the lanes 2, 3, 6 and 7, which corresponds to the molecular weight of the GST–NS5A$_{191–369}$ fusion protein. In comparison the lanes 1 and 5 do not show any over expression band. These are the lanes with the samples before expression induction. Bacterial harvest per 1 l culture medium resulted in between 3–4 g pellet wet weight. The cell pellets were stored at –20° C for further processing.

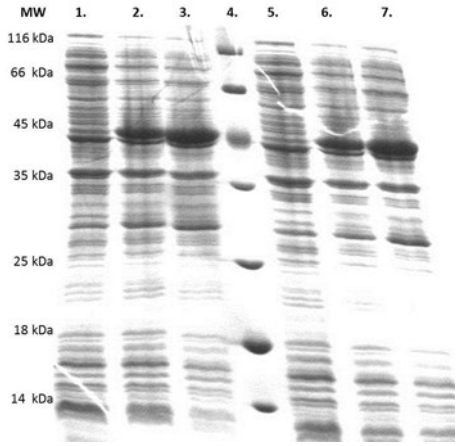

Fig.III.1.5.1: 16 % SDS PAGE of $NS5A_{191–369}$ Expression in *E. coli Rosetta* strains. Lane 1 and 5 show the bacterial expression profiles before the induction of recombinant $NS5A_{191–369}$ by IPTG. The lanes 2 and 6 show GST–$NS5A_{191–369}$ expression after 2 hours and lanes 3 and 7 after 5 hours post IPTG induction. GST–$NS5A_{191–369}$ has a molecular weight of 45 kDa

The bacterial cell pellets were suspended in lysis buffer and sonicated for cell lysis. The lysate was centrifuged. The fusion protein in the supernatant was bound to GSH sepahrose via its GST tag. After several washing and equilibration steps with the optimal buffer for HRV 3C protease, the tag was cleaved with 2 mg GST–HRV 3C protease on column overnight at 4 °C. The cleaved $NS5A_{191–369}$ was now in the flow through. The different fractions were analysed via SDS PAGE (figure III.1.5.2).

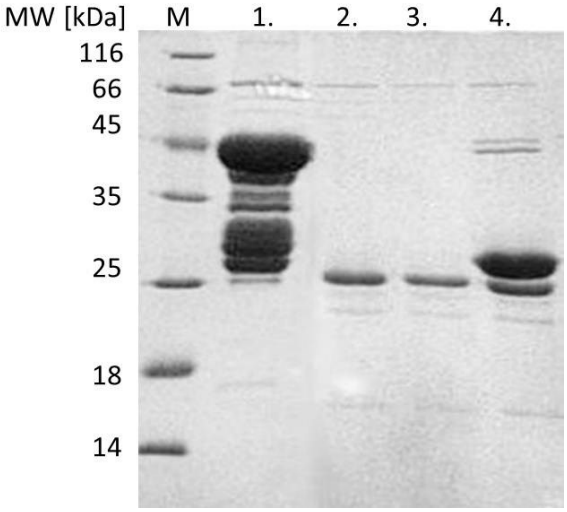

Fig.III.1.5.2: On column cleavage of GST–$NS5A_{191–369}$ with HRV 3C. On lane 1 the fusion protein at 45 kDa and its degradation products are seen on column before adding the protease to cleave the GST tag. Lanes 2 and 3 show the flowthrough fractions after overnight on column cleavage of the GST tag. The protein band at 25 kDa is $NS5A_{191–369}$ with the N–terminal GPLGS peptide overhang caused by HRV 3C digestion. Lane 4 displays the column material after the digestion and elution of the $NS5A_{191–369}$ fragment from the column. There is a dominant GST band slightly above 25 kDa, below that is still $NS5A_{191–369}$. Around 45 kDa there is uncleaved Gst $NS5A_{191–369}$ and Gst–HRV–3C protease.

The cleaved $NS5A_{191–369}$ sample shows in the SDS PAGE still impurities in the elution fraction with higher and lower molecular protein in lanes 2 and 3 in figure III.1.5.2. In lane 4 the column material is shown. The GST tag is bound to the column. There is still $NS5A_{191–369}$ attached to the column as it can be seen beneath the GST band. Another washing step with buffer eluted this remaining $NS5A_{191–369}$. Those impurities were successfully separated with anion exchange chromatography. Thus the sample was dialysed against 10 mM $NaPO_4$, pH 7.0, 2 mM DTT and applied on the anion exchange column. The chromatography was carried out at the bench and a salt gradient as described in chapter

II.2.3.7.2 was used to separate the $NS5A_{191–369}$ from the higher and lower molecular weight protein pollutions. SDS PAGE analysis shows that the lanes 2–9 have now relatively pure $NS5A_{191–369}$ protein. Lane 1 contains the crude sample before applying on column. Whereas $NS5A_{191–369}$ did not bind tightly to the DEAE sepharose and was found in the flow through and washing fractions as well as when applying low salt concentrations of 50 mM to 200 mM, the impurities were eluted at salt concentrations from 300 mM to 1000 mM.

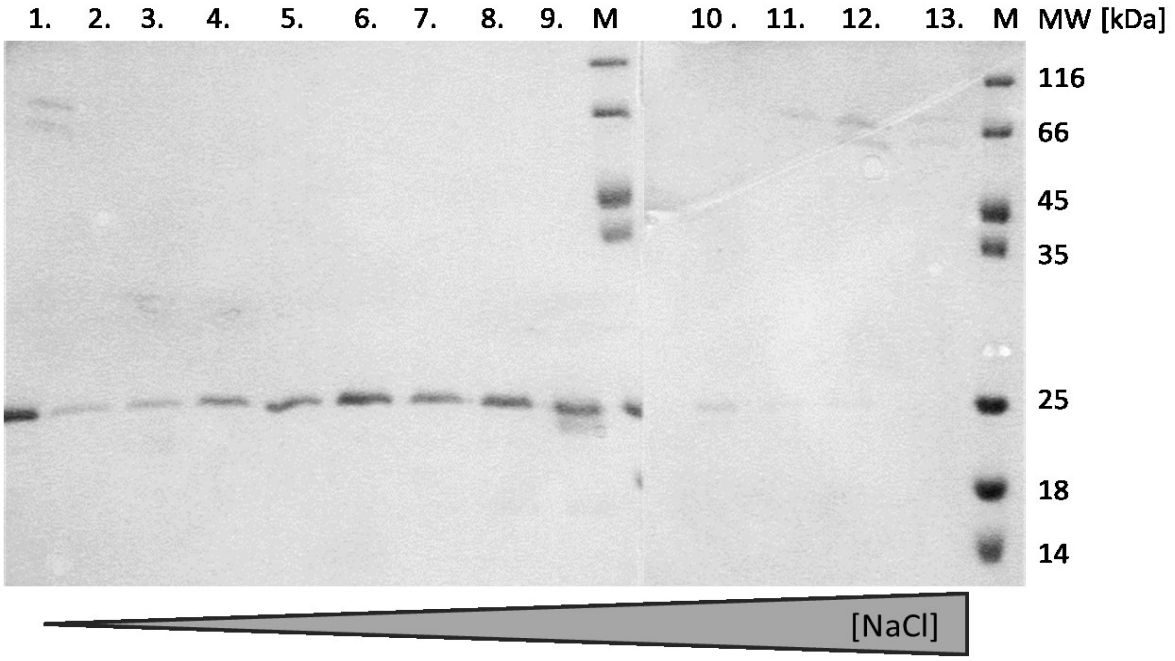

Fig. III.1.5.3: Anion exchange purification step of $NS5A_{191–369}$ on 16% SDS PAGE, NaCl gradient elution fractions using DEAE sepharose. Lane 1 contains the crude $NS5A_{191–369}$ with the lower and higher molecular impurities. Lane 2 shows the flow through and 3 the wash fraction. Lanes 4 and 5 as well as lanes 6 and 7 were eluted with 50 mM or 100 mM NaCl, respectively. Lanes 8 to 13 were from elutions with 150, 200, 300, 400, 500 and 1000 mM NaCl, respectively.The marker M is from MBI Fermentas.

The fractions 2–10 were pooled and dialysed either against 10 mM $NaOP_4$, 50 mM NaCl and 2 mM DTT, pH 6.5 or 10 mM Sodium acetate buffer, 2 mM DTT at different pH values as described in detail in the SPR chapter II.2.6.1. The $NS5A_{191–369}$ was stored with 1 complete tablet against proteolytic degradation at -80 °C for further experiments.

The overall protein yield was determined using UV–Vis at 280 nm spectroscopy (chapter II.2.2). 1 litre of *E. coli* LB medium culture yielded in 2 mg of $NS5A_{191–369}$ protein.

III.1.6. Sub–cloning of the NS5A $_{191–340}$ fragment into pGEX–6P–2 vector

Based on the pGEX–6P–2_NS5A191–369 clone (chapter III.1.4) a deletion mutant was created using PCR amplification technique. The shortened variant of $NS5A_{191–369}$ contained a deletion of the canonical SH3–binding motif, now spanning the residues 191–340. The new $NS5A_{191–340}$ fragment was inserted into a pGEX–6P–2 vector. Clones which carried an insert with the right length as judged by a digestion with BamHI and NotI and subsequent gel electrophoresis were sequence verified (Seqlab, Göttingen).

Tab.III.1.6 Amino acid sequence of $NS5A_{191–340}$. The N–terminal GPLGS peptide overhang caused by HRV 3C digestion is highlighted in red.

$NS5A_{191–340}$	**GPLGS**GTGSLRGGEPEPDVTVLTSMLTDPSHITAETAKRRLARGSPPSLASSSASQLSA PSLKATCTTHHDSPDADLIEANLLWRQEMGGNITRVESENKVVILDSFEPLHADGDER EISVAAEILRKSRKFPSALPIWARPDYNPPLLESWKDPDYVPPVVH*

III. 2. Biophysical experiments to analyse the interaction between SH3 domain and NS5A

III.2.1.Determining the dissociation constant K_D by surface plasmon resonance (SPR)

To characterise the binding affinity of Bin1 SH3 domain to the $NS5A_{333–369}$ peptide surface plasmon resonance (SPR) experiments were performed using a Biacore X device (chapter II.2.6). Bin1 SH3 domain was immobilised on the CM5 ship surface using the amine coupling technique as described in chapter II.2.6.1. For this Bin1 SH3 was kept in a sodium formiate buffer pH 3.8. The immobilised amount of Bin1 SH3 correlated to 1000 Response units (RU), corresponding to 1.2 mM SH3 domain (Howell et al. 1998). Different $NS5A_{333–369}$ concentrations were randomly injected for 2 minutes at a flow rate of 10 µl/min at 21° C in HBSEP buffer with 2 mM DTT. The injected concentrations are listed figure III.2.1.1 The sensograms were processed using BiaEvaluation software as described in methods (II.2.6.3). The overlay of all sensograms is shown in figure III.2.1.1. Because of the very rapid association and dissociation behaviour of the molecules the kinetics for the Bin1 SH3 $NS5A_{333–369}$ interaction could not be determined from the sensograms. Thus the *steady state* model was applied to estimate the affinity as described in chapter II.2.6. The blue lines over the sensograms (curves) as seen in fig. III.2.1.1 show the *steady state* phase of the respective binding event.

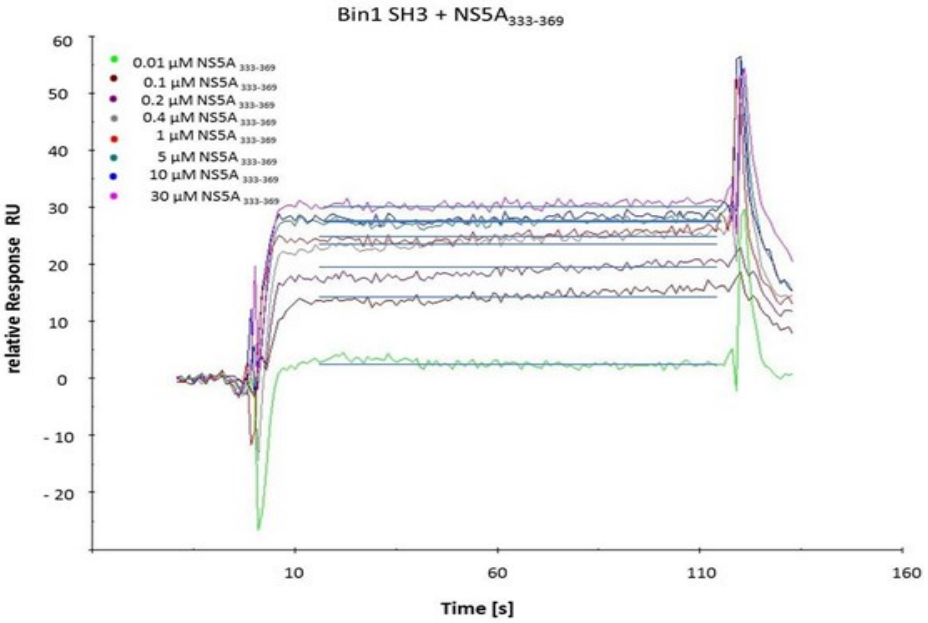

Fig.III.2.1.1 Probing the Bin1 SH3 binding to NS5A$_{333–369}$ with surface plasmon resonance (SPR). Overlay of sensograms from injections of different NS5A$_{333–369}$ peptide concentrations on a CM5 chip immobilised with BIN1 SH3. The peptide was injected for 2 minutes at 10 µl/min flow rate at 21 °C. The blue bars indicate the averaged response of the injection at *steady state*. Different colours indicate different peptide concentrations

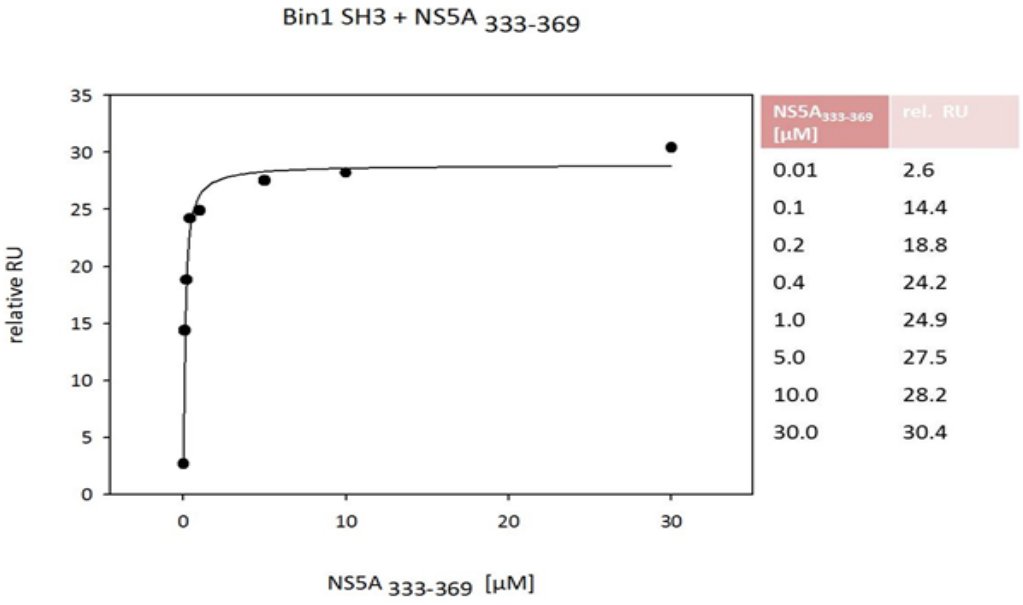

NS5A$_{333-369}$ [µM]	rel. RU
0.01	2.6
0.1	14.4
0.2	18.8
0.4	24.2
1.0	24.9
5.0	27.5
10.0	28.2
30.0	30.4

Fig.III.2.1.2 1:1 Langmuir fitting of Bin1 SH3 binding to NS5A$_{333–369}$, probed with surface plasmon resonance (SPR). The curve shows the Langmuir 1:1 fit of the averaged responses at the steady state phase of the respective binding event. The table right to the fit shows the averaged responses vs. the NS5A$_{333–369}$ peptide concentration

The lines are the averaged response between 15 and 115 s of the binding event of the respective $NS5A_{333–369}$ concentration. The averaged data were fitted using the 1:1 Langmuir binding model at *steady state* (figure III.2.1.2). The dissociation constant K_D resulting from the fit for Bin1 SH3 $NS5A_{333–369}$ interaction was 0.1 µM.

The interactions between Lyn SH3 domain and $NS5A_{333–369}$ were also probed with SPR following the same procedure as above. Lyn SH3 domain was immobilised on the CM5 chip via amine coupling. The immobilised amount correlated to 740 RU. Same buffers and flow rate were elaborated here as well except the 2 mM DTT in the solutions. $NS5A_{333–369}$ was injected in 14 steps with concentrations ranging from 0.05 µM up to 400 µM. The resulting sensograms were processed in the same fashion as above and fitted applying the *steady state* model to estimate the affinity. The averaged steady state values (between 15 and 115 s) were used for the 1:1 Langmuir binding model. The dissociation constant K_D resulting from this fit for the Lyn SH3 $NS5A_{333–369}$ interaction is 5 µM.

III.2.2 Studying the $NS5A_{191–369}$ interaction with Bin1 SH3 using SPR

Solution state NMR studies (Feuerstein et al. 2012) indicated that more than one Bin1 SH3 domain binds to the $NS5A_{191–369}$. Both binding events show different binding dynamics and affinity to $NS5A_{191–369}$, suggesting a second binding site other than the canonical SH3 PxxP motif. Two binding events could be observed at least tendentially by SPR analysis when applying immobilised $NS5A_{191–369}$ (amine coupling, chapter II.2.6.1) and injecting increasing concentrations of Bin1 SH3. The experiments were carried on with the Biacore T200 device. Approximately 80 RU $NS5A_{191–369}$ was immobilised corresponding to 40 µM $NS5A_{191–369}$ protein (Howell et al. 1998). Bin1 SH3 was injected in alternating concentrations for 3 minutes at a flow rate of 30 µl/min at 25 °C. HBSEP buffer with 2 mM 2–mercaptoethanol was used to run the experiment. Bin1 SH3 domain was dialysed against the running buffer to avoid any experimental artifacts. A wide concentration range from 0.3 to 700 µM of Bin1 SH3 was chosen to make sure that the second predicted low affinity binding site is saturated. Some concentrations were injected two to three times reassure quality of the set up. The buffer response was blanked from the SH3 injections and the sensograms were processed using BiaEvaluation T200 software as described in the methods (chapter II.2.7.). The buffer response was already blanked from the SH3 injections. All sensograms show a little jump around 100 s. with increasing values for concentrations higher than 20 µM and decreasing for lower concentration. The curves return back to average after 20 s. This effect was also observed for the buffer. An injecting mistake by the experimentalist can be excluded as the BiaCore T200 is an automated system. It could be speculated as a pumping artifact.

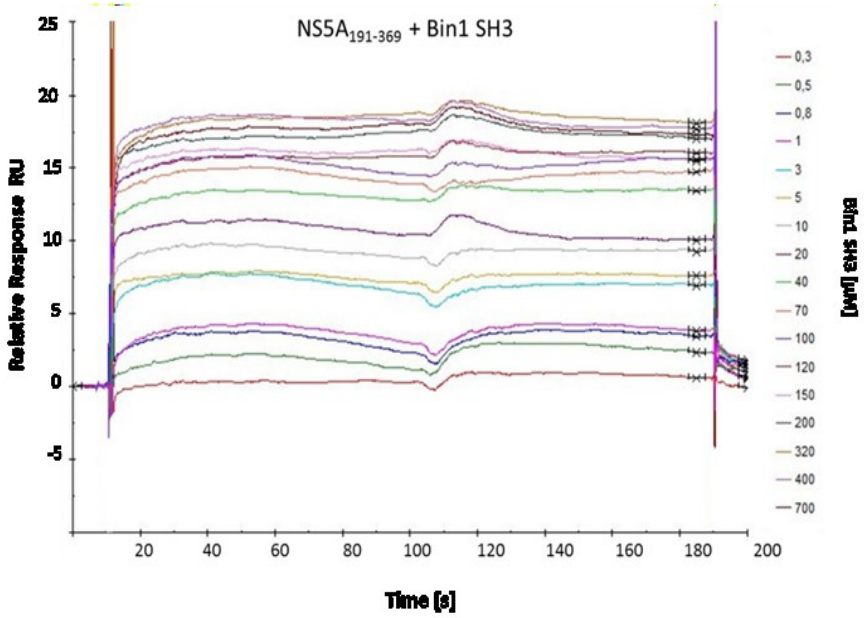

Fig. III.2.2.1 SPR analysis of the Bin1 SH3 binding to NS5A$_{191–369}$. Overlay of sensograms of the binding of different Bin1 SH3 concentrations on a CM5 S chip immobilised with NS5A$_{191–369}$. Bin1 SH3 was injected for 3 minutes at 30 µl/min flow rate at 25 °C. The black bars indicate the averaged response for 15 s of the injection at *steady state* before dissociation. Different colours indicate different SH3 concentrations

The sensograms do not give any information about the binding kinetics of the interaction. Therefore the dissociation constant K_D was obtained the from the averaged *steady state* phase of the NS5A$_{191–369}$ interaction as described in chapter II.2.6. The averaged values for each concentration were determined only from a 15 s window of the steady state phase shortly before dissociation (black bars in fig. III.2.2.1). This window is also not affected by the small “jump” in the sensograms.

First the averaged data was fitted using the Langmuir 1:1 binding model to display the experimental data. The resulting dissociation constant from the fit is 9.3 µM shown in fig III.2.2.2**.** As seen in the same figure the fit based on 1:1 Langmuir binding does not match well the experimental data at several points. Especially the data recorded for the higher concentrations at 200 µM, 320 µM and 400 µM vary significantly from the fitted curve. Also the experimental data for the concentrations 40 µM and 70 µM show slight variance.

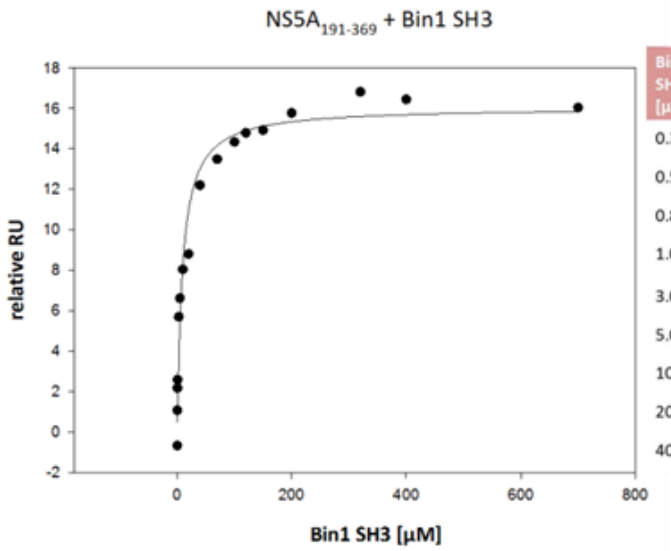

Bin1 SH3 [µM]	rel. RU	Bin1 SH3 [µM]	rel. RU
0.3	- 0.6	70.0	13.5
0.5	1.08	100.0	14.35
0.8	2.18	120.0	14.8
1.0	2.6	150.0	14.9
3.0	5.7	200.0	15.78
5.0	6.63	320.0	16.82
10.0	8.04	400.0	16.45
20.0	8.81	700.0	16.04
40.0	12.2		

Fig. III.2.2.2: Data fit of Bin1 SH3 in a Langmuir 1:1 binding model to NS5A$_{191–369}$. The curve shows the Langmuir 1:1 binding model fit of the averaged responses at the steady state phase of the respective binding event. The table right to the fit shows the averaged responses vs. the Bin1 SH3 concentration. The model does not meet the experimental data at 40 µM, 70 µM, 200 µm, 320 µM and 400 µM Bin1SH3 concentrations.

Secondly the averaged data were fitted using a "Two ligand binding" model (chapter II.2.6) shown in figure III.2.2.3. The dissociation constants K_D resulting from the fit for the NS5A$_{191–369}$ Bin1 SH3 interaction are 2.4 µM for the first binding site site and 48.9 µM for the second binding site. As seen in the figure III.2.2.3 the model is more suitable to match the experimental data. Variation of experimental data from the fit is seen for 320 µM and 700 µM SH3 domain concentrations.

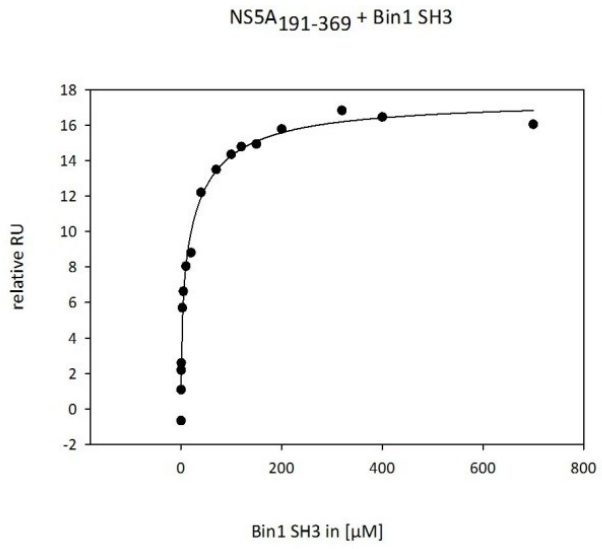

Bin1 SH3 [µM]	rel. RU	Bin1 SH3 [µM]	rel. RU
0.3	- 0.6	70.0	13.5
0.5	1.08	100.0	14.35
0.8	2.18	120.0	14.8
1.0	2.6	150.0	14.9
3.0	5.7	200.0	15.78
5.0	6.63	320.0	16.82
10.0	8.04	400.0	16.45
20.0	8.81	700.0	16.04
40.0	12.2		

Fig. III.2.2.3 Two ligand binding model fit for the Bin1 SH3 NS5A$_{191–369}$ interaction. The curve shows the "two ligand binding" model fit of the averaged responses at the steady state phase of the respective binding event. The table right to the fit shows the averaged responses vs. the Bin1 SH3 concentration.

III.2.3 Studying the NS5A$_{191–369}$ interaction with Fyn SH3 using SPR

The interaction between NS5A$_{191–369}$ and Fyn was investigated using the SPR technique. Therefor NS5A$_{191–369}$ in 10 mM Sodium acetate pH 4.0 buffer, was immobilised on a CM5 S chip using amine coupling technique. The immobilised protein complies with 850 RU, which equals approximately 430 µM NS5A$_{191–369}$ protein. The experiments were run using HBSEP buffer with 2 mM 2–mercaptoethanol at a 10 µl/ min flow rate at 25 °C. The Fyn SH3 domain was dialysed against the running buffer and was injected with alternating concentrations to minimize measuring errors. The Injected concentrations are listed in the figure III.2.3.1.

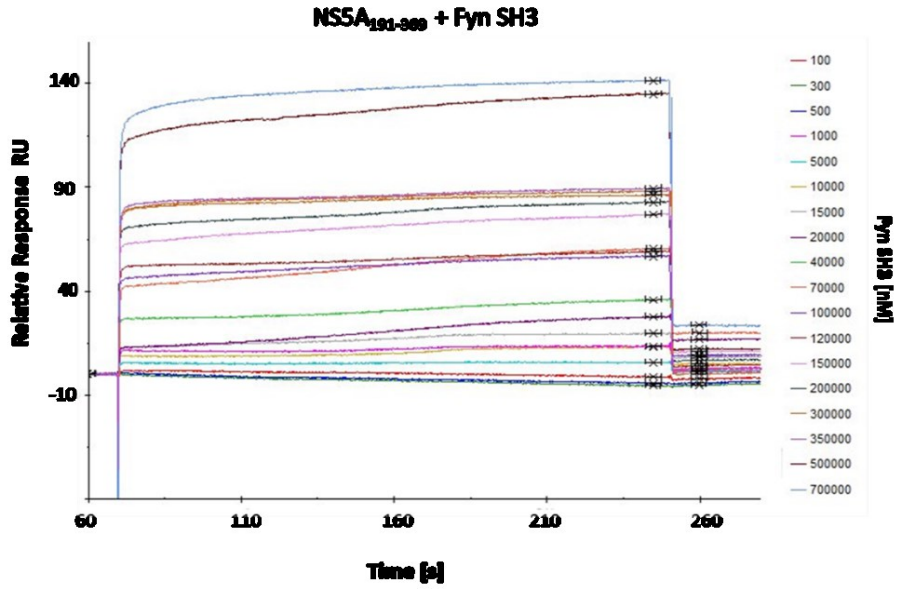

Fig. III.2.3.1.: Fyn SH3 domain binding to NS5A$_{191–369}$ probing with SPR. Overlay of sensograms of the binding of different Fyn SH3 concentrations on a CM5 S chip immobilised with NS5A$_{191–369}$. Fyn SH3 was injected for 3 minutes at 10 µl/min flow rate at 25 °C. The black bars indicate the averaged response for 15 s of the injection at *steady state* before dissociation. Different colours indicate different SH3 concentrations

Every protein concentration was injected for 3 minutes. The alignment of all sensograms shows something like saturation around 300 µM and 350 µM Fyn injection. There is no significant change in the relative response units. The sensograms in figure III.2.3.1 were processed and aligned using BiaEvalution T200 software. The buffer injection was blanked from the protein injections. The data does not give any information about the kinetics of the binding event, because of fast association and dissociation of the SH3 domain. Thus averaged data points from the *steady state* phase were taken as basis for fitting the above data firstly into a Langmuir 1.1 binding model (chapter II.2.6). The

averaged values were again taken from a 15 s time window in the *steady state* phase (black bars around 240 s in fig III.2.3.1). As the last two highest concentrations points 500 and 700 µM Fyn SH3 injection were distorting the fitting curve(fit not shown), they were taken out from the fit for a 1:1 binding model as seen in figure III.2.3.2. The fit was subjected to a Wilk Shapiro Test and passed with a W = 0.95 value. Yet some experimental data does slightly not match the fitted curve progression. These are the values measured for 100 µM, 120 µM and 150 µM Fyn SH3 injections. The dissociation constant obtained from the *steady state* phase is for a 1:1 binding model is K_D = 94.8 µM.

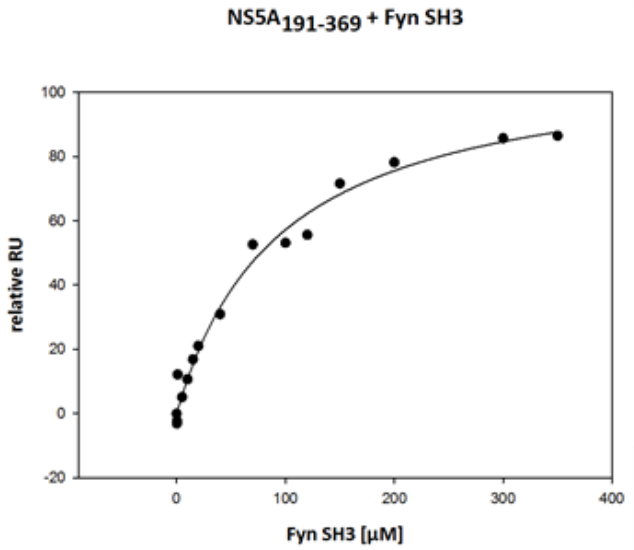

Fyn SH3 [µM]	rel. RU	Fyn SH3 [µM]	rel. RU
0.1	-0.13	40.0	30.9
0.3	-3.19	70.0	52.6
0.5	-2.47	100.0	53.1
1.0	12.1	120.0	55.6
5.0	5.1	150.0	71.6
10.0	10.6	200.0	78.2
15.0	16.8	300.0	85.7
20.0	21.0	350.0	86.5

Fig. III.2.3.2: Data fit of Fyn SH3 in a Langmuir 1:1 binding model to NS5A$_{191–369}$. The curve shows the Langmuir 1:1 binding model fit of the averaged responses at the steady state phase of the respective binding event. The table right to the fit shows the averaged responses vs. the Fyn SH3 concentration. The model does slightly vary from the experimental data at the concentration points 100 µM, 120 µM and 150 µM.

The same experiment was also subjected to a “two ligand binding” model fit (fig. III.2.3.3). Same averaged data was used for the fit, spanning a 15 s window (black bars in Fig. III.2.3.1). The values for the 300 µM and 350 µM concentrations were not used to fit the model as they were distorting the curve progression (fit not shown). Dissociation constants resulting from “two ligand binding” model fitting of the data were K_D = 24.1 µM for the first binding event and 523 µM for the second binding event.

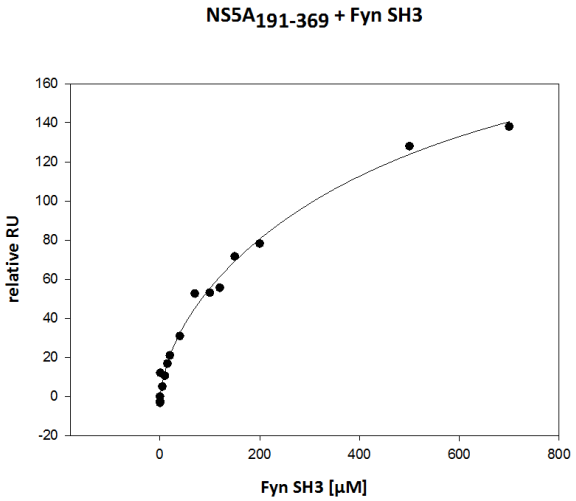

Fyn SH3 [µM]	rel. RU	Fyn SH3 [µM]	rel. RU
0.1	-0,3	40.0	30.9
0.3	-3.2	70.0	52.6
0.5	-4.73	100.0	53.1
1.0	12.1	120.0	55.6
5.0	5.1	150.0	71.6
10.0	10.6	200.0	78.2
15.0	16.8	500.0	128.0
20.0	21.0	700.0	138.0

Fig. III.2.3.3 Two ligand binding model fit for the Fyn SH3 NS5A$_{191–369}$ interaction. The curve shows the "two ligand binding" model fit of the averaged responses at the steady state phase of the respective binding event. The table right to the fit shows the averaged responses vs. the Fyn SH3 concentration

III.2.4 Studying the NS5A$_{347–361}$ interaction with Yes SH3 using fluorescence spectroscopy

The binding affinity of NS5A$_{372–361}$ to Yes SH3 was determined monitoring the change of the intrinsic tryptophan fluorescence of the SH3 domain in the PxxP motif binding pocket upon peptide adding (chapter II.2.8). A simple fluorescence titration experiment was set up to investigate the dissociation constant K_D. 0.9 µM Yes SH3 was prepared and NS5A$_{372–361}$ was gradually titrated to the sample, monitoring the fluorescence change. The NS5A$_{372–361}$ concentrations used for the titration are listed in the figure III.2.4. The titration experiment was run twice and the changes of fluorescence were blanked with the buffer fluorescence and averaged for each peptide concentration. The change of fluorescence as a function of increasing peptide concentration was used to calculate the K_D value assuming a 1:1 Langmuir model for the binding as a nonlinear regression function (Fig.III.2.4.). The buffer background was blanked before plotting the fit. The calculated K_D value for Yes SH3 interaction with NS5A$_{347–361}$ is 23 µM.

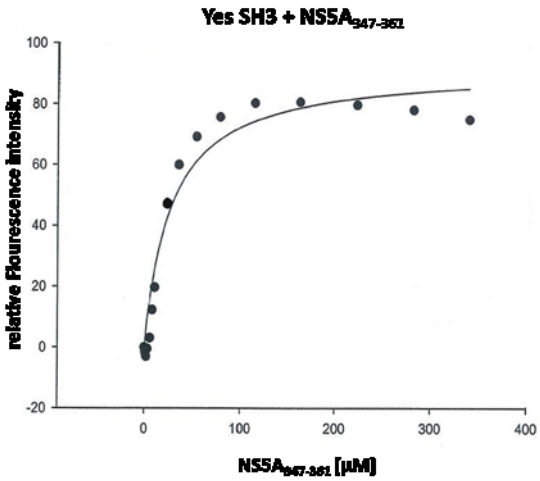

$NS5A_{347-361}$ [µM]	$NS5A_{347-361}$ [µM]
0.62	35.4
1.25	53.86
1.87	78.4
3.12	115.0
5.61	163.5
8.1	223.3
10.57	282.4
22.97	340.8

Fig. III.2.4 Fluorescence titration of $NS5A_{347–369}$ to Yes SH3 domain. 0.9 µM Yes SH3 in 1.6 ml 1x PBS, 1 mM DTT were used as starting point for the titration experiments. $NS5A_{347–369}$ was titrated in increasing concentrations to Yes SH3. The change of intrinsic fluorescence intensity is blotted as a function of $NS5A_{347–369}$ as a nonlinear regression function. The fit based on a 1:1 binding model. The excitation wavelength was 290 nm and the emission wavelength was 345 nm.

III.2.5 Hydrodynamic radius estimation of Bin1 SH3 using DLS

Dynamic Laser light scattering was employed to determine the hydrodynamic radius of potential Bin1 SH3 oligomers for different concentration at 25 °C. The Bin1 SH3 samples at different concentrations are the same samples as used in the SP experiments described in chapter III.2.2. The association and dissociation behavior of high concentrated Bin1 SH3 to the immobilised $NS5A_{191–369}$ in the initial SPR experiments (data not shown) gave rise to the possibility of oligomer formation of the SH3 domain on higher concentrations. In the following table the results of the DLS measurements are shown.

Tab.III.2.5 Dynamic light scattering experiments on the oligomerization of Bin1 SH3

Bin1 SH3 [µM]	R_H [nm]	Polydispersity %	M_w [kDa]
20	0.3	17.3	0
70	2.1	43.1	18
100	16.3	143	2305
150	4.3	8.3	104
320	2.4; 13.0	48.1, 47.5	27 ; 1360
500	4.4	81.7	107
700	2.3; 16.3	42.1; 49.1	24; 2317
1000	2.4; 20.5	42.8; 67.1	27; 3924

The DLS results suggest (table III.2.5**)** that in all sample concentrations higher molecular Bin1 SH3 domains are present. At least as a trimer and as higher molecular aggregates, which can not be classified clearly by analysing the fitted molecular weight for the hydrodynamic radius. This data is consistent with the initial SPR experiments.

III.3. CD spectroscopy to analyse the secondary structure of $NS5A_{333–369}$

A far UV CD spectrum of the $NS5A_{333–369}$ was recorded to analyse the secondary structure conformation of the free peptide. CD spectroscopy provides information about the overall secondary structure of a protein or peptide. The NS5A fragment comprises the residues which form the PxxP motif. PxxP motifs are known to form so called PPII helices. Figure II.3.1 shows the CD spectrum of the $NS5A_{333–369}$. The spectrum shows characteristics for PPII helices with a minimum at 199 nm which fits the minimum at 200 nm as described in literature (Manning et al. 1991 and Kelly et al. 2001). However the spectrum does not show the postulated maximum at 230 nm for PPII helices (figure III.3.1). The 37–mer NS5A fragment spans more than the two canonical PxxP motives and therefore deviate from the predicted maximum

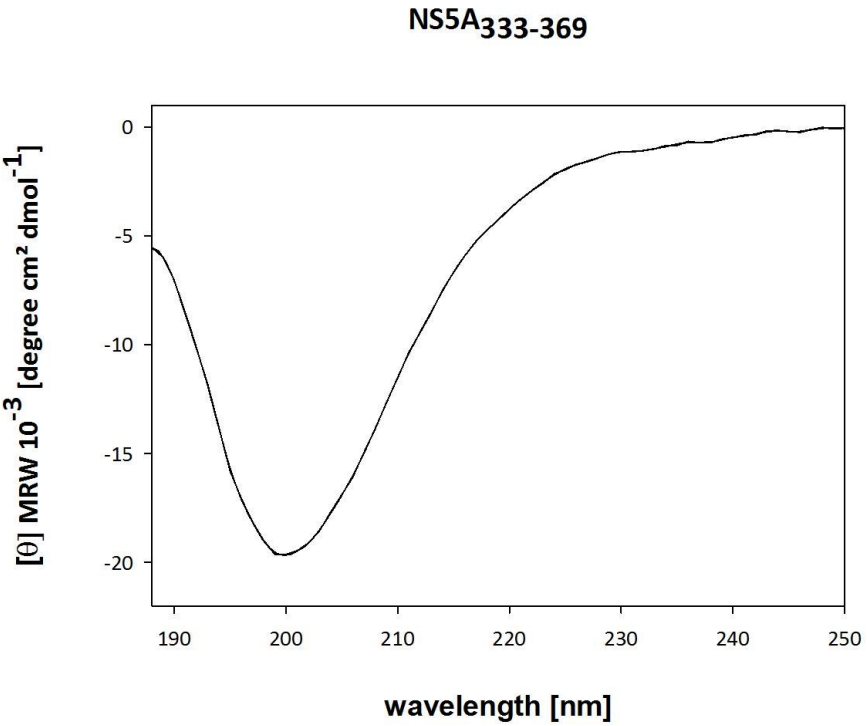

Fig.III.3.1 Far UV CD spectrum of $NS5A_{333–369}$. The spectrum was recorded in Potassiumphosphate buffer at 21 °C with 10 µM $NS5A_{333–369}$ fragment concentration. The spectra were recorded using 0.2 cm cuvette. The peptide shows a distinct minimum at 199 nm.

III.4. Structural characterisation of the Bin1 SH3: NS5A$_{333–369}$ complex with NMR

All NMR spectra were recorded at 303 K on Varian^{Unity} Inova or Varian NMR systems operating at 900, 800 or 600 MHz proton frequency equipped with cryoprobe. The protein:peptide complex was dealt as a single construct and both partners were employed as [*U*–^{13}C/^{15}N] labeled molecules for all NMR experiments to determine the complex structure(list of experiments see table II.2.7.1). The [*U*–^{13}C/^{15}N] labeled NS5A$_{333–369}$ peptide was gradually added to [*U*–^{13}C/^{15}N] labeled Bin1 SH3 domain and ^{1}H^{15}N HSQC experiments were recorded to monitor correlation resonances of protein and peptide. This step was taken to avoid populations of free SH3 domain and NS5A $_{333–369}$ peptide which would appear as extra signals and confuse during data analysis. Temperature conditions from 288 K to 303 K with 5 Kelvin steps were screened to improve signal to noise ratio and peak linewidth. The final sample composition and temperature is listed in tab.III.2.6.1 below. ^{1}H^{15}N HSQC experiments were recorded after every triple resonance experiment in order to ensure the quality of the sample. The sample was stable for several months although small amounts of protein precipitations were observed, but that did not affect the NMR experiments. All NMR spectra were processed using NMRPipe/nmrDraw (Delaglio et al. 1995). Spectra and correlation signals were assigned using CARA (Keller, 2004).

Tab. III.2.6.1 Sample composition and temperature during the NMR Experiments

Sample	Temperature	NMR
500 µM [*U*–^{13}C/^{15}N] Bin1 SH3 ~ 550 µM [*U*–^{13}C/^{15}N] NS5A$_{333–369}$ 50 mM KPi, pH 6.4 20 mM NaCl 2 mM DTT	303 K	two–and three dimensional experiments for complex structure calculation
100 µM [*U*–^{15}N] NS5A$_{333–369}$ 50 mM KPi, pH 6.4 20 mM NaCl 2 mM DTT	298 K	2D ^{1}H^{15}N HSQC experiments
100 µM [*U*–^{15}N] Bin1 SH3 50 mM KPi, pH 6.4 20 mM NaCl 2 mM DTT	298 K	2D ^{1}H^{15}N HSQC experiments

2D ^{1}H^{15}N HSQC correlation experiments of the free Bin1 SH3 and Bin1 SH3: NS5A$_{333–369}$ well dispersed signals, suitable for resonances assignment using two– and three dimensional triple NMR experiments (fig.III.2.6.1). The well dispersion of correlation signals indicates also folded protein with a well–defined tertiary structure. Based on the amino acid sequence of employed Bin1 SH3 and NS5A$_{333–369,}$ 81 ^{15}N–^{1}H correlation signals are expected for the SH3 domain and 26 for the NS5A peptide in the 2D ^{1}H^{15}N HSQC spectrum, excluding prolines which do not have amide protons and the first N–terminal amino acid which is in rapid exchange with the solution. The ^{1}H^{15}N HSQC spectrum

counts 76 correlation signals for free Bin1 SH3 (fig.III.2.6.1 (A)) and 22 correlation signals for $NS5A_{333–369}$ (fig.III.2.6.1 (B)). Five signals are missing for Bin1 SH3 already in the free–state and four signals are missing for the NS5A peptide. For the Bin1 SH3: $NS5A_{333–369}$ complex 103 ^{15}N–^{1}H correlation signals are expected. Furthermore, the side chain signals for three aspartic and nine glutamic acid signals are also expected, including five side chain signals for arginine. However only 91 signals are detected for the complex in the $^{1}H^{15}N$ HSQC experiment, twelve H_N correlation signals are missing. From the expected twelve side chain signals only eight are present.

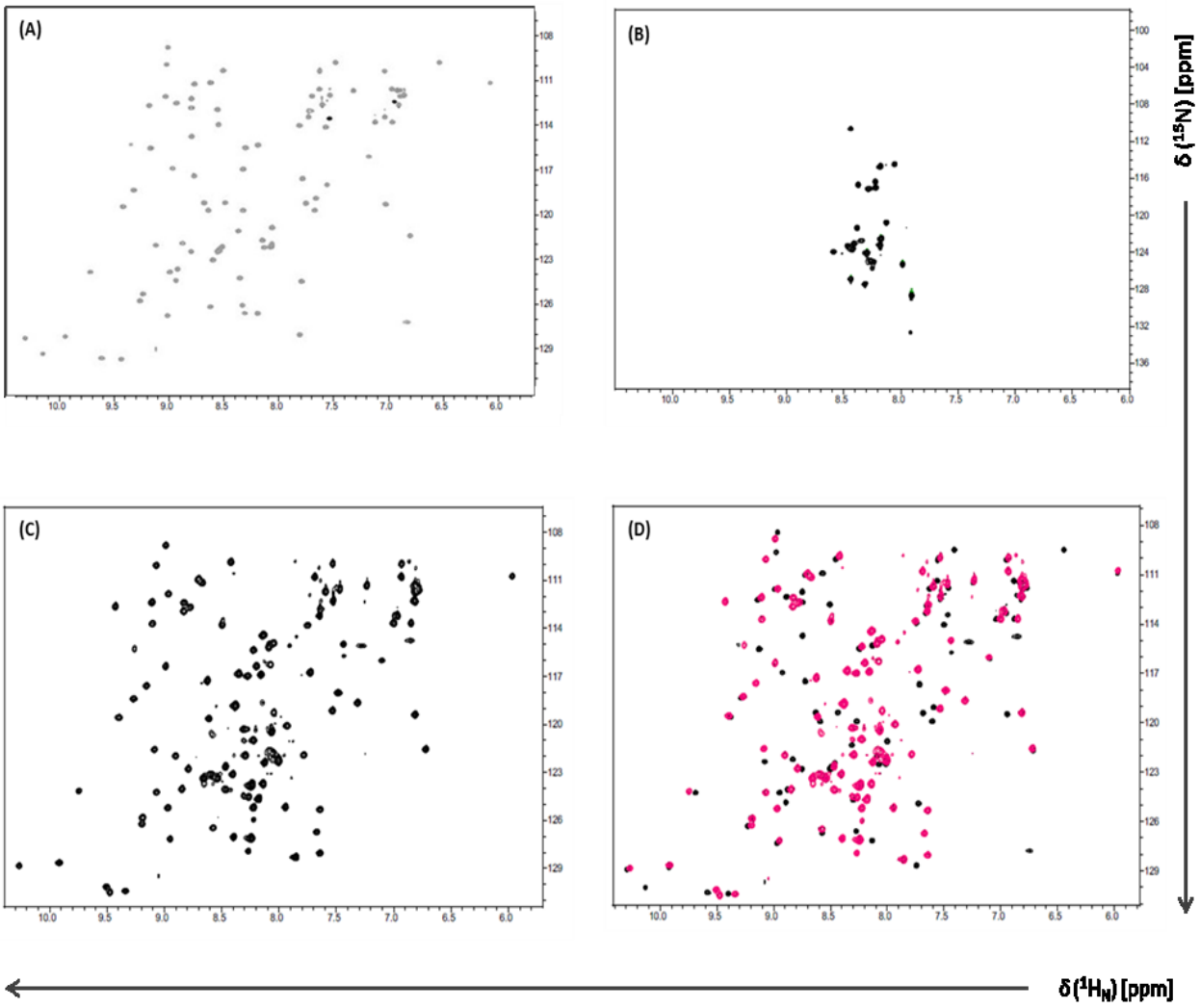

Fig. III.4.1 $^{1}H^{15}N$ HSQC spectra of (A) Bin1 SH3 free state, (B) $NS5A_{333–369}$, (C) Bin1 SH3: $NS5A_{333–369}$ complex and (D) overlay spectrum of Bin1 SH3 free state in black and Bin1 SH3: $NS5A_{333–369}$ complex in pink. Bin1 SH3 in free–state shows good dispersion of amide correlation signals, whereas $NS5A_{333–369}$ shows a poor dispersion, indicating no tertiary fold. Bin1 SH3: $NS5A_{333–369}$ complex shows good signal dispersion, indicating a well–defined tertiary structure. The overlay spectrum the free and bound states for Bin1 SH3 (D) shows the shift of many signal after NS5A peptide binding.

III.4.1.1. Bin1 SH3: NS5A$_{333–369}$ backbone assignment

The sequence specific protein backbone assignment for backbone amide groups (H^N and N), for the C^α and side chain C^β resonances for the Bin1 SH3:NS5A$_{333–369}$ complex was performed from a 3D triple resonance HNCACB experiment (Wittekind & Müller, 1993). In this experiment the amide resonance H^N and N are correlated with the $C^\alpha{}_i$– and side chain $C^\beta{}_i$ resonances of the amino acid of interest and the preceding one $C^\alpha{}_{i-1}$ and $C^\beta{}_{i-1}$. The latter correlation is weaker and results in weaker signals. The C^α correlation signals show 180° phase difference to the C^β signals, which is denoted in the spectrum by two different colours for the two carbon correlation signals. Furthermore characteristic chemical shift values of certain amino acid supports sequence specific assignment.

For example glycine residues do not have a C^β correlation and the C^α correlation chemical shifts appear around 45 ppm in the spectrum. Serine and Threonine residues show a down field shift for their C^β resonances (60– 70 ppm) due to the bond to the oxygen atom within the neighbouring hydroxyl group. Alanine residues display an extreme high field shift for their C^β resonances (18–20 ppm) which are part of the methyl group. With the help of such amino acids more or less all resonances could be assigned in a sequence specific manner. In figure III.4.1.1 stripes of 3D HNCACB experiment for 10 amino acids is shown, displaying the sequential assignment of the amide groups. Out of the 91 ^{15}N–^{1}H correlation signals, 79 residues were possible to assign. The assigned amide residues are shown in the $^{1}H^{15}N$ HSQC spectrum of the Bin1 SH3: NS5A$_{333–369}$ complex in fig III.4.1.2. The assignment of side chain atoms using the respective NMR experiments was done by M. Schwarten using the two and three dimensional NMR experiments recorded by me as described in methods (Table 2.8.1) Therefore, in the following assignment progress and results for Bin 1 SH3: NS5A$_{333–369}$ complex structure will be only mentioned briefly. During side chain assignment more correlation signals were observed than expected for the respective residues, indicating that the Bin1 SH3: NS5A$_{333–369}$ was not a homogenous sample. Moreover NMR experiments clearly showed a change of correlation signals for even assigned nuclei over time. This made it impossible to proceed for further NOE assignment and structure calculation.

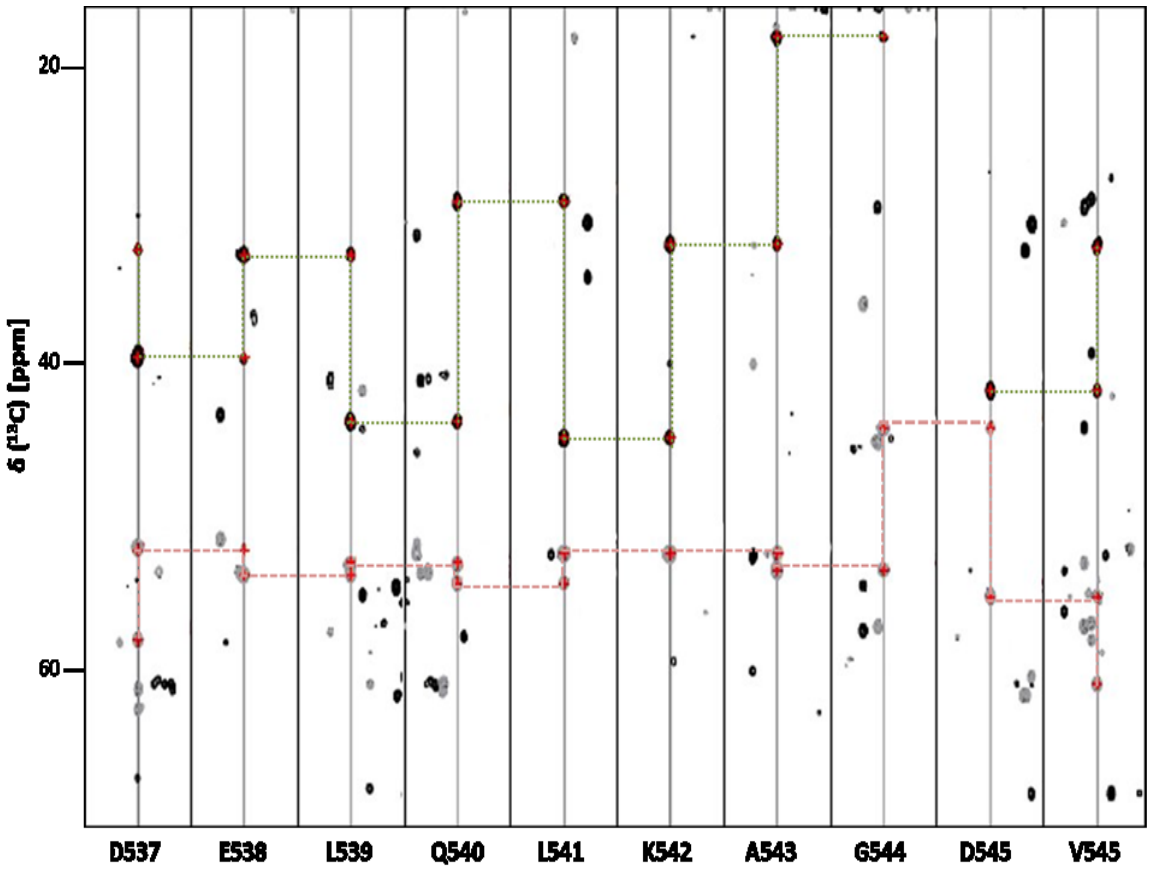

Fig.III.4.1.1 Sequence specific resonance assignment of the Bin1 SH3: NS5A$_{333–369}$ of 3D HNCACB spectrum of the residues from D537 to V545. ^{13}C(f1)– ^{1}H(f3) strips corresponding the H^{N}– and N– chemical shifts from the F2 and F3 dimensions were sequentially arranged. The C$^{\alpha}$ and side chain C$^{\beta}$ connectivities are marked with lines (C$^{\alpha}$ = red; C$^{\beta}$ = green). The typical high field shift of the alanine 543 and and the cut of C$^{\beta}$ connectivity at glycin 544.

The assignment of side chain atoms using the respective NMR experiments was done by M. Schwarten using the two and three dimensional NMR experiments recorded by me as described in methods (Table II.2.7.1). Therefore, in the following assignment progress and results for Bin 1 SH3: NS5A$_{333–369}$ complex structure will be only mentioned briefly. During side chain assignment more correlation signals were observed than expected for the respective residues, indicating that the Bin1 SH3: NS5A$_{333–369}$ was not a homogenous sample. Moreover NMR experiments clearly showed a change of correlation signals for even assigned nuclei over time. This made it impossible to proceed for further NOE assignment and structure calculation.

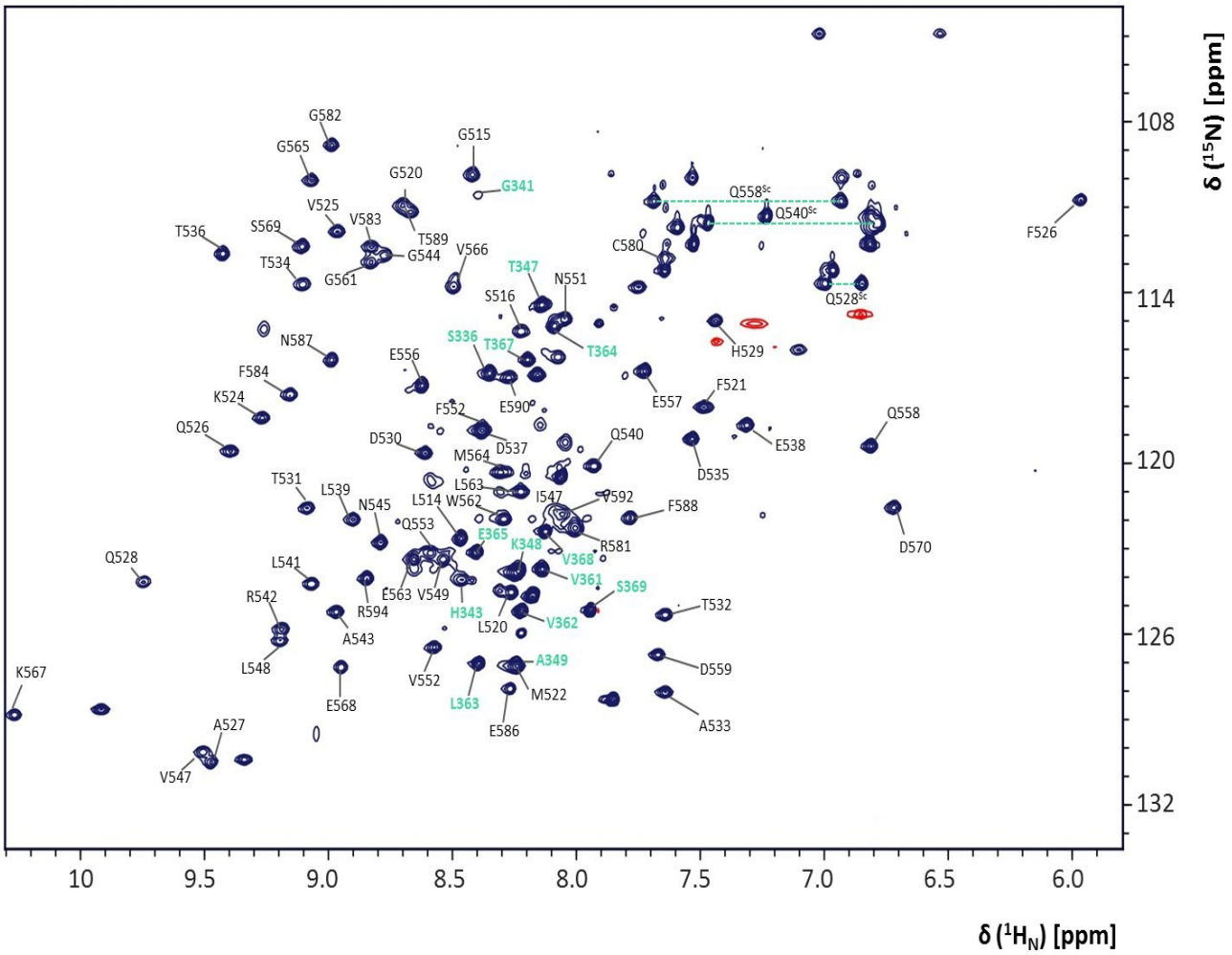

Fig. III.4.1.2. Assigned $^{1}H^{15}N$ HSQC spectrum of the Bin1 SH3: $NS5A_{333–369}$ complex. Shown here are the assigned amid correlation resonances of the Bin1 SH3 domain (black) and the $NS5A_{333–369}$ fragment (green). Out of the 91 picked $^{15}N–^{1}H$ correlation signals, 79 residues could be assigned as labeled in the spectrum.

Tab.III.4.1. Bin1 SH3: $NS5A_{333–369}$ complex backbone assignment report

Amino acid	number	Assigned amide
Ala	4	4
Arg	5	3
Asn	3	3
Asp	5	5
Cys	1	1
Gln	6	5
Glu	10	8
Gly	7	7

His	3	2
Ile	2	1
Leu	7	7
Lys	8	3
Met	2	2
Phe	5	5
Ser	5	5
Thr	8	7
Trp	2	1
Tyr	2	1
Val	13	7

III.4.2. NMR studies of NS5A fragments with SH3 domains

The interaction dynamics of NS5A with SH3 domain is not described, yet. Therefore, chemical shift perturbation (CSP) were carried out to examine the binding dynamics of the SH3 domains of Fyn, Yes and Bin1. The overall spectral change upon ligand titration gives information about kinetics of the binding event (Zuiderweg et al. 2002). $NS5a_{333–369}$ was titrated to [*U*–^{15}N] labeled SH3 domains. The concentration of each SH3 domain was 100 µM in 50 mM KPi pH 6.5 with 2 mM 2–mercapthoethanol. For the Yes SH3 domain, the binding dynamics with $NS5A_{347–361}$, a shorter fragment was probed as well. In figure III.4.2.1 only the ^{15}N–^{1}H correlation signals of the [*U*–^{15}N] labeled Fyn SH3 are visible. Upon $NS5a_{333–369}$ titration the chemical environment of the corresponding nuclei changes due to peptide binding. The gradual shift (black to green) for most of the resonances here indicates fast exchange of $NS5A_{333–369}$ on and off the Fyn SH3 binding site (Hall et al. 2001). Dissociation of complex occurs fast, observed for low affinity binding.

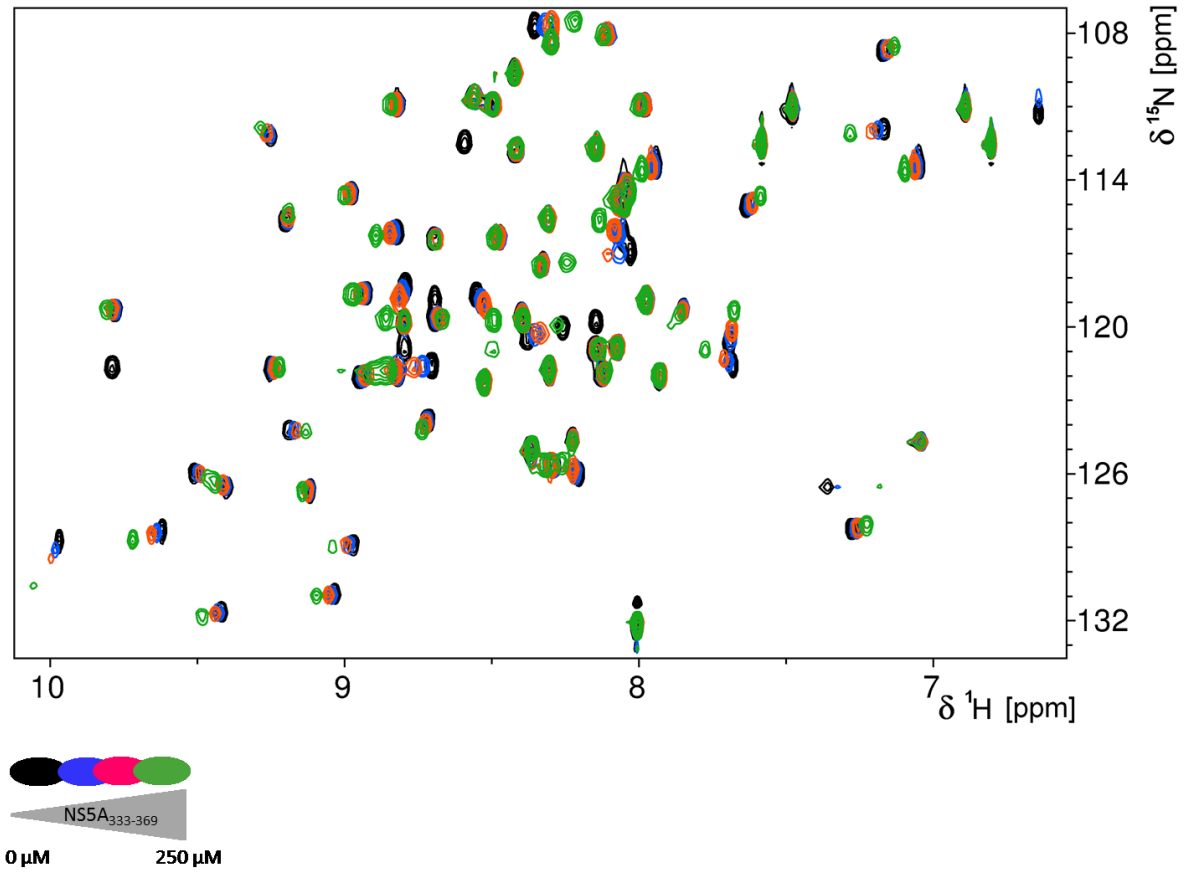

Fig. III.4.2.1. Analysis of Fyn SH3 –NS5A$_{333–369}$ interaction by HSQC titration experiments. Superposition of four spectra obtained upon titration of Fyn SH3 with increasing amounts of NS5A$_{333–369}$ ligand (from black to green). The initial Fyn SH3 concentration was 100 µM. Fyn SH3 amide resonances show a linear shift upon peptide titration.

The same experimental set up was used for Yes SH3. 100 µM [*U*–^{15}N] labeled Yes SH3 in 50 mM KPi pH 6.5 with 2 mM 2–mercapthoethanol was used for titration experiments. NS5A$_{333–369}$was gradually titrated in five steps to Yes SH3 domain. The final concentration of peptide was 250 µM in the sample whereas the SH3 domain had a concentration of 95 µM. Some resonances disappeared already during the initial peptide titration step as shown in figure III.4.2.2 (A), whereas some resonances displayed a linear shift to new positions upon gradual peptide binding. Figure III.4.2.2 (B) shows a section of the overlaid spectrum which is exemplary for disappearing ^{15}N–^{1}H correlations. These resonances are typical for a so called intermediate exchange, indicating a strong binding (McAllister et al. 1996).

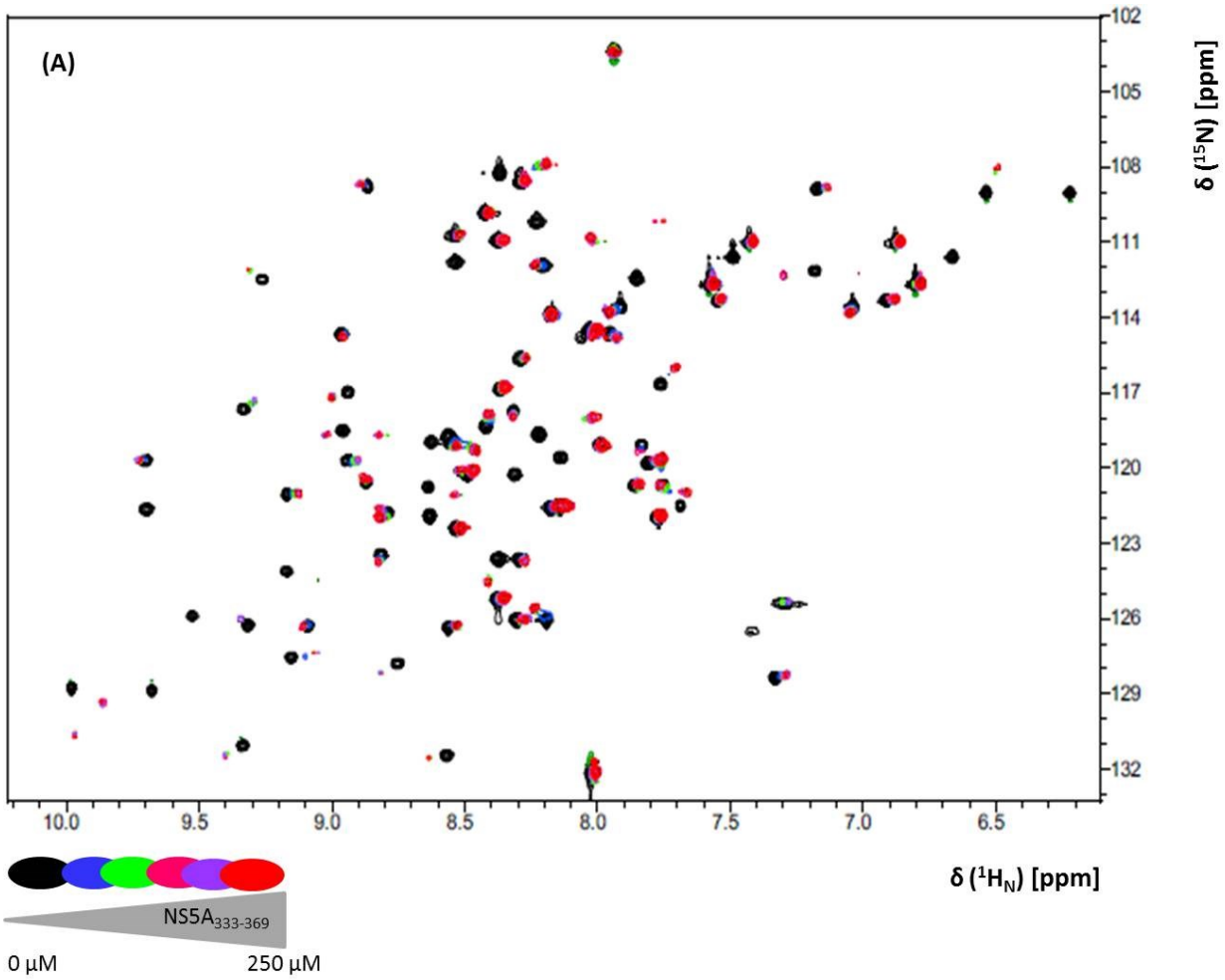

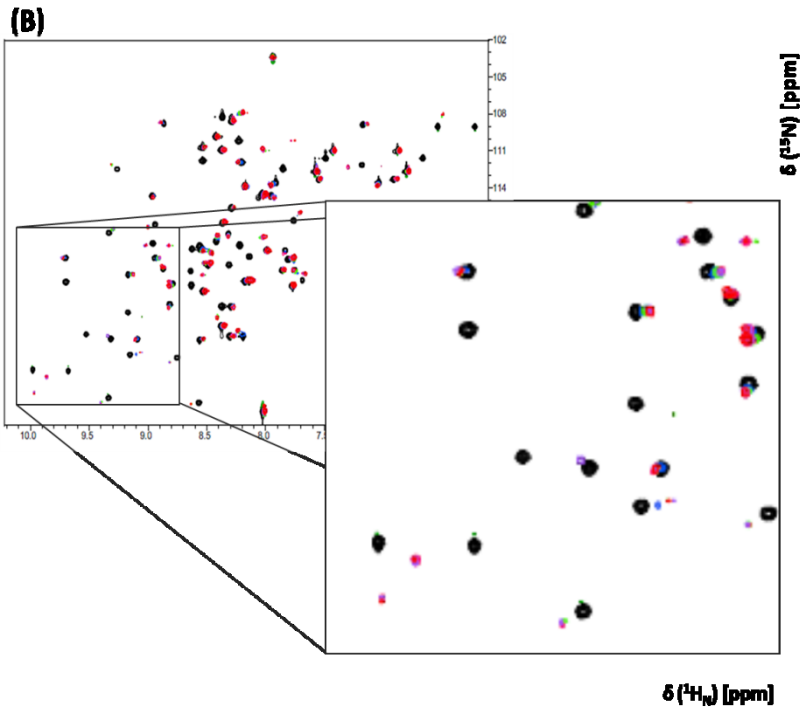

Fig. III.4.2.2. Analysis of Yes SH3 –NS5A$_{333–369}$ interaction by HSQC titration experiments. (A). Superposition of four spectra obtained upon titration of Fyn SH3 with increasing amounts of NS5A$_{333–369}$ ligand (from black to pink). The initial Yes SH3 concentration was 100 µM. (B) Section of the same spectrum showing amide resonances which disappear upon peptide binding. Some resonances follow fast exchange kinetics.

Complex dissociation is relatively slow for these resonances. Looking at other parts of the spectrum fast exchange kinetics is also observed and in some cases there is merely a change of chemical shift seen. The interaction is a combination of both exchange kinetics.For the Yes SH3 domain the same experiment was repeated with a shorter version of the NS5A peptide comprising the residues 347–361, with the canonical PxxP SH3 binding motif. The conditions were the same. $NS5A_{333–369}$ peptide was titrated using the same titration steps and concentrations to the [*U*–^{15}N] labeled Yes SH3 domain. The overlay spectrum of all six spectra from the titration in figure III.4.2.3 shows that most of the amide correlations appear to have a linear shift upon binding of peptide. The kinetics can be classified as fast exchange and the affinity is expected to be low. Comparing this result with the Yes SH3 titration with $NS5A_{333–369}$ peptide (fig. III.4.2.2.), one can conclude that not only the canonical binding motif PxxP is important for binding, but also contacts outside this conserved motif.

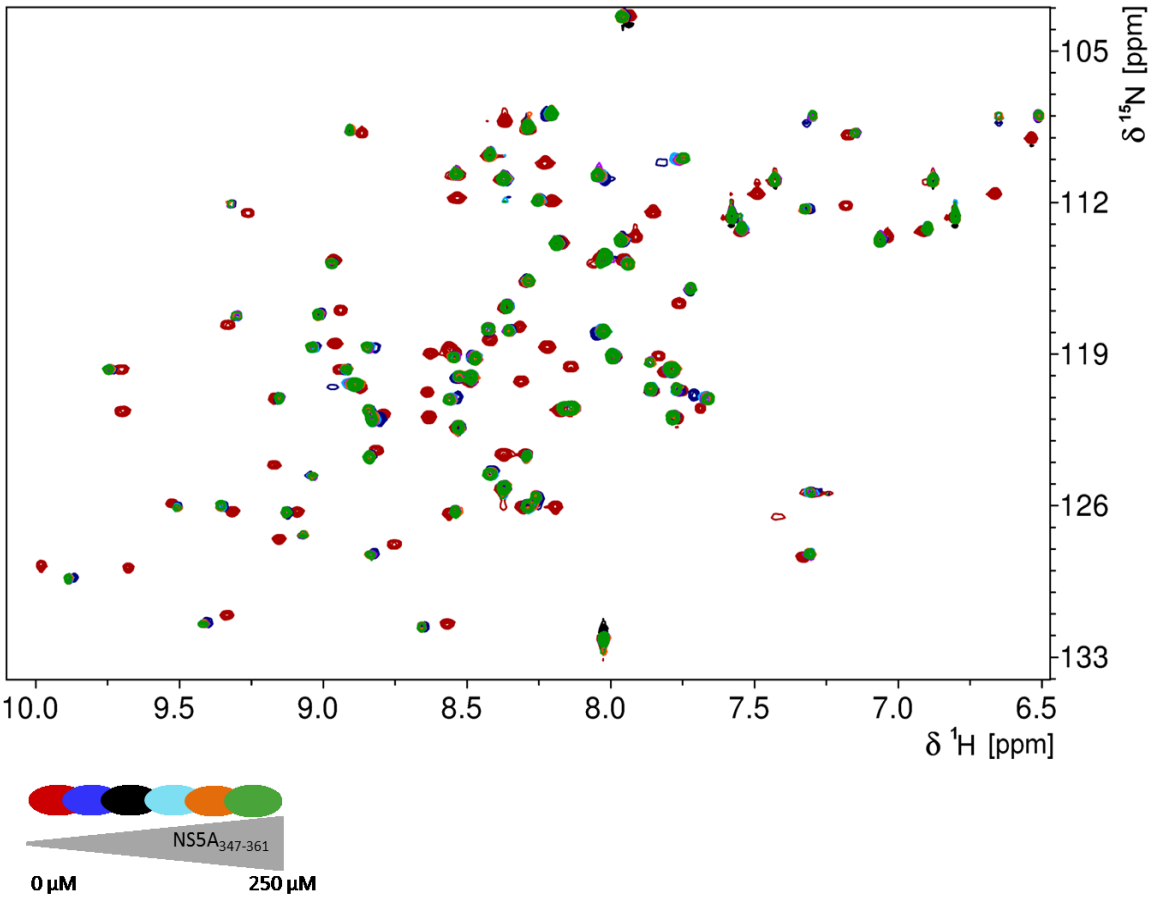

Fig. III.4.2.3. Analysis of Yes SH3 –$NS5A_{347–361}$ interaction by HSQC titration experiments. Superposition of six spectra obtained upon titration of Yes SH3 with increasing amounts of $NS5A_{347–361}$ ligand (from red to green). The initial Yes SH3 concentration was 100 µM. Yes SH3 amide resonances show a linear shift upon peptide titration

[*U*–^{15}N] labeled Bin1 SH3 domain NS5A$_{333–369}$ interaction was analysed employing the same experimental set up as already described for the HSQC titrations. The peptide was titrated in five steps to the SH3 domain. With increasing NS5A$_{333.369}$ concentrations some Bin1 SH3 ^{15}N–^{1}H correlations started to shift in a linear manner from free–state (black spectrum) to bound state (gradually: blue, orange, red, green and turquoise). Some amide correlations disappeared upon peptide binding and change of the chemical environment for those nuclei. Overall the Bin1 SH3 NS5A$_{333–369}$ interaction shows elements of fast exchange as well as slow exchange kinetics.

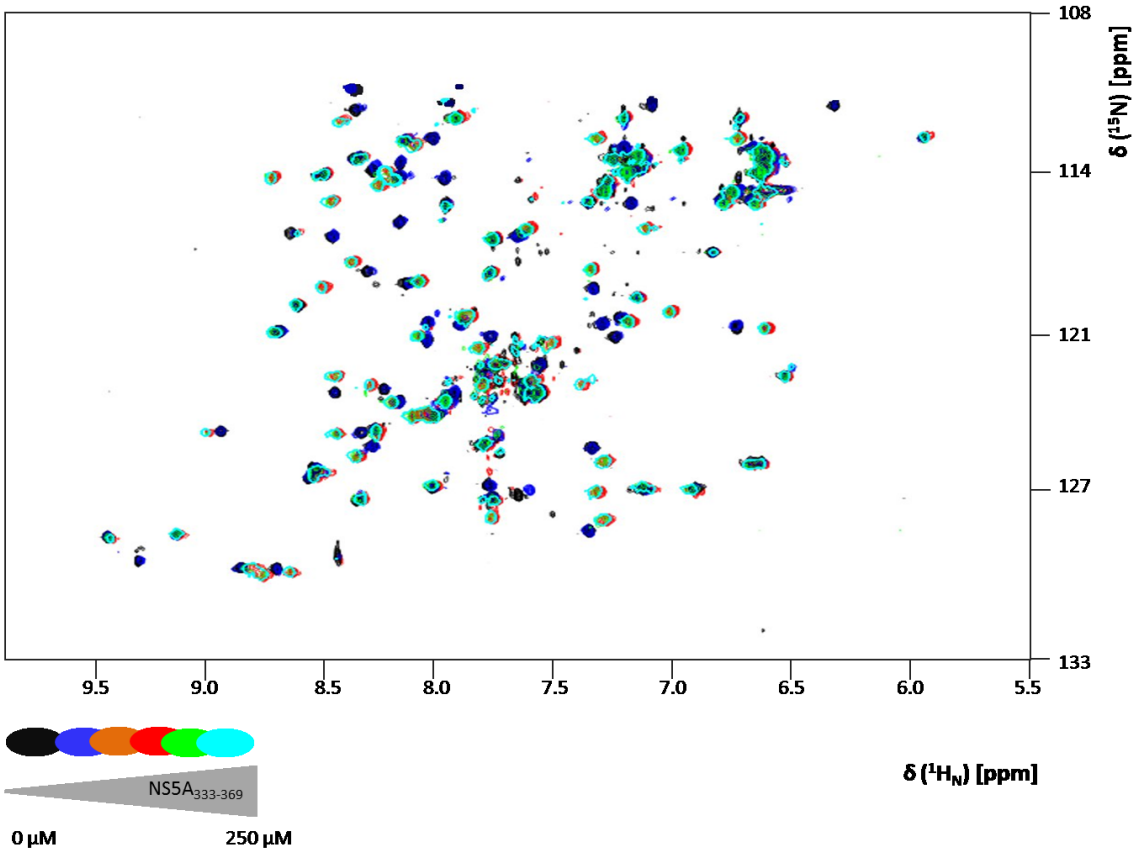

Fig. III.4.2.4. Analysis of Bin1 SH3 –NS5A$_{333–369}$ interaction by HSQC titration experiments. Superposition of six spectra obtained upon titration of Bin1 SH3 with increasing amounts of NS5A$_{333–369}$ ligand (from black to turquoise). The initial Bin1 SH3 concentration was 100 µM. Bin1 SH3 overlay spectrum shows for some resonances linear shift and some resonances disappear upon peptide binding.

III.4.3 $^{1}H^{15}N$ HSQC spectrum of $NS5A_{191–369}$

$^{1}H^{15}N$ HSQC NMR experiments are a powerful and relatively fast tool to have a first glance at the overall folding of the protein of interest. Chemical shifts can be described as a function of backbone torsion angles. Therefore, for proteins in a folded state, ring currents and other dipolar interactions lead to increased chemical shift dispersion. In unfolded or partly folded proteins these effects are near to zero and chemical shift values are close to random coil values. The chemical shift dispersion is narrowed to a typical part of the spectrum. In a typical folded protein, the dispersion of the amide correlation signals is spread between 6.5 ppm and 9.5 ppm, ideally. The signal dispersion of mainly unfolded proteins is narrowed down to a 2 ppm range (Yao et al 1997). Figure III.4.3.1 shows the $^{1}H^{15}N$ HSQC spectrum for 100 µM $NS5A_{191–369}$ in 10 mM NaPi pH 6.5 and 2–mercaptoethanol. The ^{15}N and ^{1}HN amide correlation signals do not show characteristic dispersion for folded proteins. Most of the correlation signals are between 7.4 ppm and 8.7 ppm, displaying characteristics of intrinsically unfolded proteins. The signal dispersion ranges 1.3 ppm. It is described that intrinsically disordered proteins undergo local folding or ordering upon molecular recognition (Wright and Dyson, 1999; Dyson and Wright, 2002). NS5A is known to interact with a set of SH3 domains (MacDonald et al. 2004). The ability of $NS5A_{191–369}$fragment to undergo transition to local ordering and structure upon ligand binding is probed in the following experiment. Unlabeled Lyn SH3 domain was titrated gradually to [*U*–^{15}N] $NS5A_{191–369}$. ^{15}N–^{1}H correlation signal shifts were observed for almost every amide correlation upon Lyn SH3 binding. The change in signal dispersion is shown in figure III.4.3.2. The black amide resonances are from the free $NS5A_{191–369}$ whereas the red resonance signals arise from $NS5A_{191–369}$: Lyn SH3 complex formation. Even though huge shift are observed for NS5A fragment upon ligand binding, the ^{15}N–^{1}H correlation signal dispersion remains within the range of unfolded or partially unfolded proteins for the $^{1}H_{N}$ dimension. A greater dispersion is reached for the ^{15}N dimension, a weak indication for α–helical conformations.

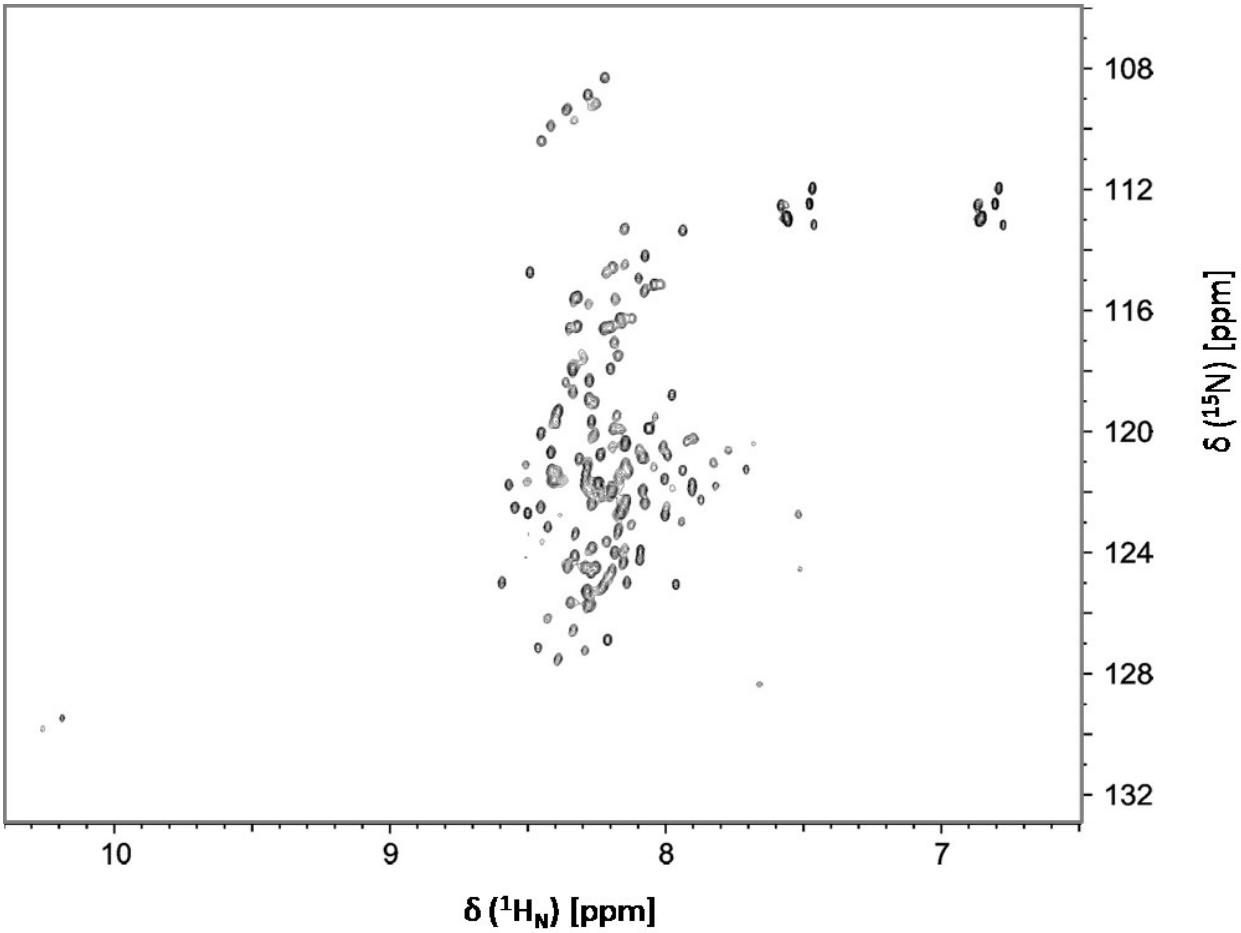

Fig. III.4.3.1.: $^{1}H^{15}N$ HSQC´spectrum of the $NS5A_{191–369}$ fragment from hepatitis C virus. Sample composition is 100 µM [*U*–^{15}N]–$NS5A_{191–369}$ in 10 mM NaPi pH 6.5 and 2–mercaptoethanol at 25 °C. $^{15}N–^{1}H$ correlation signals are not well dispersed. The signal dispersion ranges from 7.5 ppm to 8.6 ppm. This is typical for unfolded or partly unfolded proteins.

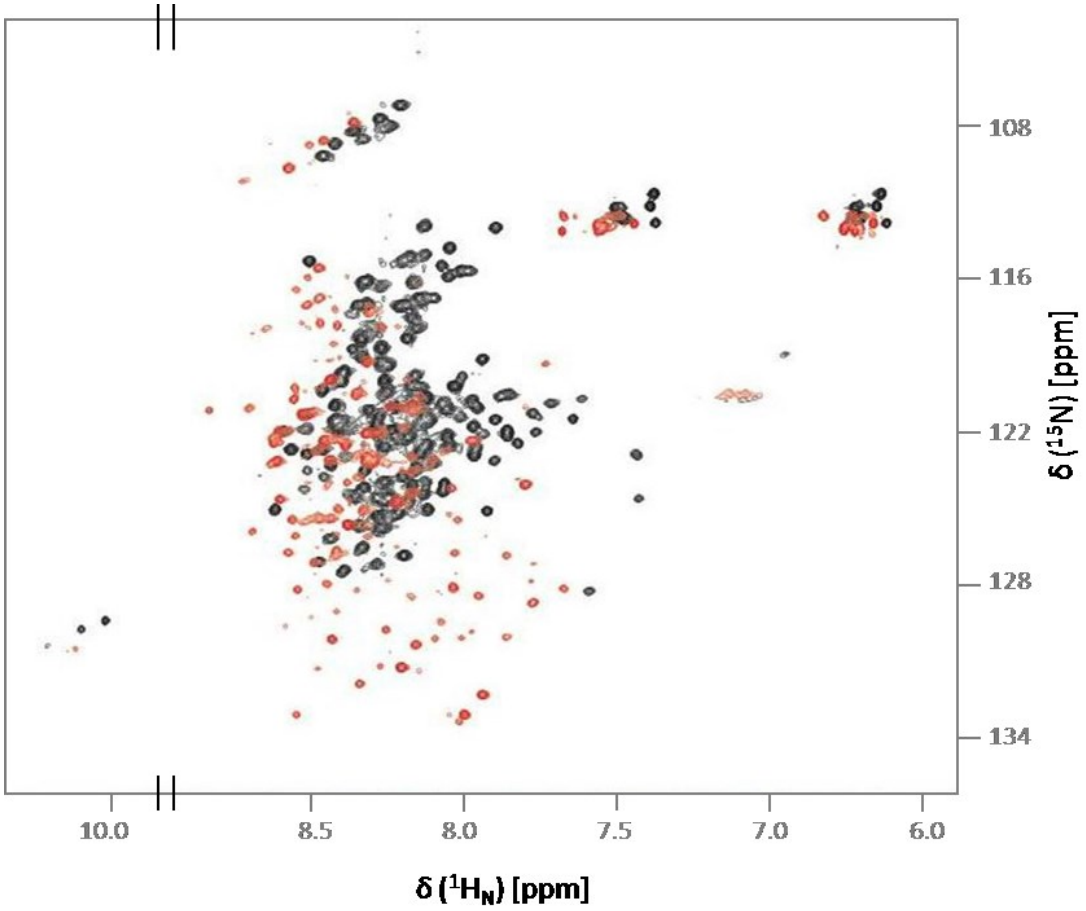

Fig. III.4.3.2 $^{1}H^{15}N$ HSQC´overlay spectrum of the $NS5A_{191–369}$ fragment from hepatitis C virus in free–state and upon Lyn SH3 adding. The black spectrum shows $NS5A_{191–369}$ in unbound form and the red spectrum shows $^{15}N–^{1}H$ correlation signals for $NS5A_{191–369}$ upon Lyn SH3 binding. Here the final titration step is shown in five times molar abundance of Lyn SH3 to $NS5A_{191–369}$.

III.5 Structural characterisation of Bin1 SH3 Myc interaction with and without NS5A fragment

In the previous chapters the interaction of mainly Bin1 SH3 with three different NS5A fragments was analysed elaborating different biophysical techniques. Furthermore, the interaction dynamics of the NS5A peptide with the SH3 domains of Fyn and Yes was described using NMR.

Myc Bin1 interaction was already investigated by Pineda–Lucena et al. (2005). To characterise the dynamics of the Bin1SH3 $Myc_{55–68}$ interaction $^{1}H^{15}N$ HSQC NMR titration experiments were done. They allow classifying binding dynamics based on the overall spectral changes observed during titration (Zuiderweg et al. 2002). Pineda–Lucena et al. 2005 determined from their NMR titration data the dissociation constant K_D for $Myc_{55–68}$ Bin1 SH3 interaction to be 4.9 µM. The dissociation

constant K_D for Bin1 SH3 $NS5A_{333–369}$, determined using SPR was about 0.1 µM (this work).This difference in binding affinity between the two peptides to Bin1 SH3 and its effect on binding dynamics was addressed with $^{1}H^{15}N$ HSQC NMR titration experiments in the following chapters.

III.5.1 Comparison of complex dynamics of Bin1 SH3: $NS5A_{347–361}$ with Bin1 SH3: $Myc_{55–6869}$

Unlabeled peptides $Myc_{55–69}$ and $NS5A_{347–361}$ were gradually titrated to a ^{15}N labeled Bin1 SH3 protein solution, separately. 100 µM of [U–^{15}N] labeled Bin1 SH3 in 50 mM KPi, 20 mM NaCl pH 6.5; 1 mM 2–mercaptoethanol was used for each peptide titration series. First the $^{1}H^{15}N$ HSQC NMR spectrum of the free Bin1 SH3 domain was recorded at 298 K. The peptides were washed first with H_2O first to get rid of TFA artifacts. After lyophillisation they were solved into 10 mM concentration in the same buffer as the SH3 domain to avoid buffer effects. Afterwards the peptides were titrated in 5 steps gradually to the free Bin1 SH3 till Bin1 SH3 peptide equimolarity was reached (see fig. III.4.1. for peptide concentrations). $^{1}H^{15}N$ HSQC spectra of each titration step were recorded using exactly the same parameters for each experiment. Spectra superposition of all titration steps shows the ligand induced changes in the SH3 domain and can deliver information about the binding dynamics. In fig. III.5.1.1(A). an overlay of all five titration steps is shown for the Bin1 SH3 $Myc_{55–69}$ interaction. We can see how upon peptide titration the chemical environment of the free state NH correlation signals from a time zero (black spectrum) change and thus the signals shift from their former positions gradually to new positions (orange spectrum). This shows the conformational change from free–state Bin1 SH3 to Bin1 SH3: $Myc_{55–68}$ bound state. The whole “shift” of the NH correlation signals depends on the peptide concentration as indicated by the colour code for each spectrum in the overlay. For most of the signals, the chemical shift change is linear indicating “fast exchange” for these residues upon peptide binding (see arrows in fig.III.5.1.1 (A)) This is due to fast dissociation of the SH3:peptide complex, typical for low affinity binding.

In figure III.5.1.1(B), the same experiment was repeated for the Bin1 SH3 $NS5A_{347–361}$ interaction. The peptide titration steps were the same, but however the overlay of all titration steps reveals a different binding dynamics for Bin1 SH3 $NS5A_{347–361}$ interaction. Titration with ligand causes disappearance of some of the free–state signals (black correlation signals) in parallel with appearance of new resonances (orange correlation signals). These new signals arise from the bound state protein conformation. This is typical for a strong interaction between protein and ligand and is referred as a “slow exchange”.

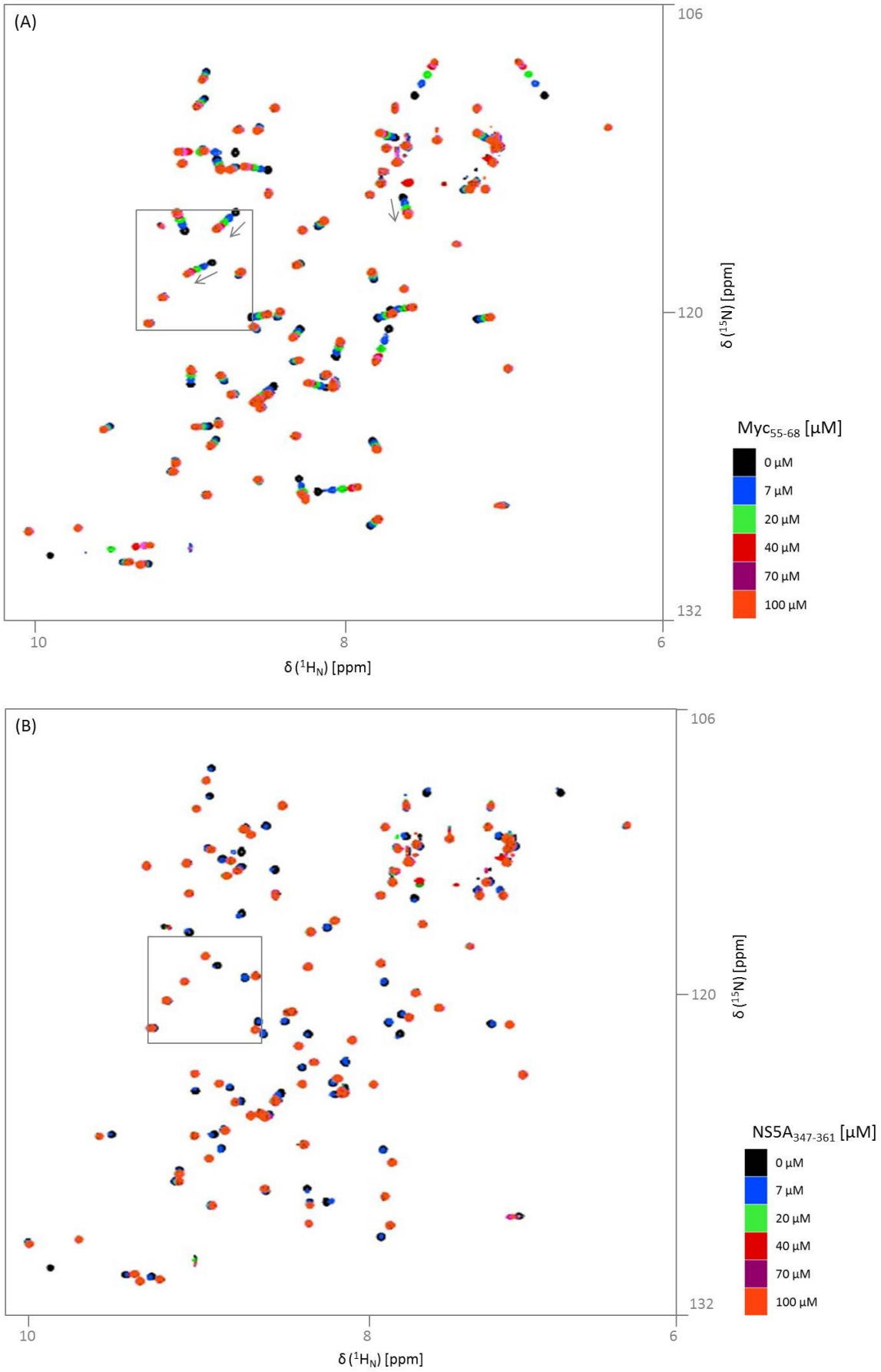

Figure description see next page.

Fig. III.5.1.1: $^{1}H^{15}N$ HSQC spectra of Bin1 SH3 during titration with $Myc_{55–69}$ (A) and $NS5A_{347–361}$ (B). Both figures (A) and (B) show an overlay of $^{1}H^{15}N$ HSQC spectra for the increasing SH3:peptide complex concentration. The black spectra (A) and (B) show the NH correlation signals for 100 µM [*U*–^{15}N]–Bin1 SH3. The peptides $Myc_{55–69}$ (A) and $NS5A_{347–361}$ (B) were gradually added to the free SH3 domain till equimolarity was reached (orange spectrum). Titration steps are shown on the right side of the spectra showing the colour code with the corresponding peptide concentration, respectively. The part in the square was selected to discuss further experiments.

The peptides $Myc_{55–69}$ and $NS5A_{347–361}$ interact with Bin1 SH3 with different binding kinetics. Comparing the final step of both peptide titrations for a selected region of the spectra reveals that the NH correlation signals for the respective residues behave differently upon Myc or NS5A binding (fig.III.5.1.2). The first window shows the free Bin1 SH3 domain spectrum (black). The next window from left displays Bin1 SH3:$Myc_{55–69}$ complex spectrum in orange, overlaid over the free Bin1 SH3 spectrum in black. The third windows from left is an overlay of Bin1 SH3 free (black), Bin1 SH3:$Myc_{55–69}$ complex (orange) and Bin1 SH3: $NS5A_{347–361}$ complex (blue) spectra. There is a clear difference for both interactions shown for the residues F587 and T537 in this selected part of the spectrum.

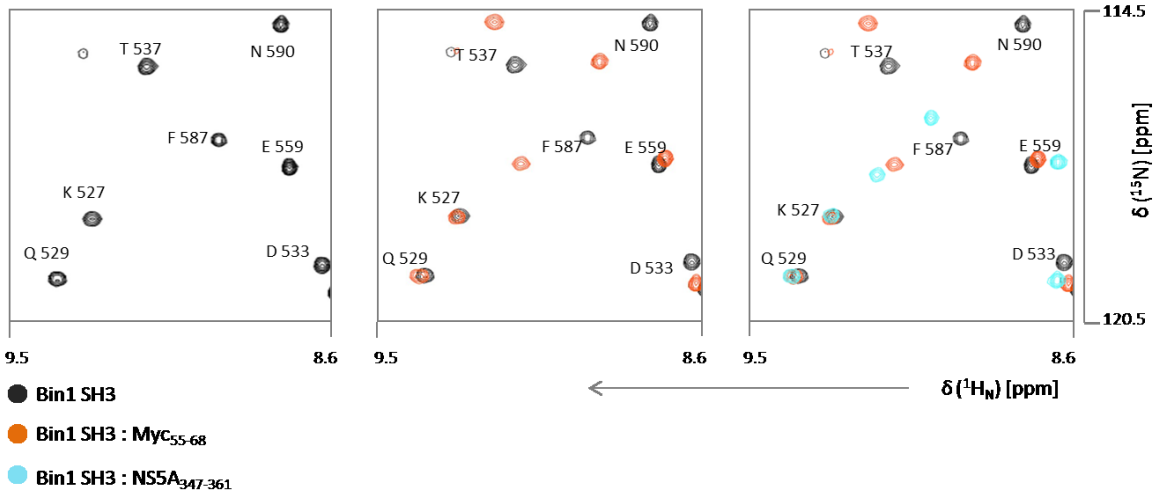

Fig. III.5.1.2 Comparison of selected region of $^{1}H^{15}N$ HSQC spectra of Bin1 $SH3_{free}$ (black), Bin1 SH3:$Myc_{55–69}$ complex (orange) and Bin1 SH3: $NS5A_{347–361}$ complex. The complex spectra show the final titration step of the respective peptide. Both peptides bind with different affinity and dynamics to the Bin1 SH3 domain hence showing two different spectra (see overlay in the last window from left).

III.5.2. Competition of $NS5A_{347–361}$ and $Myc_{55–69}$ for Bin1 SH3 binding

$NS5A_{347–361}$ and $Myc_{55–69}$ show different binding dynamics and affinity to the Bin1SH3 domain as shown in the previous chapter, indicating $NS5A_{347–361}$ binding to Bin1 SH3 is stronger. To address this question both peptides were probed in a $^{1}H^{15}N$ HSQC "competition" experiment for the Bin1 SH3 binding site. Knowing how both Bin1 SH3:peptide complex spectra look like (Fig. III.5.1.1), adding either $NS5A_{347–361}$ to Bin1 SH3:$Myc_{55–69}$ complex in equimolar concentrations or adding $Myc_{55–69}$ in the same manner to the Bin1 SH3: $NS5A_{347–361}$ complex which should give information about the competing potential of each peptide. $^{1}H^{15}N$ HSQC spectra of the two samples from the previous experiment with Bin1 SH3: $NS5A_{347–361}$ complex and Bin1 SH3:$Myc_{55–69}$ complex were recorded. In the next step the competing peptide was added in equimolar concentration to the existing complex and $^{1}H^{15}N$ HSQC spectra of this state were recorded. In figure III.5.2.1 a selected region of the spectrum for the Bin1 SH3:$Myc_{55–69}$ complex is shown (orange). The next window shows overlay spectra of the same region after adding $NS5A_{347–361}$ for completion to the complex. Significant changes are seen for the NH correlations for the residues N590, E 559 and F587. In the last window the overlay spectra of Bin1 SH3:$Myc_{55–69}$ complex, of Bin1 SH3:$Myc_{55–69}$ complex + $NS5A_{347–361}$ and of Bin1 SH3: $NS5A_{347–361}$ complex for comparison are shown. Adding $NS5A_{347–361}$ peptide to the existing Bin1 SH3:$Myc_{55–69}$ complex resulted in replacing Myc with NS5A from the SH3 binding site as the spectra of Bin1 SH3:$Myc_{55–69}$ complex + $NS5A_{347–361}$ and of Bin1 SH3: $NS5A_{347–361}$ complex align perfectly.

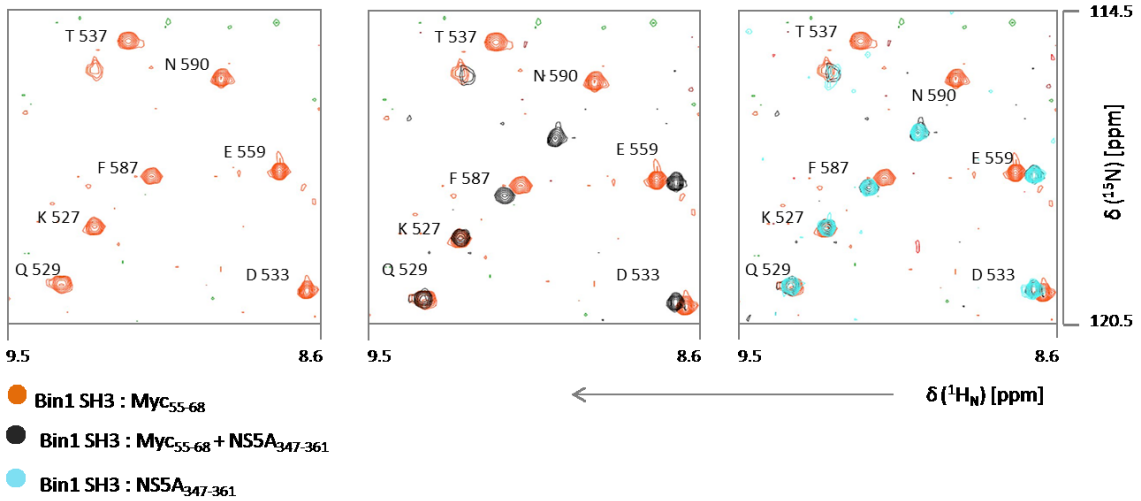

Fig. III.5.2.1 Competition experiment. Three different spectra and overlays are shown here. The first window from left shows the Bin1 SH3:$Myc_{55–69}$ complex in orange. The next window in the middle shows the overlay of the Bin1 SH3:$Myc_{55–69}$ complex (orange) and the new spectrum after adding NS5A peptide to this complex (black). The last window shows the overlay of three spectra as indicated by the colour code below left.

The same experiment was run for the opposite situation. To the Bin1 SH3: $NS5A_{347–361}$ complex (blue spectrum in fig.III.5.2.2) $Myc_{55–69}$ peptide equimolar to the complex concentration was added and $^{1}H^{15}N$ HSQC spectrum of this new state was recorded (fig.III.5.2.2) orange spectrum. The new state shows not any difference to the Bin1 SH3: $NS5A_{347–361}$ complex spectrum as seen in the second window of fig.III.5.2.2. The adding of $Myc_{55–69}$ peptide had no effect on the complex. The Bin1 SH3: $NS5A_{347–361}$ complex remains stable. As a control the Bin1 SH3:$Myc_{55–69}$ complex spectrum (black spectrum) was overlaid to the other two spectra in fig.III.5.2.2 last window. There is no congruence between the both spectra. $Myc_{55–69}$ peptide could not displace $NS5A_{347–361}$ from the Bin1 SH3 binding site. The *in vitro* experiments show that a 12–mer NS5A fragment can successfully compete with an equally big fragment of the physiological interaction partner Myc for Bin1 SH3 binding.

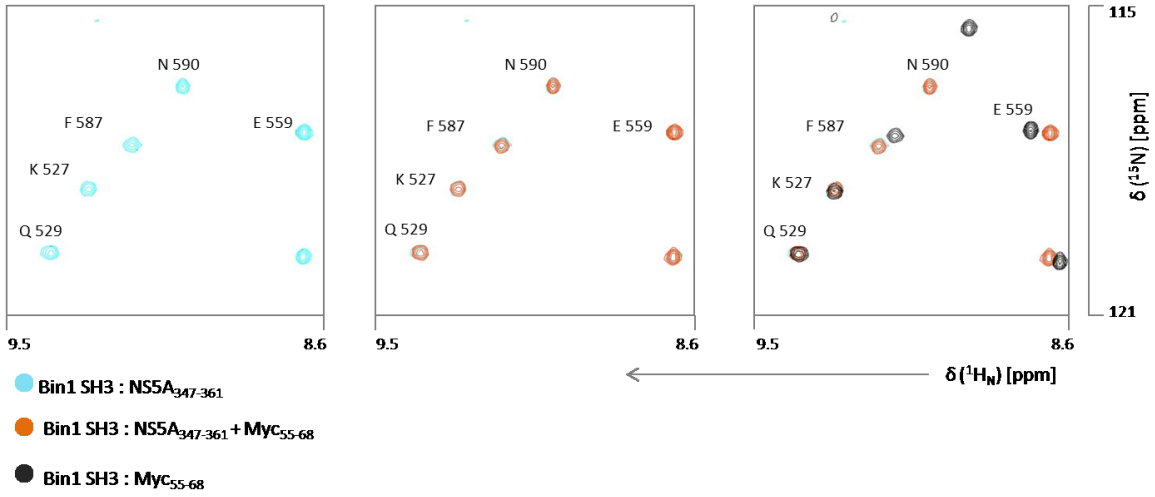

Fig.III.5.2.2 Competition experiment. Three different spectra and overlays are shown here. The first window from left shows the Bin1 SH3:$NS5A_{347–361}$ complex in blue. The next window in the middle shows the overlay of the Bin1 SH3:$NS5A_{347–361}$ complex (blue) and the new spectrum after adding Myc peptide to this complex (orange). The last window shows the overlay of three spectra as indicated by the colour code below left.

III.5.3 Chemical shift perturbation experiments and mapping of Bin1 SH3 residues involved in binding to $NS5A_{333–369}$ and $Myc_{55–69}$

The chemical shift perturbation (CSP) was performed to map protein–ligand interactions to the surface of the protein. The ligand was not labeled whereas the other interaction partner was ^{15}N labeled. The chemical shift changes of the interacting $^{1}H^{15}N$ amide correlations with increasing amounts of ligand. Upon ligand binding the chemical environment for the nuclei around the binding

interface changes, thus a “perturbance” of their chemical shifts are recorded with a set of HSQC experiments.

The HSQC data from chapter III.5.1 and the assignment data from chapter III.4.1.1 were used here to map the binding sites for $Myc_{55–69}$ and $NS5A_{333-369}$ on the molecule surface of Bin1 SH3 domain. For molecule visualization, the PDB entry for free Bin1 SH3 (PDB: 1MUZ) was used to map the interaction site. The difference in chemical shifts upon ligand binding for $^{1}H_{N}$ and ^{15}N correlations was calculated separately at first and normalized to an overall chemical shift difference using the formula described in methods (chapter II.2.8.3.1). The results for both ligands are shown in the figures III.5.3.1 and Fig. III.5.3.2. The figures include the normalized chemical shift difference Δ δ between free SH3 domain and SH3 domain after peptide binding (B) for each amino acid. Furthermore, a table (C) with the list of amino acids classified according to their apparent normalized chemical shift difference. The chemical shift differences were classified into three categories, “strong”, “middle” and “weak”. The threshold for the three “categories” was chosen arbitrarily. The amino acids in this table where then mapped on the surface of the 3D molecular surface model of free Bin1 SH3 domain following the indicated colour for the respective chemical shift difference classification.

In figure III.5.3.1 the $NS5A_{333–369}$ Bin1 SH3 interaction based on HSQC and HNCACB experiments is described. The normalized chemical shift difference Δ δ shows that peptide binding affects the residues in the RT–loop area of the SH3 domain strongest (see figure III.5.3.1(B)). Residues forming the 3_{10}helix 1, the adjacent β–sheet #3, 3_{10}helix 3 and 3_{10}helix 4 are affected moderately upon peptide binding. The residues with the strongest change of their chemical environment are 535 and 537 aspartic acid. The following residue 538 glutamic acid is also relatively strongly affected by peptide binding. These residues are all negatively charged and located in the RT–loop. The hydrophilic amino acids 557 glutamic acid, 558 glutamine and 559 aspartic acid in the first 3_{10} helix show also strong overall chemical shifts. These Residues are mapped on the molecule surface as shown in fig.III.5.3.1 (A) following the indicated colour code in table (C). The classic PxxP binding region as described by Feng et al 1994 and Yu et al. 1994 which is based on hydrophobic interaction between protein and ligand through aromatic residues of the SH3 domain and aliphatic side chains of the respective ligand, flanked by RT–loop and N–Src–loop is not the main interaction interface for $NS5A_{333–369}$ Bin1 SH3 interaction. In figure III.5.3.2 the $Myc_{55–69}$ Bin1 SH3 interaction based on HSQC–titration experiments is analysed. The SH3 domain conserved tryptophan 562 in the classic binding pocket shows the most dominant change of chemical environment upon Myc peptide binding. The other two residues which are mainly affected upon Myc binding are 578 glutamic acid and aromatic amino acid 588 phenylalanine.

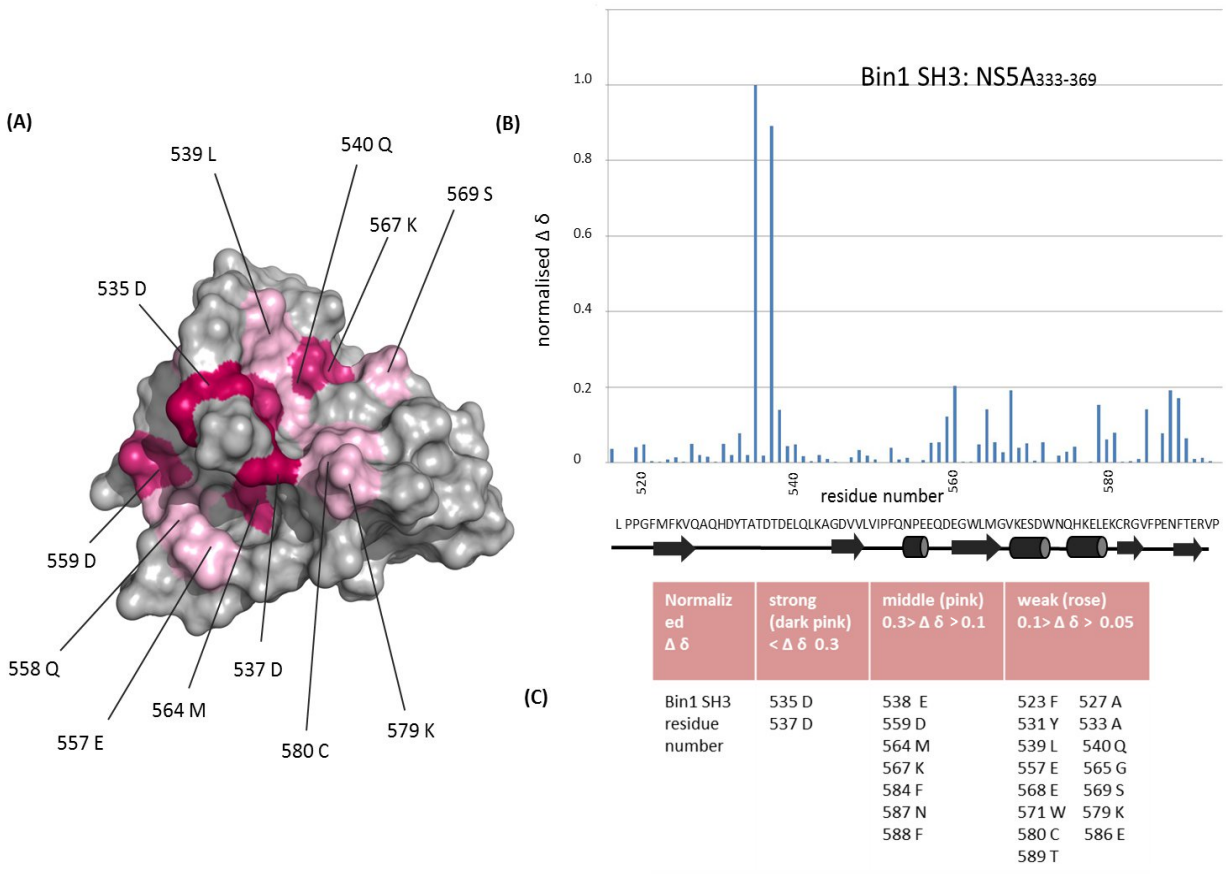

Fig. III.5.3.1 Chemical shift perturbation mapping of NS5A$_{333–369}$ interaction with Bin1 SH3. The NMR high resolution structure of the free SH3 domain (PDB: 1MUZ) was used for mapping the residues with the highest chemical shift perturbances upon ligand binding (A).The residues with the highest normalized chemical shift difference upon NS5A peptide binding were mapped. In (B) the normalised chemical shift difference upon NS5A peptide binding for all SH3 residues are shown. In C the residues with the major changes are classified in a table arbitrarily to be mapped on the molecule surface model of Bin1 SH3. The main shifts are happening in a negatively charged area of the RT–loop.

These residues are mapped on the molecular surface model of free Bin1 SH3 as shown in (C). The weaker interactions spots are also mapped and concern mainly the C–terminal β–sheets 4 and 5 and the neighborhood of the conserved tryptophan 562. Both peptides show remarkable differences upon binding to the Bin1 SH3 domain, keeping in mind that the NS5A peptide is a 37mer and Myc a 15–mer peptide.

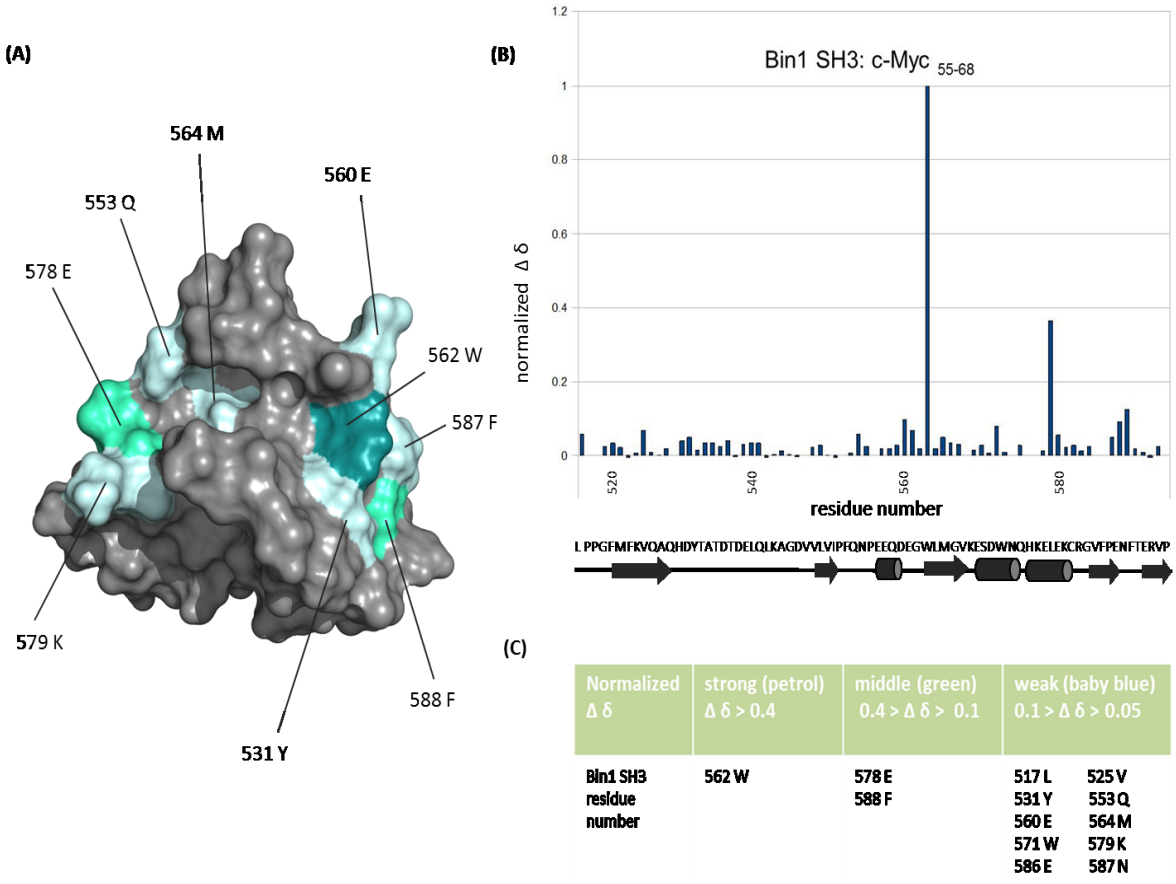

Normalized Δ δ	strong (petrol) Δ δ > 0.4	middle (green) 0.4 > Δ δ > 0.1	weak (baby blue) 0.1 > Δ δ > 0.05	
Bin1 SH3 residue number	562 W	578 E 588 F	517 L 531 Y 560 E 571 W 586 E	525 V 553 Q 564 M 579 K 587 N

Fig. III.5.3.2. Chemical shift perturbation mapping of $Myc_{55–69}$ interaction with Bin1 SH3. The NMR high resolution structure of the free SH3 domain (PDB: 1MUZ) was used for mapping the residues with the highest chemical shift perturbances upon ligand binding (A).The residues with the highest normalised chemical shift difference upon Myc peptide binding were mapped. In (B) the normalized chemical shift difference upon Myc peptide binding for all SH3 residues are shown. In C the residues with the major changes are classified in a table arbitrarily to be mapped on the molecule surface model of Bin1 SH3. The main shifts are observed for the conserved tryptophan 562 in the SH3 binding pocket and for residues c–terminal to this.

III.6 Full–length NS5A cloning into DsRed and CFP vectors for cell culture experiments

The interaction between the tumor suppressor Bin1 and the oncogene Myc in human cells and NS5A as a prospective competitor in this interaction is a highly interesting topic as it addresses NS5A's and the role of Hepatitis C virus infection in HCC formation and infected cells evading the process apoptosis. To address this interaction between the three proteins co–localisation and co–immunoprecipitation experiments in cell culture system are planned. HCV 1b geneotype (HC–J4) NS5A full–length gene was commercially bought from Lifetechnologies. The synthetic gene was incorporated into a pMK–RQ vector flanked with the restriction sites for the enzymes HindIII at 5' and BamHI 3' end of the gene. NS5A was sub cloned into the multiple cloning sites of the target

vectors for eukaryotic cells pDsRedN1 and pCFPN1 (clontech) using the two mentioned enzymes HindII and BamH1 (Fermentas). Both vectors carry the fluorescent protein tag genes C–terminally aligned to the MCS region and therefore the fluorescent–protein tag will be attached C–terminally to the target gene. This is important, because NS5A interacts N–terminally via the amphipathic helix with membranes. *E.coli Mach* 1 cells were transformed with the target vectors pDsred–N1, pCFP–N1 and the target gene NS5A in pMK–RQ vector and amplified and purified using anion–exchange columns (Macherey& Nagel, Düren) following manufacturer`s protocol. Target vectors and gene were digested with HinIII and BamH1. The DNA of interest in both cases was purified by gel electrophoresis and a follow up gel extraction step before ligation of NS5A into the pDsREd–N1 and pCFP–N1 vectors. *E.coli Mach 1* cells were transformed with the Ligation and clones were picked and the DNA was sent away for sequencing (Seqlab, Göttingen) to confirm the success of cloning. Full length 1b NS5A was successfully cloned into the pDsRed–N1 and pCFP–N1 vectors. These vectors can be used for transfecting Huh– 7 cells which is a hepatocyte derived cellular carcinoma cell line and subjected to the above mentioned experiments.

IV Discussion

In this work the interaction of HCV NS5A protein fragments with diverse SH3 domains, especially with that of Bin1 was characterised using different biophysical methods. In order to find suitable candidates for a NS5A:SH3 NMR complex structure, binding dynamics of Bin1 SH3 to NS5A peptides was compared to other SH3 domains using HSQC titration. Binding affinity of Bin1 SH3 NS5A fragment interactions were investigated using surface plasmon resonance spectroscopy. The binding affinity of NS5A fragments towards the Fyn and Yes SH3 domains were obtained using SPR for Fyn SH3 and fluorescence spectroscopy for the Yes SH3 interaction. The 3D solution NMR complex structure of Bin1 SH3: $NS5A_{333–369}$ was started, but could not be finished due to problems during $NS5A_{333–369}$ resonance assignment. The information gained through SH3 backbone assignment in the complex was used to map the binding region of $NS5A_{333–369}$ on the free SH3 molecule surface. The same was done for $Myc_{55–69}$, a peptide from Myc an oncogene which is controlled by Bin1 using HSQC titration results. The competition potential between NS5A and Myc for the SH3 binding was probed in vitro using $^{1}H^{15}N$–HSQC experiments.

IV.1 NS5A–fragments and SH3 domains were expressed, purified and isotopically labeled in mg yields

Human Bin1– and Yes SH3 domains were cloned into a recombinant expression vector for E. coli for further studies. Furthermore a NS5A fragment with 178 amino acids, comprising domain 2, the SH3 binding motif PxxP within the C–terminal LCS region and the flanking N–terminal LCS region as well, was sub cloned into a recombinant expression vector for E. coli expression (chapter III.1.4). Additionally for control experiments a NS5A fragment (191–340) lacking the C–terminal PxxP motif was sub–cloned into the same vector. Cloning success for pGEX–6P–2–Bin1–SH3, pGex–6P–2–Yes–SH3; pGEX–6P–2–$NS5A_{191–369}$, pGEX–6p–$NS5A_{191–340}$, pDsRed–NS5A–1b and pCFP–NS5A–1b was verified by DNA sequencing (chapters III.1.1; III.1.4 and III.4.3).

Bin1 SH3 and Yes SH3 purification was performed following the standard SH3 domain expression and purification protocols for GST–tagged proteins (Schmidt et al. 2007).The cleavage of the GST tag followed the protocol in chapter II.2.3.6.2**.** The Bin1 SH3 domain required further adding of reducting

agent 2 mM DTT or the 2–mercaptoethanol equivalent to avoid protein aggregation. Both protein expressions yielded in mg pure protein. For biophysical experiments which required no labeling both SH3 domains were expressed in LB medium. For NMR $^{1}H^{15}N$ HSQC experiments GST– SH3 was expressed as [*U*–^{15}N] enriched SH3. Bin1 SH3 domain was also expressed in mg yield as [*U*–^{13}C/*U*–^{15}N] enriched Bin SH3 (chapter III.1.2). Both SH3 domains could be concentrated up to 2 mM using ultracentrifugation tubes without precipitation of protein, important for Surface Plasmon Resonance (SPR) experiments where a SH3 excess in mM range was used.

$NS5A_{333–369}$ was expressed as a His_{10}–ubiquitin–construct either in LB or as [*U*–^{15}N] enriched or [*U*–^{13}C/*U*–^{15}N]–enriched $NS5A_{333–369}$ protein in E. *coli* system depending of experimental requirements. The His_{10}–ubiquitin system used in this work is specially designed for the expression of isotope labeled peptides in E. *coli* (Kohno et al. 1998). The initial conditions for expression and purification were done by T. Tran but the final steps and optimization of expression and purification protocol is part of this work. The 37–mer NS5A peptide was purified under native conditions using a Ni–NTA column. Elution of the fusion protein was done with step wise increasing concentrations of imidazole. The eluted His–ubiquitin fusion–peptide was digested with YUH–hydrolase without creating overhang residues. Finally cleavage products and the hydrolase were separated from each other using reversed phase chromatography. Peptide fractions were lyophilized and stored at 4 °C (chapter III.1.3).

A GST–fusion system was chosen to express $NS5A_{191–369.}$ This is a different strategy from Liang et al. 2007, which used a His–ubiquitin–fusion system to express $NS5A_{240–335}$, a fragment strictly spanning only domain 2 of NS5A. $NS5A_{191–369}$ was expressed in E. *coli* in LB medium for SPR experiments which did not require labeling. For NMR experiments the protein was expressed as [*U*–^{15}N]–$NS5A_{191–369}$ and as [*U*–^{13}C/*U*–^{15}N]–$NS5A_{191–369}$. The protocol for purification was established and optimised in this work, showing that the alternative expression system in a GST context also works fine for NS5A expression in E. *coli*. All buffers contained 2 mM DTT due to two cysteines in the NS5A fragment. Purification of NS5A fragment employed affinity chromatography which was followed by on–column cleavage of the GST tag over–night with HRV–3A protease. The resulting NS5A fraction needed further purification steps due to higher and lower molecular impurities. These impurities could be cleared by employing anion exchange chromatography immediately after dialysis of the sample against the respective buffer. The resulting protein included Gly and Pro as the HRV–3A protease cleavage site and an additional linker region consisting of seven amino acids (Leu, Gly, Ser, Leu, Arg, Gly, Gly) N–terminally to the $NS5A_{191–369}$ fragment. The protein could be concentrated up to 200 µM without precipitation using ultracentifugation tubes and was stable for months when stored at -80° C. This concentration is suitable for 2D and 3D NMR experiments.

IV.1.1 NS5A$_{333–369}$ reveals characteristics for PPII helices

The formation of left handed polyproline helices (PPII) is important for structural integrity and protein protein interactions. PxxP motives in protein sequences are known to adopt this structure as described in Manning et al. 1991 and Kelly et al. 2001 and thus play an important role as structural recognition determinants. Typically polyproline helices show a minimum at 200 nm and a maximum at 228 nm. The far–UV–CD spectrum of NS5A$_{333–369}$ shows a minimum at 199 nm (figure III.3.1.). Comparing this with the spectra describing PPII helices we can clearly state that NS5A$_{333–369}$ shows in free–state already certain characteristics of PPII helices with the minimum at 199 nm. Compared to the model peptides which were analysed in the literature (Kelly et al. 2001) NS5A$_{333–369}$ is a 37 residue peptide and consists also of residues such as asparagine, valine and isoleucine which are in disfavour of PPII helix formation. In contrast to that it has only one alanine reside which shows a high propensity for PPII helix formation. It can be concluded that there are secondary structure elements which resemble a PPII helix, but certainly other elements such as random coil or even β–sheet elements which do account for the CD spectrum of NS5A$_{333–369.}$

IV.2. Probing physiological interaction partners of NS5A suitable for NMR complex structure determination

The hepatitis C virus protein NS5A is a 448 residue phosphoprotein that interacts with a vast number of cellular proteins with multiple effects on cell physiology (Macdonald and Harris 2004). NS5A is organised in three domains. The structure of domain one is determined (Tellinghuisen et al. 2005). During the starting period of this work there was no information on the structural nature of the domains 2 and 3. In the course of this work NS5A$_{191–369}$ fragment was shown as intrinsically disordered (chapter III.4.4). Liang et al. 2007 have reported for domain 2 intrinsically disordered protein character and Hanoulle et al. 2010 showed the same for domain 3 of NS5A, independently. Domains 1 and 2 as well as domains 2 and 3 are linked through a linker described as low complexity sequence (LCS). The LCS region between domain 2 and 3 contains three consensus PxxP motifs. Macdonald et al. investigated in 2004 the interaction of these PxxP motifs with the SH3 domains of Fyn, Lyn, Hck and Lck by pull–down experiments using the respective the SH3s in a GST context and eukaryotic cell lysates as NS5A source. These findings neither give any significant information about

the quality of the NS5A interaction with the respective SH3 domains nor quantitative information about the respective binding affinity. Knowing the binding characteristics and atomic resolution of the binding interface may help to understand NS5A promiscuity and the selection mechanism towards the different SH3 domains which all play important roles in the human cell is the main motivation of this work.

NS5A fragment	Sequence
$NS5A_{333–369}$	DYVPPVVHGSPLPPTKAPPIPPPRRKRTVVLTESTV
$NS5A_{347–361}$	TKAPPIPPPRRKRTV

Table.IV.2.1. NS5A fragments used in the interaction studies. The $NS5A_{333–369}$ comprises three PxxP motifs, displayed in grey. The first motif is referred as PP2.1 and is not conserved and not important for SH3 interaction for most of the cases (Macdonald et al. 2004), whereas the second motif is referred as PP2.2 and is conserved over the HCV genotypes. The bold positive residue stands for the anchor rest in a class I PxxP motif (fig I.1.2).

IV.2.1.$NS5A_{333–369}$ shows different affinity to selected SH3 domains of various Src type kinases

In this work the interaction of selected Src family SH3 domains (MacDonald et al. 2004 and Nanda et.al. 2006) with two short NS5A fragments (tab IV.2.1), comprising the core binding region as displayed by a synthetic 15–mer peptide $NS5A_{347–361}$ and the recombinant fragment $NS5A_{333–369}$ consisting of the conserved PxxP motif (red letters) as well of the less conserved motif depicted in tab.IV.2.1. in green, was investigated with SPR and fluorescence spectroscopy in order to find suitable candidates to describe the complex structure of NS5A peptide with SH3 domains using NMR. Only high affinity binding partners meet the needs of a stable complex to determine structural information.

For the Yes SH3 domain the interaction with $NS5A_{347–361}$ was studied by fluorescence titration, measuring the change of the intrinsic tryptophan fluorescence of Yes SH3, due to alterations around the conserved tryptophan of the Yes SH3 binding pocket upon $NS5A_{347–361}$ binding. The measured K_D value is 23 µM. Lyn SH3 $NS5A_{333–369}$ interaction was quantified with SPR. The resulting dissociation

constant derived from the steady state data of each binding was K_D= 5 µM. Just by looking at the affinity, Lyn SH3 seems to be a promising candidate for further NMR experiments, aiming for a complex structure, but unfortunately Lyn SH3 domain binds to both PxxP motifs on $NS5A_{333–369}$ (MacDonald et al. 2004). Therefore it would be a difficult candidate for a NMR complex structure as two independent populations binding NS5A peptide might exist. The K_D values for the other Src family SH3 domains Hck and Lck are 6.8 µM for Hck and 16 µM for Lck using SPR (Aladag diploma thesis, data not shown). In the context of Src family kinases the SH3 domain of Yes interaction shows the lowest affinity to the respective NS5A fragment compared to the other SH3 domains (III.2.4).

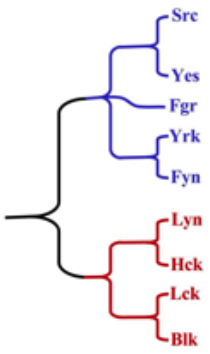

Fig. IV.2.1.2 Phylogenic scheme of the Src family kinases. Based on differences the family can be seperated into two groups. Depicted here in blue and red. The blue group consists of Fyn,Yrk, Fgr, Yes and Src. The red family members are Blk, Lck, Hck and Lyn. (http://www.hxms.neu.edu/research/chime/Fig1.JPG)

In figure IV.2.1.2. the phylogenic family relations of the kinases are depicted. Lyn shows together with Hck the strongest affinity towards $NS5A_{333–369}$, followed by Lck and Yes. This finding is consistent with the phylogenic relation of the investigated kinases. Lyn SH3 is the sole Src family kinase which has been shown by others to bind both PxxP motifs, PP2.1 and PP2.2 as shown in Tab.IV.2.1.1. Mutations of the PxxP motifs and GST– pulldown assays confirmed this (MacDonald et al. 2004). It may be a reason why Lyn shows strongest affinity towards the investigated NS5A fragment. However, HCV infection takes place mainly in the liver and manifests itself in hepatoma cells. Therefore interaction of NS5A with Lck and Hck, which are mainly expressed in T–lymphocytes and lymphatic cells, can be neglected. Lyn, Fyn and Yes out of the Src family kinases are rather physiologically relevant.

IV.2.2 NS5A $_{333–369}$ interaction with Bin1 SH3 yields in an unexpected high affinity

Bin1 is not member of the Src type kinase family and its SH3 domain shows slight differences in its 3D structure compared to the highly conserved structure of Src type SH3s. It has extended n–Src–loop

and distal loop regions compared to Src family kinase SH3 domains. Notably, Bin1 was identified three times as NS5A interaction partner. Zech et al. 2003, Masumi et al. 2005 and Nanda et al. 2006, discovered independently from each other using two different methods that NS5A interacts with the recently as tumor suppressor described Bin1 via its SH3 domain. No quantitative data regarding the affinity of NS5A to Bin1 has been reported, so far. In this work the NS5A Bin1 SH3 domain interaction was quantified using SPR experiments. Here the $NS5A_{333–369}$ fragment was used in the SPR experiments (see Tab.IV.2.1.1). The $NS5A_{333–369}$ peptide shows, with a K_D of 0.1 µM, an extreme high affinity the Bin1 SH3 domain. The also measured K_D = 0.15 µM for the $NS5A_{347–361}$ 15–mer peptide with NS5A is within the same range as for the 37–mer peptide (data not shown, because measurement was run only once)

SH3 domains are involved in many signal transduction pathways in the cell and must interact with many partners in respect to the cellular needs and environment. Their interactions with their cellular targets are transient and thus the affinities are usually in the mM to µM range. Viral proteins compete successfully with the physiologic SH3 binding partner often simply because of a higher affinity to the SH3 domain of interest. The viral protein Tip (herpes virus) shows a high affinity to the SH3 domain of Lyn in low µM range (Schweimer et al. 2002). Several truncations of the Tip protein showed that tertiary contacts outside the PxxP core binding motif are important for high affinity binding. The HIV–1 protein Nef shows also a remarkable affinity to the SH3 domain of human Hck. The interaction of Hck SH3 domain with Nef has been quantified as K_D = 0.25 µM (Lee et al. 1995). The affinity of a Nef derived PxxP motif comprising 12–mer peptide to Hck was 91 µM, suggesting that other molecular contacts outside the PxxP region are required for Nef Hck interaction. For example contacts of Nef in the RT–loop region of the Hck SH3 domain are important for specificity of binding. A 12–mer peptide does not span the RT–loop region (Saksela et al. 1995). Shelton et al (2008) showed that the NS5A (Δ250 truncated N–terminally) Fyn SH3 interaction is among the strongest viral protein SH3 domains interactions with a K_D = 0.6 µM. All these groups have shown that additional tertiary contacts outside the core binding motif with the virus are crucial for high affinity binding. Remarkably, in this work just a 37–mer peptide ($NS5A_{333–369}$) derived from NS5A, displays high affinity to Bin1 SH3. The result is in sub micro molar range and is comparable to the data for full –length Nef to Hck SH3 and NS5A to Fyn SH3, suggesting that the selected 37–mer region contains enough determinants crucial for Bin1 binding. Preliminary data with the 15 aa containing $NS5A_{347.361}$peptide, suggests that this short peptide contains determinants that are needed to yield a K_D of around 0.1 µM binding (data not shown). This finding is indeed exceptional but not impossible. This is consistent with the data shown by Schmidt et al. 2007. A similar high affinity binding was shown previously for an artificial 12–mer peptide, derived from phage display selection for Hck SH3.

This notable aspect of NS5A Bin1 SH3 interaction is very interesting for structural characterisation of the binding interface between the two proteins.

IV.2.3 The interactions of NS5A $_{333–369}$ with the SH3 domains of Bin1, Fyn and Yes show diverse binding dynamics

The binding of $NS5A_{333–369}$ peptide to the SH3 domains of Bin1 and Yes was already quantified with SPR and fluorescence spectroscopy, demonstrating Bin1 to be high affinity binding partner and Yes to be a rather moderate binding partner. Here the binding dynamics and kinetics of the binding of Bin1, Fyn and Yes SH3 domains with the NS5A derived 37–mer peptide will be discussed and classified using NMR. $^{1}H^{15}N$–HSQC titration experiments were run with the (*U*–^{15}N) labeled SH3 domains and unlabeled $NS5A_{333–369}$ peptide. These experiments monitor ligand induced change of chemical environment of the SH3 domain with increasing ligand concentrations. The change of the chemical environment depends on the kinetics of an interaction, giving a reliable hint for the stability of a complex (Zuiderweg et al. 2002).

IV.2.3.1 NS5A $_{333–369}$ interaction with Fyn SH3 follows fast exchange kinetics

Notably, although a very tight binding between FynSH3 and NS5A (Δ250) was described by Shelton at al. the NMR titration experiments of this work performed with the 37–mer peptide derived from NS5A (Tab.IV.2.1.) showed for Fyn SH3 $NS5A_{333–369}$ HSQC titration experiments fast exchange kinetics, indicating a fast dissociation of the SH3:–peptide complex (chapter III.4.2; fig.III.4.2.1 **)**. During the titration process only one set of signals could be observed, which are the weighted chemical shift averages of the free and bound state. The nuclei immediate to the binding interface move continuously during titration. This is usually the case for low affinity interaction. The trajectories of the shifting resonances are following the same rate and the direction is similar (Hall et al. 2001). However, the high affinity SPR data from Shelton et al. 2008 were measured using a NS5A protein which comprised the domains 2 and 3. The combination of the here presented data and Shelton`s

data suggest that Fyn needs more contact sites inside NS5A than the 37–mer that includes the canonical PxxP motif can deliver. Protein complexes displaying fast exchange kinetics are not very desirable for 3D solution NMR structure experiments, which eliminates Fyn SH3 from the list of candidates.

IV.2.3.2 NS5A $_{333–369}$ interaction with Yes SH3 follows intermediate and fast exchange kinetics

As can be seen in figure III.4.2.3, HSQC titration experiments with Yes SH3 and the NS5A$_{347–361,}$ containing the core PxxP binding site (tab.IV.2.1.1) show all characteristics of fast–exchange kinetics. The resonances shift in a linear manner. No line broadening effects can be seen. This kind of kinetics is typical for low affinity complexes. This is consistent with the fluorescence titration derived K_D= 23 µM for Yes SH3 with NS5A$_{347–361}$. Whereas the same HSQC experiments with the 37–mer NS5A$_{333–369}$ peptide, induce changes in the spectrum which are characteristic for fast exchange and intermediate exchange kinetics. Some resonances show a linear shift upon peptide titration, typical for fast exchange and fast dissociation of complex and other resonances disappear during the measuring regime due to line broadening, typical for intermediate exchange (fig.III.4.2.2.)(McAlister et al. 1996). The HSQC titration with the longer NS5A$_{333–369}$ fragment, displaying intermediate exchange for some residues, hints that for the Yes SH3 NS5A interaction, more than the canonical PxxPxR residue contacts, lead to a stabilization of SH3:NS5A complex. It is clear that the role of molecular contacts outside the core PxxP binding region seem to be important for Yes NS5A interaction. None the less also the Yes SH3 domain shows rather unfavourable binding dynamics for further 3D solution NMR structure experiments to elucidate the complex structure.

IV.2.3.3 NS5A $_{333–369}$ interaction with Bin1 SH3 follows slow exchange kinetics and qualifies Bin1 for determining the Bin1 SH3: NS5A $_{333–369}$ complex solution NMR structure

The Bin1 SH3 interaction with NS5A$_{333–369}$ peptide is quantified measuring the dissociation constant K_D with 0.1 µM. As a thumb rule in NMR titration experiments slow exchange interactions usually show

K_D < 10 µM. As expected, the Bin1 SH3 $NS5A_{333–369}$ HSQC titration overlay spectra show slow and fast exchange kinetics for the resonances (chapter III.4.2; fig.III.4.2.4 **).** In slow exchange the dissociation is slow and one will observe resonances for free and bound state. During the titration process the free–state resonances disappear and only the bound state signals are visible. The shifts are not linear and the new locations of the resonances cannot be assigned clearly (Zuiderweg 2002). Slow exchange kinetics is typical for high affinity binding and the protein: ligand complex are considered as stable and suitable for further structural NMR studies.

IV.3 Triple resonance NMR experiments with Bin1 SH3:$NS5A_{333–369}$ complex, reveal more than one SH3: peptide complex species

As both interaction partners are relatively small molecules with Bin1 SH3 being 8 kDa and the $NS5A_{333–369}$ peptide being 4 kDa, and display a nice signal dispersion in $^{1}H^{15}N$–HSQC spectra, both proteins were directly [*U*–^{13}C/*U*–^{15}N] labeled and NMR experiments recorded. Different triple resonance NMR experiments were employed for obtaining assignment and restraints for the determination of the Bin1 SH3: $NS5A_{333–369}$ complex structure. Backbone assignment of the complex showed no problem in identifying the residues and was successful. The assignment was completed to 72% with assigning 79 residues from picked 91 ^{15}N–^{1}H correlation signals with twelve signals from $NS5A_{333–369}$ missing respectively (chapter III.4.1.1). However, assigning the side chains for the $NS5A_{333–369}$ showed more than one correlation signals for several residues in the respective spectra, indicating the existence of more than one Bin1 SH3:$NS5A_{333–369}$ population in the sample. Fig.VI.3.1 shows such an example of double set of signals for several residues for the NS5A peptide, depicted in the blue and red spectra for aromatic residues. Looking at the experiments in a time line showed also a change of the correlation signals for the NS5A peptide over time. This could not been observed by $^{1}H^{15}N$ HSQC experiments which were recorded throughout the time to monitor possible protein degradation. Unfortunately, the heterogeneity of the Bin1 SH3:$NS5A_{333–369}$ NMR sample disabled the proceedings towards a structure calculation as planned within the PhD period of this work. The problems raised throughout the NMR assignment procedure are evidence for the complexity of the HCV NS5A interaction with Bin 1 SH3. One aspect of the complex interaction will be addressed in VI.6.

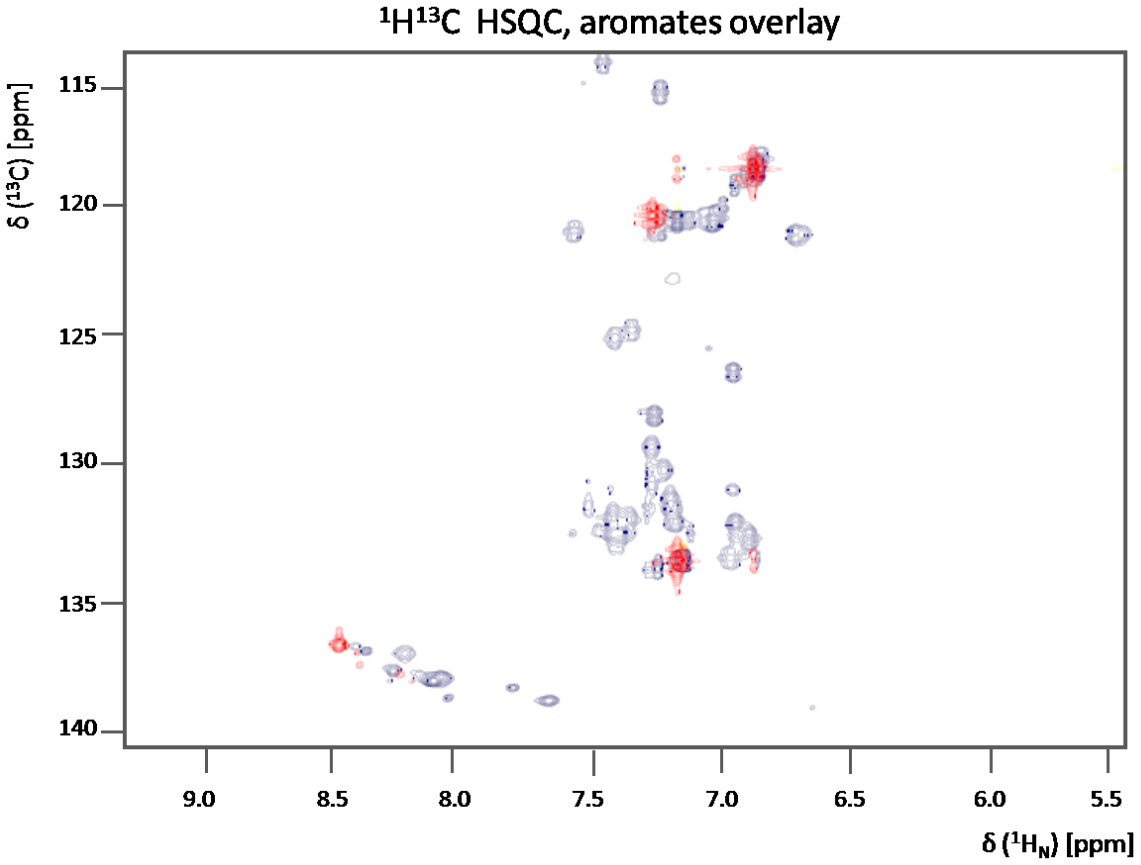

Fig. VI.3.1. Overlay of $^{1}H^{13}C$ HSQC spectrum, aromatic residues of NS5A333–369. The blue spectrum shows [*U*–^{13}C/*U*–^{15}N] Bin1 SH3 in complex with [*U*–^{13}C/*U*–^{15}N] NS5A333–369. The red spectrum shows the complex with only the NS5A333–369 peptide [*U*–^{13}C/*U*–^{15}N] enriched. (Red spectra recorded and analysed by M. Schwarten, former member of our laboratory.)

IV.4 NS5A $_{347–361}$ competes successfully with Myc $_{55–69}$ peptide for Bin1 SH3 binding

Bin 1 Myc interaction was first described by Sakamuro et al. 1996 and investigated Bin1 role as a possible tumor suppressor in the Myc interaction. They designated a rather C–terminal domain as the Myc–binding domain (fig.I.2.1) (MBD) as the major interaction interface for Myc and Bin1. Pineda–Lucena showed that deletion of the MBD region did not abolish Bin1 binding in a yeast two hybrid system, which is suitable to assay transcriptionally active baits. These results strongly suggested another interaction region in Bin1 protein which was identified as the SH3 in the same manuscript

(Pineda–Lucena et *al.* 2005). They were also able to characterise the Bin1 SH3 interaction with a Myc derived polyproline rich peptide (tab.IV.4.1.) by NMR.

Here $^{1}H^{15}N$ HSQC titration experiments as discussed in the chapter IV.3 earlier were recorded to investigate the Bin SH3 interaction with the synthetic $Myc_{55–69}$ and $NS5A_{347–361}$ peptide (chapter III.4). The 15–mer NS5A fragment with only PP2.2 was chosen in this experiment to guarantee same conditions for Myc and NS5A peptide for the interaction with Bin1 SH3.

Tab.IV.4.1. Peptide sequences of NS5A and Myc used in the NMR experiments and their respective dissociation constants K_D (Myc: Pineda–Lucena et al. 2005).

$Myc_{55–61}$	LLPTPPLSPSRRSGL	K_D =4.9 µM
$NS5A_{347–361}$	TKAPPIPPPRRKRTV	K_D = 0.1 µM

Both peptides were titrated in two separate NMR experiments with the same set up to the [U^{15}N] labeled Bin1 SH3 domain. Both ligands induced a shift of Bin1 SH3 resonances (Fig. III.5.1). As expected, the short NS5A 15–mer peptide shows all signs of a slow exchange for the interaction with Bin1, indicating a high affinity binding which fits well with our SPR finding. The complex is dissociating slow and is thus considered to be stable. In comparison the Myc 15 induced spectral changes of the Bin1 SH3 resonances display fast exchange kinetics. The shifts are linear and the trajectories are following the same rate, characteristic for low affinity binding. The data fits the K_D value which is derived from fluorescence titration experiments for Myc–peptide by Pineda–Lucena (2005). The two spectra, induced by the perturbation through the two peptides $NS5A_{347–361}$ and $Myc_{55–69}$ show different binding dynamics and differ from each other in last titration experiment (fig.III.5.2.). $NS5A_{347–369}$ interactions mostly occur with the negatively charged asparagines D535 and D537 of the Bin1 SH3 in the peptide binding pocket, which are unique for the Bin1 SH3 compared to other SH3 domains.

The question which arises from these experiments is: Can NS5A compete with Myc, the physiological binding partner of Bin, for the Bin1 SH3 binding region since it shows a higher affinity to the SH3? A simple HSQC spectrum after adding equimolar amount of $NS5A_{347–361}$ peptide to the existing Bin1 SH3:$Myc_{55–69}$ complex was recorded and confirmed the hypothesis. $NS5A_{347–361}$ induced a shift of the Bin1 SH3:$Myc_{55–69}$ complex resonances and towards the position of resonances of a typical Bin1SH3:$NS5A_{347–369}$ complex (fig.III.5.3.**)**. NS5A peptide was able to displace Myc peptide from SH3 binding interface, demonstrated by destroying of the SH3:Myc complex resonances and forming of

new resonances in the HSQC spectrum. The respective control experiment for the reverse situation was performed as well. Myc peptide was added to the existing Bin1 SH3:$NS5A_{347–361}$ complex and an HSQC spectrum was recorded. The adding of Myc peptide did not induce any shifts of the complex resonances indicating that Myc peptide is not capable to displace NS5A peptide from SH3 binding interface.

It could be shown *in vitro* that a 15–mer $NS5A_{347–361}$ peptide can successfully compete for the Bin1 SH3 binding with a 15–mer $Myc_{55–69}$ peptide. To investigate the physiological relevance of the in vitro results, further studies in mammalian cells with the respective full–length proteins are necessary to confirm this. Initial experiments for co–immunoprecipitation of Myc with endogenous Bin1 with and without the presence of NS5A (1a) were carried out in NS5A (1a) transfected Huh 7 cells to gain further molecular insights of into the interactions of these three players within the human cell system. However, the results suggested that the used Myc anti–bodies were not suitable for co–immunoprecipitation experiments. Given the fact that Myc is an oncogene, Myc protein levels in the cell are controlled strictly and thus Myc has a very short half–life and is prone to fast degradation during experimental procedure, adding up to the difficulties of the system (data not shown, this work).

Experiments in order to show co–localisation of NS5A with Bin1 and Myc in Huh–7 cells were performed (data not shown, this work), but the first results did not show any co–localisation of Bin1 with Myc due to secondary antibody problems. These experiments are stuck in the progress of optimization and were not further pursued in this work. To overcome the multiple difficulties which were all linked to lack of suitable antibodies for the Myc–Bin1–NS5A interaction circle, full–length NS5A 1b (HC–J4) protein in context of the fluorescent–proteins DsRed– and CFP– tag in mammalian vectors (Clontech) was successfully cloned in this work.

IV.5 $NS5A_{191–369}$ displays characteristics of intrinsically disordered proteins

The $NS5A_{191–369}$ fragment of the hepatitis C virus was expressed and purified as [*U*–^{15}N] $NS5A_{191–369}$. The protein is a 178 residue fragment, spanning domain 2, the flanking LCS regions plus C–terminal parts of domain 1 as well N–terminal parts of D3 of NS5A 1b (HC–J4) protein (Fig.I.2). This fragment included also the two class II PxxP motifs PP2.1 and PP2.2 (Fig.I.2), canonical binding motifs for SH3 domains. The selected fragment showed in the recorded ^{15}N HSQC spectrum well defined ^{1}H ^{15}N correlations, but not well dispersed. The correlations were rather concentrated to a narrow window of the spectrum which is typically observed for intrinsically unfolded/disordered proteins

(Fig.III.4.7.1). Independent from this work Liang et al. reported for a smaller fragment comprising only domain 2 the characteristics of intrinsically unfolded proteins (Liang et al. 2007), confirming this results. Recently domain 3 is also reported to be intrinsically disordered (Hanoulle et al. 2010). Intrinsically disordered proteins (IDPs) are characterised by a high degree of structural flexibility. The number of proteins reported as IDPs is lately increasing very much so for proteins which are involved in regulatory processes. NS5A is involved in viral replication and virus particle assembly as well as in various virus host interactions which require molecular recognition and interaction. NS5A benefits from its structural disorder of the domains 2 and 3. This way NS5A would be able to meet its various functions either directly from the disordered state or from local ordering upon molecular recognition (Dyson and Wright 2002). Ligand induced transition or local folding is well reviewed and described. NS5A is reported to bind to a set of Src family SH3 domains (MacDonald et al. 2004). To investigate the effect of ligand binding to the $NS5A_{191–369}$ fragment Lyn SH3 domain was added to the $NS5A_{191–369}$ sample (III.4.7.2). Lyn SH3 clearly induced conformational changes in the disordered protein backing the hypothesis molecular recognition leads to local folding. Assigning and characterising the structure of relatively large disordered proteins by NMR require special pulse sequences meeting the problem of extensive signal overlap. Hence further experiments addressing $NS5A_{191–369}$ were carried out in cooperation with the Brutscher laboratory, Institut de Biologie Structurale, Centre National de Recherche Scientifique in Grenoble who work in the development of special NMR techniques (Rasia et al. 2011 and Feuerstein et al. 2012). Most of the NMR experiments regarding the structural propensity of the $NS5A_{191–369}$ fragment were investigated by S. Feuerstein and Bernhard Brutscher.

To meet the difficulties given by high conformational dynamics special NMR experiments such as iHADamard–encoded AMino–ACid–typeediting (iHADAMAC) pulse sequences were employed to discriminate amino acid types. With this strategy $NS5A_{191–369}$ has been successfully assigned (Feuerstein et al. 2011). To describe the conformational dynamics, ^{15}N relaxation experiments were performed. Long distance information was gained through PRE experiments. The data suggests that $NS5A_{191–369}$ has partial fold and propensities for three transient helical structures: H1 (198–231), H2(251–266) and H3(292–306) which may be important for recognition of interaction partners (figure I.2. and IV.5.1) (Feuerstein et al. 2011). The pure [U–^{13}C/U–^{15}N] $NS5A_{191–369}$protein was provided was provided in the course of the here presented work.

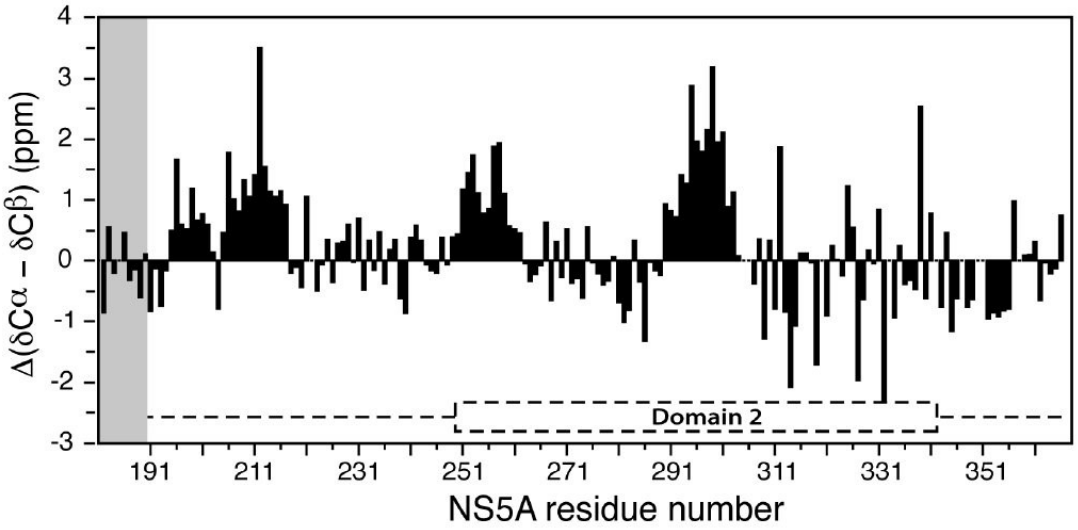

Fig. IV.5.1 Secondary chemical shifts Δ(δCα – δCβ) obtained from the difference between measured resonance frequencies and tabulated random coil values taking into account next neighbor effects. Consecutive positive values indicate polypeptide regions with increased propensity to adopt α–helical conformations (taken from Feuerstein et al. 2011).

IV.6 $NS5A_{191–369}$ shows different binding behavior to the SH3 domains of Bin1, Lyn, Src, Fyn and PI3K

Beside the assignment of $NS5A_{191–369}$, the cooperation also included characterisation of the $NS5A_{191–369}$ interaction with Bin1 SH3 domain (pure protein and DNA provided in the course of this work) and with the SH3 domains of Lyn, Fyn, PI3K and Src (provided in the course of this work) (Feuerstein et al. under revision). The assigned $NS5A_{191–369}$ allows mapping of binding regions of several SH3 domains upon performing chemical shift perturbation (CSP) experiments (chapter II.2.7.4) done by S. Feuerstein. The CSP experiments show in fact different binding activity of $NS5A_{191–369}$ toward different SH3 domains (figure IV.6.1.). Shown are the chemical shift differences for the Δδ (^{1}H, ^{15}N) of the $NS5A_{191–369}$ backbone plotted against the NS5A primary sequence upon SH3 titration. All SH3 domains were initially titrated to a 1:1 molar ratio and later on up to 5 times molar excess. The Src SH3 domain shows only contacts in the core PxxP region of NS5A even in a 5:1 molar ratio to NS5A. This is in contrast to the GST–pull–down experiments performed by MacDonald et al 2004 where they do not see any Src NS5A interaction. The SH3 domains of PI3K and Lyn make contacts within the similar range in the helix 1(H1) region of NS5A. Lyn SH3 has been reported by MacDonald et al. 2004 to make the strongest interaction with NS5A. In comparison Fyn SH3 domain makes similar contacts in the α1

(H1) but additional contacts as well in the α3 (H3). This indicates slightly that Fyn SH3 domain may require contacts outside the canonical PxxP binding motif for NS5A binding. This data is consistent with the results in chapter VI.2.3.1, where HSQC titration experiments with a 15–mer containing the canonical PxxP motif only were performed.

CSP experiments revealed for the Bin1 SH3 $NS5A_{191–369}$ interaction slow exchange kinetics with a high binding affinity of the two proteins. Mainly residues in the region between 342– 366 comprising the two PxxP motifs were affected when titrated in 1:1 molar ratio. Notably, the data revealed a second low binding region to the transiently populated helices α1(H1) and α3 (H3)(figure IV.7.1) This binding occurs only after 5–fold excess of Bin1 SH3, suggesting a low affinity binding event that might stabilize the transient helical fold that is present in the regions between positions 198–231 and 294–330.

IV.7 $NS5A_{191–369}$ displays bi–valence for Bin1 SH3 interaction

The potential of $NS5A_{191–369}$ to bind two Bin1 SH3 domains in a non cooperative manner was tested with SPR measurements. Approximately 40 µM $NS5A_{191–369}$ was immobilised via amine coupling on a CM 5 chip. Bin1 SH3 domain was titrated up to 17–fold excess to meet the conditions for the second low affinity binding event as observed in NMR (Feuerstein et al*. 2012*). The data showed the best fit, when considering a two binding model which delivers two dissociation constant values for respective binding site. The first high affinity binding site has a K_D = 2.4 µM and the second low affinity binding site 48.9 µM (chapter III.2.2). The measured K_D value for the high affinity binding site varies from the SPR data measured, when Bin1 SH3 is immobilised and $NS5A_{333–369}$ is injected (chapter III.2.1). The newly measured affinity is 24 times lower. One of the reasons for the discrepancy between the two measurements could be found in the different experimental set up. Here $NS5A_{191–369}$ was immobilised via amine coupling which affects also lysine residues. Five of the eight lysine residues are located either inside the binding interface or its close proximity which may have a negative effect on binding. This set up was absolutely necessary to display the possible two binding events

The obtained data suggest that Bin1 SH3 domain can bind to non canonical binding motifs and confirms the NMR data reported in our cooperation laboratory in Grenoble. The high affinity binding site is the canonical PxxP binding motif on NS5A, whereas the low affinity binding site includes the two transient alpha helices H1 and H3 as described in chapter VI.6 (fig.IV.6.1), see also figure VI.7.1

which displays the CSP experiments on $NS5A_{191–369}$ upon a 1:1 Bin1 SH3 molar ratio, a 1:5 and 1:10 ratio. Importantly, further SPR experiments with Fyn SH3 injected to immobilised $NS5A_{191–369}$ (same CM 5 chip), could only fitted best with a 1:1 Langmuir model (chapter III.2.3). This confirms the CSP data from chapter VI.6 which compared to the Bin1 SH3 data shows relatively weak interactions in the H1 and H3 region of $NS5A_{191–369}$.

However, this does not exclude eventual other important binding contacts outside the chosen NS5A fragment. According to data presented by Shelton et al. 2008 this contacts are likely to be located at domain 3 as for NS5A Fyn SH3 interaction the N–terminal amphipathic helix and domain I are unimportant, although here the NMR data clearly shows contacts of Fyn SH3 in domain 1 (α1; figure IV.6.1).

Over the last years, data reporting SH3 domains binding to proteins in a polyproline independent manner accumulated (Kang et al. 2000 and Duke Cohan et al. 2006). In this work Bin1 SH3 binds to such a non canonical region on $NS5A_{191–369}$ after Bin1 SH3 saturation of the polyproline binding region. The biological relevance of such a complex binding process remains speculative. The Bin1 protein is described to able to form dimers via its' BAR domain (Casal et al. 2006). The advantage of a bivalent Bin1 SH3 binding motif of NS5A can lay in the discrimination for proteins containing two SH3 domains or for dimers. In this manner investigating the Grb2 protein which contains two SH3 domains would be highly interesting. Grb2 NS5A interaction was reported by Tan et al. 1999, indicating that both SH3 of Grb2 bind in a cooperative manner to the NS5A. The second low binding site for Bin1 SH3 with NS5A protein overlaps with the postulated serine residues for hyperphosphorylation (S222, S225, S229 and S232) (Tanji et al. 1995). Bin1 SH3 may successfully block the hyperphosphorylation of NS5A as described already by (Masumi et al. 2005). This shows again the biological complexity of NS5A host protein interactions. Different phosphorylation patterns direct different interaction platforms of NS5A with host and HCV viral proteins during virus replication (Evans et al. 2004).

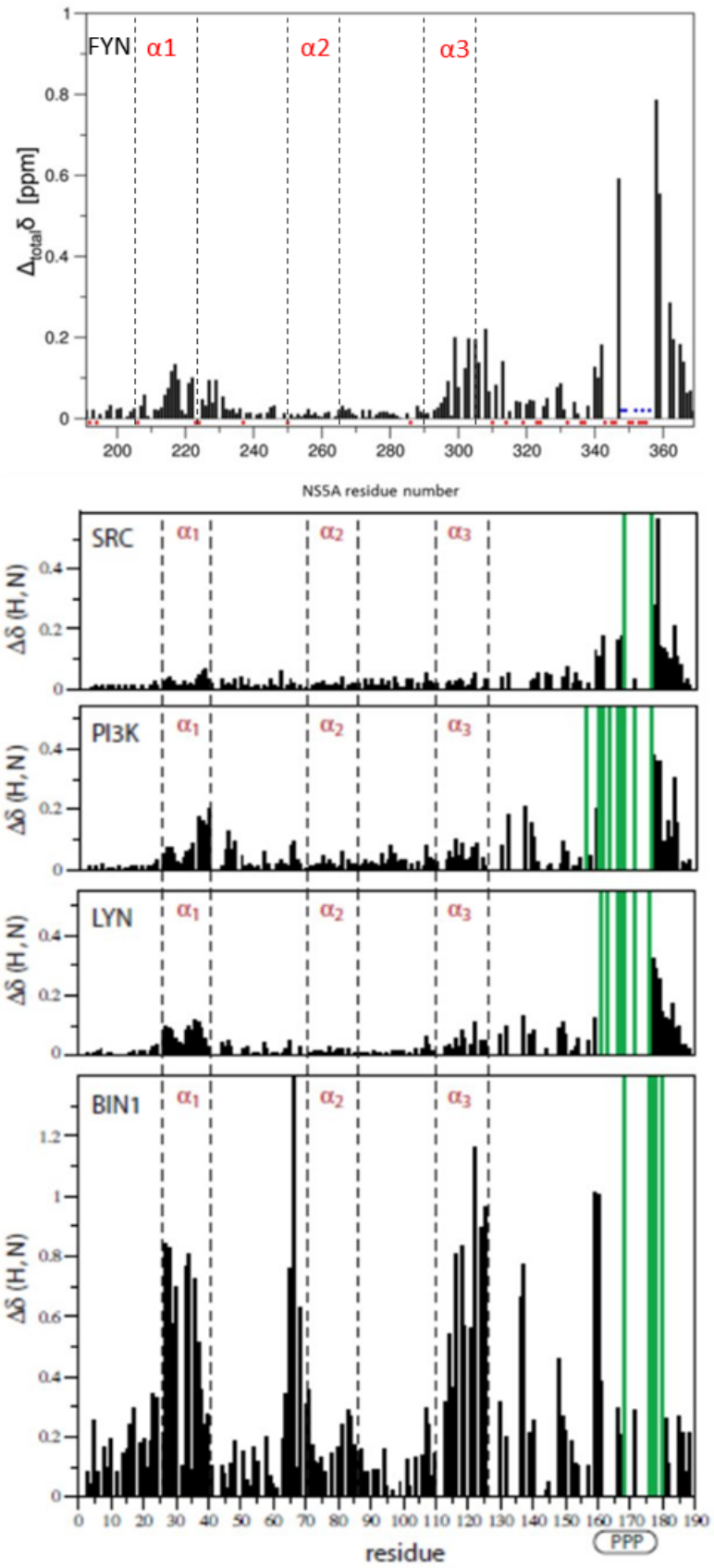

Fig. IV.6.1 Chemical shift changes Δδ(HN,N) = ((10*ΔδHN)2 + (ΔδN)2)½ plotted as a function of the primary sequence of $NS5A_{191–369}$. Shown are the plotted 5 times molar excess titration results for the SH3 domains of Fyn, SRC, PI3K, Lyn and Bin1. Furthermore the three transient α–helices are depicted as α1, α2 and α3 and the residues involved marked with the dash line. The canonical PxxP motif is displayed as PPP. (data and figures kindly provided by S. Feuerstein)

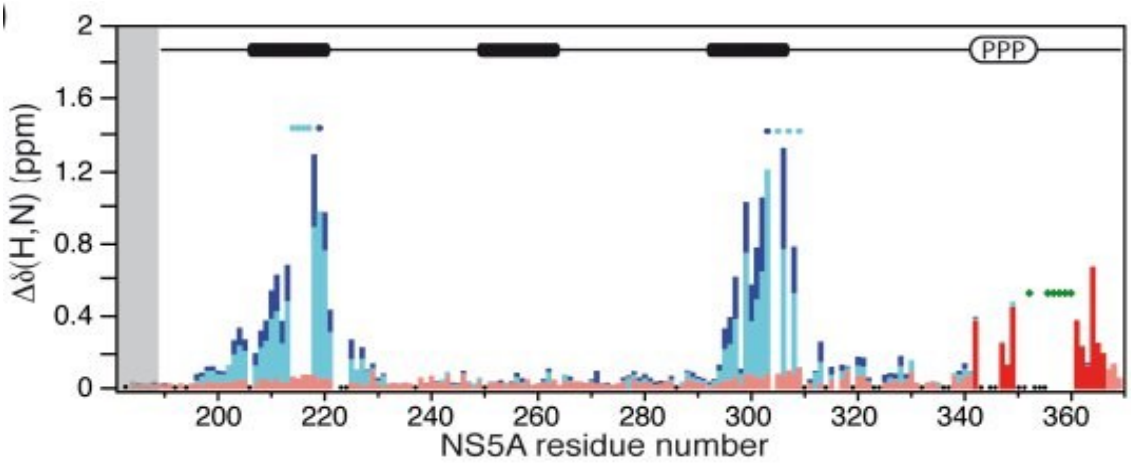

Fig. IV.7.1 Interaction of NS5A(191–369) with human Bin1–SH3. Chemical shift changes Δδ (HN,N)= ((10*ΔδHN)2 + (ΔδN)2)½ plotted as a function of the primary sequence of $NS5A_{191–369}$. Observed chemical shift changes for residues after titration of Bin1 SH3 in a 1:1 molar ratio (red bars), in a 1:5 molar ratio (cyan bars) and in a 1:10 molar ratio (blue bars). The red bars involve the canonical PxxP binding motif region for high affinity (K_D = 2.4 µM) and the green bars show the low affinity region (K_D = 48.9 µM). The low affinity binding sites include the transient α–helical regions on the NS5A fragment. Helix 1 (aa205–221) and helix 2 (aa 292–306) are clearly involved in the second Bin1 SH3 binding event. (Feuerstein et al. 2012)

However the mechanisms and downstream effects of the phosphorylation patterns are not completely understood. Figure IV.7.2 summarizes the recent experimental findings (partly in course of this work) as well as already described features and functions of NS5A protein important for the fragment spanning amino acids 191–369. The transiently formed helices described for the disordered $NS5A_{191–369}$ fragment can also be a model for a molecular interaction platform for several proteins. These kinds of platforms are already described for hub proteins, which are part of protein–protein interactions in protein networks and show similar as NS5A binding promiscuity and can be disordered (Singh et al. 2007 and Patil et al. 2010).

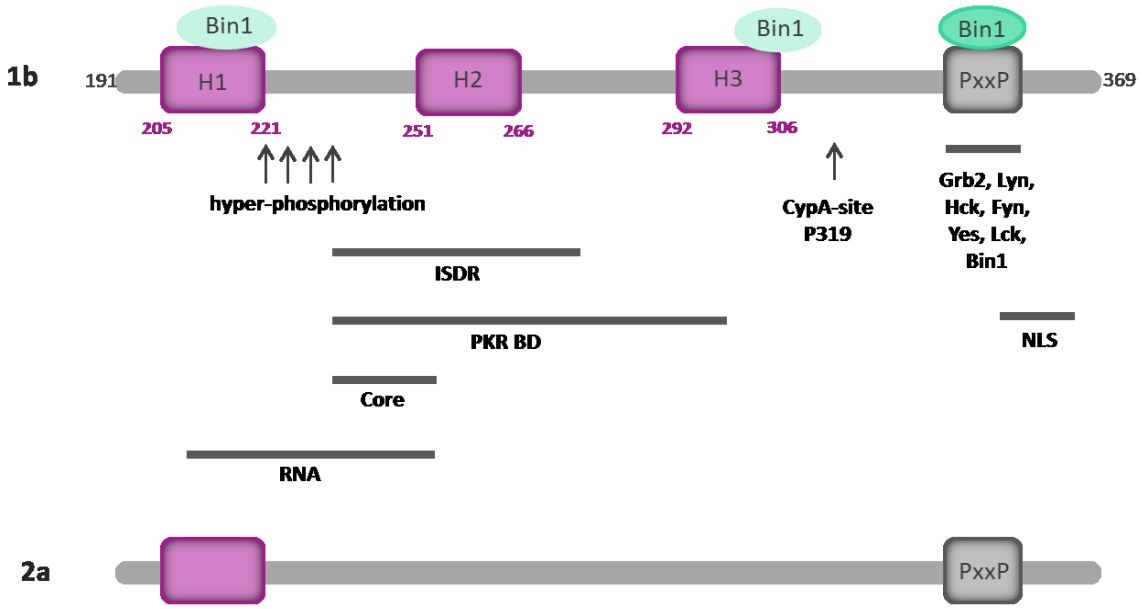

Fig. IV.7.2. A schematic diagram of the NS5A protein fragment used in this study with the experimental findings (chapter IV.5 and 6) are summarized together with a subset of already described features of NS5A in order to demonstrate the high biological complexity of this region. The position of serine residues for hyperphosphorylation (Tanji et al. 1995), the interferon sensitivity determining region (ISDR)(Tan and Katze, 2001) overlapping with the binding domain of cellular antiviral kinase PKR (PKR BD) (Gale et al. 1998), the nuclear localisation signal (NLS) (Ide et al. 1996) as well as the binding sites for several SH3 domains (Tan et al. 1999; MacDonald et al. 2003 and Zech et al. 2003), the viral core protein are depicted (Goh et al. 2001). Additionally, proline 319 (P319) a substrate for isomerization by the peptidyl–prolyl–isomerase cyclophilin A (CypA) is highlighted. CypA mediated prolyl isomerization stimulates the RNA binding activity of domain 2 (Foster et al. 2011). Finally, the position of a recently described RNA binding low complexity sequence 1 region is shown, which encompasses according to Hwang et al. 2010 together with domain 1 the minimal RNA binding site of NS5A. Finally, a speculative view at the conformation of genotype 2a $NS5A_{191–369}$ based on AGADIR prediction is shown. It is known that genotypes respond differently to IFN–α therapy with rates up to 80% for patients infected with genotype 2b compared to only 40–50% in case of genotype 1a or 1b. The degree of variability of ISDR sequences in hepatitis C virus (HCV) genome has been postulated to predict the respond to interferon therapy. The study in cooperation with the Brutscher laboratory with NS5A from subtype 1b shows that helix 2 (H2) localises in the center of the ISDR and that this helix as well as helix 3 (H3) is probably not present in subtype 2a.

V Summary

The hepatitis C virus protein NS5A has various functions in different stages of the viral life cycle. It has the ability to interact with a great body of proteins including viral and human proteins. NS5A binds to a set of human Src homology 3 domains (SH3). Three polyproline motifs (PxxP) on NS5A, which are canonical binding sites for SH3 domains are supposed to be crucial for this event. The Bridging integrator 1 (Bin1) plays a key role in inducing actively membrane curvature via its Bin–amphiphysin–Rvs (BAR) domain. In the past years, the tumour suppressor role of Bin1 in controlling Myc activity moved more and more in the focus of research, regarding Myc`s importance in apoptotic signalling pathways. There is clear evidence that the Bin1-Myc-interaction is mediated through the SH3 domain of Bin1.

Aim of this work is the characterisation of the NS5A interaction with certain SH3 domains and the understanding discrimination determinants for the binding interface of its promiscuous interaction with SH3 domains. Therefore, the binding behaviour of NS5A fragments to the SH3 domains of physiological binding partners of NS5A was studied using different biophysical methods, such as surface plasmon resonance (SPR) spectroscopy and nuclear magnetic resonance (NMR) spectroscopy. The main focus of the current thesis was to characterise the binding of NS5A to the Bin1 SH3 domain, additionally the interaction with the SH3 domains of Fyn, Yes and Lyn was characterised.

The quantification of the affinity between NS5A and Bin1 SH3 by using SPR spectroscopy resulted in an unexpected high affinity with a dissociation constant K_D= 0.1 µM. The obtained K_D value is rare for SH3-ligand-interactions, which usually transient with affinities in the mM to µM range. However, this kind of affinity is typical for viral proteins, which have to compete successfully with the physiological ligands of SH3 domains. The K_D values of the NS5A to the SH3 domains of Lyn, Yes and Fyn resulted in affinities ranging from 6 µM for Lyn, 25 µM for Yes and 95 µM for Fyn. $^{1}H^{15}N$ HSQC NMR titration experiments were conducted to analyse the dynamics of these interactions, where a 35—mer NS5A fragment was gradually titrated to the [$U—^{15}N$] labelled SH3 domains. The investigated NS5A complexes with Fyn and Yes SH3 displayed fast exchange kinetics, consistent with the SPR data. As expected, only the binding dynamics of the NS5A-Bin1-interaction, revealed slow exchange kinetics for most of the SH3 residues and fast exchange kinetics for a few. Slow exchange kinetics in $^{1}H^{15}N$ HSQC NMR experiments are observed for stable complexes and are suitable for further structural NMR experiments. In order to gain structural information, triple resonance NMR experiments to elucidate the Bin1 SH3: $NS5A_{333-369}$ complex structure, were conducted. The backbone assignment and mapping of the binding region of the NS5A peptide on the Bin1 SH3 domain surface could be carried out successfully. The unforeseen formation of various SH3:NS5A complex species in the

sample, presumably due to the usage of more than one PxxP motif as binding site the structure of the entire complex could not be solved.

The interaction of Bin1 with its physiological binding partner Myc follows, compared to the interaction with NS5A, fast exchange kinetics, which can be observed for not long lived complexes. In this work the potency of NS5A to compete and replace Myc from binding to Bin1 SH3 was probed *in vitro* with chemical shift perturbance experiments using NMR spectroscopy. 15—mer peptides of NS5A (aa 347—361) and Myc (aa 55—69) were applied to demonstrate the ability of NS5A to compete with a physiological binding partner. The replacement was monitored by following the change in the chemical shift of the residues involved in the binding in the $^{1}H^{15}N$ HSQC NMR spectra. This finding is interesting in regard of the oncologic feature of a HCV infection and should be investigated in future.

Further, the present thesis deals with the structural propensities of a NS5A fragment spanning the residues 191—369, comprising an extended domain 2. $^{1}H^{15}N$ HSQC NMR experiments revealed that this NS5A fragment shows all characteristics for intrinsically disordered proteins (IDPs). IDPs are very common in nature and some IDP classes show folding upon binding to their respective ligands. Upon adding of the SH3 domain of Lyn, chemical shift changes for the NS5A residues were observed, hinting a structural rearrangement for the NS5A extended domain 2 upon ligand binding. This finding was investigated in more detail in collaboration with S. Feuerstein and B. Brutscher (Institut de Biologie Structurale, Centre National de Recherche Scientifique in Grenoble) also for the SH3 domains of Bin1, Src, Fyn and Pi3K. Notably, their studies showed that NS5A (aa 191-369) has a second non canonical low affinity binding site for Bin1 SH3. This result could be confirmed in the course of this work using an independent SPR approach.

V Zusammenfassung

Das Hepatitis C Virus (HCV) Protein NS5A nimmt unterschiedliche Funktionen in den verschiedenen Phasen des viralen Lebenszyklus an. Es interagiert mit einer großen Anzahl an viralen sowie humanen Proteinen, um den verschieden Funktionen, die es inne hat bei zukommen. Unter anderem bindet NS5A an ausgewählten Src Homologie *3* (SH3) Domänen. Wichtig für SH3-Bindung sind drei Polyprolin-Motive (PxxP) auf dem NS5A Protein. Das Protein *Bridging Integrator 1* (Bin1) spielt eine wichtige Rolle bei der Faltung von Membranen, indem es aktiv sich mit ihrer Bin–amphiphysin–Rvs (BAR) Domäne direkt an die Membran anlagert. Allerdings rückte in den letzten Jahren Bin1 als Tumorsuppressor-Protein im Hinblick auf ihre Kontrollfunktion der Myc Aktivität in den zellulären apoptotischen Signaltransduktionswegen in den Vordergrund. Die Bin1 Kontrolle der Myc Aktivität läuft hauptsächlich über die Bin1 SH3 Domäne.

Die Zielsetzung dieser Arbeit ist die Charakterisierung der NS5A Interaktion mit bestimmten SH3 Domänen und das Verständnis von Diskriminierungsdeterminanten für die Bindungsoberfläche mit den verschieden SH3 Domänen. Aus diesem Grund wurde das Bindungsverhalten von NS5A-Fragmenten zu den SH3 Domänen von physiologischen Bindungspartnern mit biophysikalischen Methoden wie Oberflächenplasmon-Resonanz-Spektroskopie (SPR) und der Kernresonanz-Spektroskopie (NMR) untersucht. Der Fokus der vorliegenden Arbeit lag hauptsächlich in der Beschreibung der Bindung von NS5A zu der SH3 Domäne von Bin1 SH3. Außerdem wurde die Interaktion zu den SH3 Domänen von Fyn, Yes und Lyn Proteinen untersucht.

Die Quantifizierung der Affinität zwischen NS5A und Bin1 SH3 mit der SPR-Spektroskopie lieferte eine unerwartet hohe Affinität mit einer Dissoziationskonstanten (K_D) von 0.1 µM. Dieser K_D-Wert ist nicht typisch für SH3-Ligand-Wechselwirkungen in der Zelle, die meist transient sind und in eher µM bis zu mM Bereichen angesiedelt sind. Jedoch ist es gerade für virale Proteine essentiell hohe Bindungsaffinitäten zu zeigen, um erfolgreich gegen die physiologischen Liganden der SH3 Domänen zu konkurrieren. Die K_D-Werte für die Bindung zwischen NS5A und den SH3 Domänen von Lyn, Yes und Fyn betrug 6 µM für Lyn, 25 µM für Yes und 95 µM für Fyn. Um die Dynamik der Bindung näher zu untersuchen wurden $^{1}H^{15}N$ HSQC NMR Titrationsexperimente aufgenommen, bei denen ein 35mer NS5A-Fragment graduell zu der [U—^{15}N] markierten SH3 Domäne zugegeben wurde. Die untersuchten NS5A Komplexe mit den SH3 Domänen von Fyn und Yes folgen in der Titration einer schnellen Austauschkinetik, deckend zu den Ergebnissen aus den SPR Experimenten. Erwartungsgemäß zeigte die NS5A-Bin1-SH3-Bindungsdynamik für die meisten SH3 Aminosäurereste einen langsamen Austausch und schnellen Austausch für einige wenige. Langsame Austauschkinetik ist charakteristisch für stabile Komplexe und eignet sich daher für höher dimensionale NMR-Strukturexperimente. Zwecks NMR-Lösungsstrukturauflösung des Bin1 SH3:$NS5A_{333-369}$—Komplexes wurden Tripleresonanz-Experimente aufgenommen. Das Proteinrückgrat des Komplexes konnte

erfolgreich zugeordnet werden und diente als Grundlage für die Kartierung der Bindungsregion des NS5A Peptids auf der Bin1—SH3—Oberfläche. Jedoch enthielt die NMR-Probe unterschiedliche Konformationsspezies des Bin1 SH3:NS5A Komplexes, die wahrscheinlich auf mehr als ein Polyprolin—Bindungsmotiv auf der NS5A—Oberfläche zurückzuführen sind. Somit konnte die Komplexstruktur nicht gelöst werden.

Die Interaktion des Bin1 mit dem physiologischen Bindungspartner Myc, folgt verglichen mit der Wechselwirkung mit NS5A einer schnellen Austauschkinetik im Komplex, welches typisch für kurzlebige Komplexe ist. In dieser Arbeit wurde das Verdrängungspotential des NS5A Proteins in einer Konkurrenzsituation mit dem Myc Protein für die Bindungsstelle auf der Bin1 SH3 *in vitro* mit Chemische—Verschiebung—Perturbationsexperimenten (CSP) mit NMR näher untersucht. Es wurden 15mer Peptide des NS5A (347-361) und Myc (55-69) eingesetzt, um das Verdrängungsexperiment durchzuführen. Die erfolgreiche Verdrängung des Myc Peptids von der Binderegion der Bin1 SH3 mit dem NS5A Peptid konnte auf Grund der Veränderung der chemischen Verschiebungen für die Amidresonanzen in dieser Region in einem Set von $^{1}H^{15}N$ HSQC NMR Spektren verfolgt werden. Dieses Ergebnis ist im Hintergrund des onkologischen Charakters einer HCV Infektion sehr interessant und sollte im Detail untersucht werden.

Ein weiterer Aspekt der vorliegenden Arbeit ist die strukturelle Charakterisierung eines NS5A-Fragments, welches die Aminosäuren von 191—369 einspannt und somit eine erweiterte Domäne 2 darstellt. In $^{1}H^{15}N$ HSQC NMR Experimenten zeigte das NS5A-Fragment Charakteristika für intrinsisch ungeordnete Proteine (IDPs). IDPs sind in der Natur weit verbreitet und einige IDP-Klassen zeigen Faltungsmerkmale nach Ligandenbindung. Die Zugabe der SH3 Domäne des Lyn, führte zur Veränderungen in der chemischen Verschiebung für die Resonanzen des NS5A, welches auf eine strukturelle Umlagerung des NS5A in der erweiterten Domäne 2 nach Ligandenbindung deutet. Dieser Umstand wurde in einer Kollaboration mit S.Feuerstein und B. Brutscher (Institut de Biologie Structurale, Centre National de Recherche Scientifique in Grenoble) im Detail auch für die SH3 Domänen von Bin1, Src, Fyn und Pi3K untersucht. Bemerkenswerterweise konnten sie zeigen, dass NS5A (191-369) eine zweite nicht kanonische und vergleichbar niedrig affine Bindestelle für die Bin1 SH3 hat. Dieses Ergebnis konnte in dieser Arbeit mit einem unabhängigen SPR Ansatz bestätigt werden.

VI Appendix

1D, 2D and 3D	One–, two– and three–dimensional
A_{xxx}	Absorbance at xxx nm
APS	Ammonium persulfate
aa	Amino acid
Bin1	Bridging integrator 1
c	concentration
CARA	Computer Aided Resonance Assignment
δ	Chemical shift
COSY	Correlation Spectroscopy
°C	Degree Celsius
CSP	Chemical shift perturbation
CV	Column volume
d	diameter
D_2O	Deuterium oxide; ^2H_2O
Da	Dalton (unit for molecular weight for biopolymers)
DLS	Dynamic Light Scattering
ddNTP	Dideoxynucleotides
DNA	Desoxyribonucleic acid
dNTP	Deoxyribonucleotide
DTT	Dithiothreitol
E. *coli*	*Escherichia coli*
EDTA	Ethylenediamine tetraacetic acid
ER	Endoplasmatic reticulum
et al.	et allis
g	Gravitational acceleration
FPLC	Fast protein liquid chromatography

GST	Gluthatione–S–Transferase
GSH sepharose	Gluthaione sepahrose
h	hour
HAV	Hepatitis a virus
HBV	Hepatitis b virus
HCV	Hepatitis c virus
HCC	Hepatocellular carcinoma
HEPES	4–(2–hydroxyethyl)–1–piperazineethanesulfonic acid
HIV–1	Human immunodeficiency virus type 1
HNCO	NMR experiment observing peptide ^{15}N, $^{1}H^{N}$ and previous ^{13}CO
HNCACB	NMR experiment observing peptide ^{15}N, $^{1}H^{N}$, $^{13}C^{\alpha}$, $^{13}C^{\beta}$, $^{13}C^{\alpha-1}$ and $^{13}C^{\beta-1}$
HSQC	Heteronuclear single quantum coherence 1
Hz	Hertz
IDP	Intrinsically disordered proteins
IFN	Interferon
IPTG	Isopropyl–β–D–thiogalactopyranoside
IRES	Internal ribosomal entry site
kb	Kilo bases
K_D	Dissociation constant
kDa	Kilo–dalton
LB–Medium	Luria–Bertani Medium
LCS	Low complexity sequence
M	Molar (Mol/Liter)
µM	Micromol/Liter
min	Minute
mg	Milligramm
ml	Milliliter
mM	Millimol/Liter
M9–Medium	Minimal medium for isotope labeling
MWCO	Molecular weight cutoff

Myc	Myelocytomatosis
Na–EDTA	Disodium–ethylendinitrilotetraacetic acid
Ni–NTA	Nickel nitrilotriacetic acid
nm	Nanometer
NMR	Nuclear magnetic resonance
NMRPipe	Programme für processing NMR spectra
NOE	Nuclear Overhauser effect
NOESY	NOE spectroscopy
NS5A	Non structural protein 5 A
nt	Nucleotide
ORF	Open reading frame
OD_{xxx}	Optical density at xxx nm
PAGE	Polyacrylamide gel electrophoresis
PCR	Polymerase chain reaction
PDB	Protein Data Bank
PFG	Pulse field gradient
ppm	parts per million
R_H	Hydrodynamic radius
RNA	Ribonucleic acid
rpm	rotations per minute
RT	Room temperature
RU	Response Unit
s	second
SDS	sodium dodecylsulfate
SEC	Size exclusion chromatography
SH3	Src homology 3
SPR	Surface plasmon resonance
Src	Sarcouma
TALOS	Torsion angle likelihood obtained from shifts and sequence similarity
TE	Tris–EDTA
TEMED	N,N,N',N'–Tetrametylethylene diamine

TFA	Trifluoroacetic acid
Tris	Tris(hydroxymethyl)–amino–methane
U	Unit
[*U*–^{13}C], [*U*–^{15}N]	Uniform isotope labeling with nuclide ^{13}C and ^{15}N
µl	Microlitre
UV	Ultra violet
V	Volt
$^{v}/_{v}$	Volume per volume
WT	Wild type
$^{w}/_{v}$	Weight per volume
ε	Extinctions coefficient

V.1 List of amino acids with one– and three–letter codes

Alanine	Ala	A
Arginine	Arg	R
Asparagine	Asn	N
Aspartic acid	Asp	D
Cysteine	Cys	C
Glutamine	Glu	Q
Glutamic acid	Gln	E
Gylcine	Gly	G
Histidine	His	H
Isoleucine	Ile	I
Leucine	Leu	L
Lysine	Lys	K
Methionine	Met	M
Phenylalanine	Phe	F
Proline	Pro	P
Serine	Ser	S
Threonine	Thr	T
Tryptophan	Trp	W
Tyosine	Tyr	Y

Valine	Val	V

V.2 List of Tables

V.3 List of Figures

Scientific publications, poster presentations and presentations

Publications

Feuerstein S., Solyom S., Aladağ A., Hoffmann S, Willbold D., Brutscher B.; *^{1}H, ^{13}C, and ^{15}N resonance assignment of a 179 residue fragment of hepatitis C virus non-structural protein 5A*; Biomol. NMR Assign. October 5 (2):241-3 2011

Feuerstein S., Solyom S., Aladağ A.,Favier A., Hoffmann S, Willbold D., Brutscher B. ; *Transient structure and SH3 interaction sites in an intrinsically disordered fragment of the hepatitis C virus protein NS5A;* Journal of Molecular Biology, July 20; 420(4-5):310-23, 2012

Poster

Aladağ A, Hoffmann S, Stoldt M., Willbold D.; *Structural characterisation of host cell signaling pathway modulation by the hepatitis C virus protein NS5A*; 4th International Conference of the collaborative Research Center SFB 575 (2008), Düsseldorf

Aladağ A, Hoffmann S, Stoldt M., Willbold D.; *Structural basis of the interaction of Hepatitis C virus protein NS5A, Bin1 and Myc;* Annual Meeting of the German Biophysical Society (2010), Bochum

Presentation

"Hepatitis c virus protein NS5A—a molecular shielding approach"; 4th International Conference of the collaborative Research Center SFB 575 (2008), Düsseldorf

VII Bibliography

Adler, A. J., N. J. Greenfield, et al. (1973). "Circular dichroism and optical rotatory dispersion of proteins and polypeptides." Methods Enzymol 27: 675–735.

Bauer, F., E. Hofinger, et al. (2004). "Characterization of Lck–binding elements in the herpesviral regulatory tip protein." Biochemistry 43(47): 14932–14939.

Bax, A., G. M. Clore, et al. (1990). "H–1–H–1 Correlation Via Isotropic Mixing of C–13 Magnetization, a New 3–Dimensional Approach for Assigning H–1 and C–13 Spectra of C–13–Enriched Proteins." Journal of Magnetic Resonance 88(2): 425–431.

Bernado, P., C. W. Bertoncini, et al. (2005). "Defining long–range order and local disorder in native alpha–synuclein using residual dipolar couplings." J Am Chem Soc 127(51): 17968–17969.

Bodenhausen, G. and D. J. Ruben (1980). "Natural Abundance N–15 Nmr by Enhanced Heteronuclear Spectroscopy." Chemical Physics Letters 69(1): 185–189.

Bourhis, J. M., K. Johansson, et al. (2004). "The C–terminal domain of measles virus nucleoprotein belongs to the class of intrinsically disordered proteins that fold upon binding to their physiological partner." Virus Research 99(2): 157–167.

Bracken, C., L. M. Iakoucheva, et al. (2004). "Combining prediction, computation and experiment for the characterization of protein disorder." Curr Opin Struct Biol 14(5): 570–576.

Brass, V., E. Bieck, et al. (2002). "An amino–terminal amphipathic alpha–helix mediates membrane association of the hepatitis C virus nonstructural protein 5A." Journal of Biological Chemistry 277(10): 8130–8139.

Casal, E., L. Federici, et al. (2006). "The crystal structure of the BAR domain from human Bin1/Amphiphysin II and its implications for molecular recognition." Biochemistry 45(43): 12917–12928.

Cornilescu, G., F. Delaglio, et al. (1999). "Protein backbone angle restraints from searching a database for chemical shift and sequence homology." J Biomol NMR 13(3): 289–302.

De Guzman, R. N., M. A. Martinez–Yamout, et al. (2004). "Interaction of the TAZ1 domain of the CREB–binding protein with the activation domain of CITED2 – Regulation by competition between intrinsically unstructured ligands for non–identical binding sites." Journal of Biological Chemistry 279(4): 3042–3049.

Delaglio, F., S. Grzesiek, et al. (1995). "NMRPipe: a multidimensional spectral processing system based on UNIX pipes." J Biomol NMR 6(3): 277–293.

Duke–Cohan, J. S., H. Kang, et al. (2006). "Regulation and function of SKAP–55 non–canonical motif binding to the SH3c domain of adhesion and degranulation–promoting adaptor protein." Journal of Biological Chemistry 281(19): 13743–13750.

Dunker, A. K., C. J. Brown, et al. (2002). "Intrinsic disorder and protein function." Biochemistry 41(21): 6573–6582.

Dyson, H. J. and P. E. Wright (2002). "Coupling of folding and binding for unstructured proteins." Current Opinion in Structural Biology 12(1): 54–60.

Dyson, H. J. and P. E. Wright (2005). "Intrinsically unstructured proteins and their functions." Nature Reviews Molecular Cell Biology 6(3): 197–208.

Egger, D., B. Wolk, et al. (2002). "Expression of hepatitis C virus proteins induces distinct membrane alterations including a candidate viral replication complex." J Virol 76(12): 5974–5984.

Egger, D., B. Wolk, et al. (2002). "Expression of hepatitis C virus proteins induces distinct membrane alterations including a candidate viral replication complex." J Virol 76(12): 5974–5984.

Elazar, M., K. H. Cheong, et al. (2003). "Amphipathic helix–dependent localization of NS5A mediates hepatitis C virus RNA replication." J Virol 77(10): 6055–6061.

Evan, G. I., A. H. Wyllie, et al. (1992). "Induction of Apoptosis in Fibroblasts by C–Myc Protein." Cell 69(1): 119–128.

Evans, M. J., C. M. Rice, et al. (2004). "Phosphorylation of hepatitis C virus nonstructural protein 5A modulates its protein interactions and viral RNA replication." Proc Natl Acad Sci U S A 101(35): 13038–13043.

Facchini, L. M. and L. Z. Penn (1998). "The molecular role of Myc in growth and transformation: recent discoveries lead to new insights." Faseb Journal 12(9): 633–651.

Feng, S., J. K. Chen, et al. (1994). "Two binding orientations for peptides to the Src SH3 domain: development of a general model for SH3–ligand interactions." Science 266(5188): 1241–1247.

Feuerstein, S., M. J. Plevin, et al. (2012). "iHADAMAC: A complementary tool for sequential resonance assignment of globular and highly disordered proteins." J Magn Reson 214(1): 329–334.

Feuerstein, S., Z. Solyom, et al. (2011). "(1)H, (13)C, and (15)N resonance assignment of a 179 residue fragment of hepatitis C virus non–structural protein 5A." Biomolecular Nmr Assignments 5(2): 241–243.

Feuerstein S., Solyom S., Aladağ A.,Favier A., Hoffmann S, Willbold D., Brutscher B. ; Transient structure and SH3 interaction sites in an intrinsically disordered fragment of the hepatitis C virus protein NS5A; Journal of Molecular Biology, July 20; 420(4-5):310-23, 2012

Foster, T. L., P. Gallay, et al. (2011). "Cyclophilin A Interacts with Domain II of Hepatitis C Virus NS5A and Stimulates RNA Binding in an Isomerase–Dependent Manner." J Virol 85(14): 7460–7464.

Gale, M., C. M. Blakely, et al. (1998). "Control of PKR protein kinase by hepatitis C virus nonstructural 5A protein: Molecular mechanisms of kinase regulation." Mol Cell Biol 18(9): 5208–5218.

Gale, M. J., M. J. Korth, et al. (1997). "Evidence that hepatitis C virus resistance to interferon is mediated through repression of the PKR protein kinase by the nonstructural 5A protein." Virology 230(2): 217–227.

Ge, K., J. DuHadaway, et al. (1999). "Mechanism for elimination of a tumor suppressor: Aberrant splicing of a brain–specific exon causes loss of function of Bin1 in melanoma." Proc Natl Acad Sci U S A 96(17): 9689–9694.

Ge, K., J. Duhadaway, et al. (2000). "Losses of the tumor suppressor BIN1 in breast carcinoma are frequent and reflect deficits in programmed cell death capacity." International Journal of Cancer 85(3): 376–383.

Goh, G. K. M., A. K. Dunker, et al. (2008). "A comparative analysis of viral matrix proteins using disorder predictors." Virology Journal 5.

Goh, G. K. M., A. K. Dunker, et al. (2009). "Protein intrinsic disorder and influenza virulence: the 1918 H1N1 and H5N1 viruses." Virology Journal 6.

Goh, P. Y., Y. J. Tan, et al. (2001). "The hepatitis C virus core protein interacts with NS5A and activates its caspase–mediated proteolytic cleavage." Virology 290(2): 224–236.

Grodberg, J. and J. J. Dunn (1989). "Comparison of Escherichia–Coli K–12 Outer–Membrane Protease Ompt and Salmonella–Typhimurium E–Protein." J Bacteriol 171(5): 2903–2905.

Grzesiek, S., J. Anglister, et al. (1993). "Correlation of Backbone Amide and Aliphatic Side–Chain Resonances in C–13/N–15–Enriched Proteins by Isotropic Mixing of C–13 Magnetization." Journal of Magnetic Resonance Series B 101(1): 114–119.

Grzesiek, S. and A. Bax (1992). "Correlating Backbone Amide and Side–Chain Resonances in Larger Proteins by Multiple Relayed Triple Resonance Nmr." J Am Chem Soc 114(16): 6291–6293.

Grzesiek, S. and A. Bax (1992). "An Efficient Experiment for Sequential Backbone Assignment of Medium–Sized Isotopically Enriched Proteins." Journal of Magnetic Resonance 99(1): 201–207.

Grzesiek, S. and A. Bax (1992). "Improved 3d Triple–Resonance Nmr Techniques Applied to a 31–Kda Protein." Journal of Magnetic Resonance 96(2): 432–440.

Hall, D. A., C. W. V. Kooi, et al. (2001). "Mapping the interactions between flavodoxin and its physiological partners flavodoxin reductase and cobalamin–dependent methionine synthase." Proc Natl Acad Sci U S A 98(17): 9521–9526.

Han, J. D. J., N. Bertin, et al. (2004). "Evidence for dynamically organized modularity in the yeast protein–protein interaction network." Nature 430(6995): 88–93.

Hanoulle, X., A. Badillo, et al. (2010). "The Domain 2 of the HCV NS5A Protein Is Intrinsically Unstructured." Protein and Peptide Letters 17(8): 1012–1018.

He, B., K. Wang, et al. (2009). "Predicting intrinsic disorder in proteins: an overview." Cell Research 19(8): 929–949.

He, Y. P. and M. G. Katze (2002). "To interfere and to anti–interfere: The interplay between hepatitis C virus and interferon." Viral Immunology 15(1): 95–119.

Hiasa, Y., N. Horiike, et al. (1998). "Low stimulatory capacity of lymphoid dendritic cells expressing hepatitis C virus genes." Biochem Biophys Res Commun 249(1): 90–95.

Howell, S., M. Kenmore, et al. (1998). "High–density immobilization of an antibody fragment to a carboxymethylated dextran–linked biosensor surface." Journal of Molecular Recognition 11(1–6): 200–203.

Huang, Y. Q. and Z. R. Liu (2009). "Kinetic Advantage of Intrinsically Disordered Proteins in Coupled Folding–Binding Process: A Critical Assessment of the "Fly–Casting" Mechanism." J Mol Biol 393(5): 1143–1159.

Ide, Y., L. W. Zhang, et al. (1996). "Characterization of the nuclear localization signal and subcellular distribution of hepatitis C virus nonstructural protein NS5A." Gene 182(1–2): 203–211.

Ikura, M., L. E. Kay, et al. (1991). "Improved three–dimensional 1H–13C–1H correlation spectroscopy of a 13C–labeled protein using constant–time evolution." J Biomol NMR 1(3): 299–304.

Ish–Horowicz, D. and J. F. Burke (1981). "Rapid and efficient cosmid cloning." Nucleic Acids Res 9(13): 2989–2998.

Jensen, M. R., P. Bernado, et al. (2010). "Structural Disorder within Sendai Virus Nucleoprotein and Phosphoprotein: Insight into the Structural Basis of Molecular Recognition." Protein and Peptide Letters 17(8): 952–960.

Jensen, M. R., G. Communie, et al. (2011). "Intrinsic disorder in measles virus nucleocapsids." Proc Natl Acad Sci U S A 108(24): 9839–9844.

Johnson, B. A. (2004). "Using NMRView to visualize and analyze the NMR spectra of macromolecules." Methods Mol Biol 278: 313–352.

Kaneko, T., Y. Tanji, et al. (1994). "Production of 2 Phosphoproteins from the Ns5a Region of the Hepatitis–C Viral Genome." Biochem Biophys Res Commun 205(1): 320–326.

Kang, H., C. Freund, et al. (2000). "SH3 domain recognition of a proline–independent tyrosine–based RKxxYxxY motif in immune cell adaptor SKAP55." Embo Journal 19(12): 2889–2899.

Karlsson, R., P. S. Katsamba, et al. (2006). "Analyzing a kinetic titration series using affinity biosensors." Anal Biochem 349(1): 136–147.

Katze, M. G., B. Kwieciszewski, et al. (2000). "Ser(2194) is a highly conserved major phosphorylation site of the hepatitis C virus nonstructural protein NS5A." Virology 278(2): 501–513.

Kay, L. E., M. Ikura, et al. (2011). "Three–dimensional triple–resonance NMR Spectroscopy of isotopically enriched proteins. 1990." J Magn Reson 213(2): 423–441.

Kelly, M. A., B. W. Chellgren, et al. (2001). "Host–guest study of left–handed polyproline II helix formation." Biochemistry 40(48): 14376–14383.

Kohno, T., H. Kusunoki, et al. (1998). "A new general method for the biosynthesis of stable isotope–enriched peptides using a decahistidine–tagged ubiquitin fusion system: An application to the production of mastoparan–X uniformly enriched with N–15 and N–15/C–13." J Biomol NMR 12(1): 109–121.

Krawczynski, K., G. Kuo, et al. (1989). "Blood–Borne Non–a, Non–B Hepatitis (Pt–Nanb) – Immunohistochemical Identification of Disease – and Hepatitis–C Virus–Associated Antigen(S)." Hepatology 10(4): 580–580.

Kuo, G., Q. L. Choo, et al. (1989). "An Assay for Circulating Antibodies to a Major Etiologic Virus of Human Non–a, Non–B–Hepatitis." Science 244(4902): 362–364.

Laemmli, U. K. (1970). "Cleavage of Structural Proteins during Assembly of Head of Bacteriophage–T4." Nature 227(5259): 680–&.

Lee, C. H., B. Leung, et al. (1995). "A Single Amino–Acid in the Sh3 Domain of Hck Determines Its High–Affinity and Specificity in Binding to Hiv–1 Nef Protein." Embo Journal 14(20): 5006–5015.

Lemaster, D. M. (1994). "Isotope Labeling in Solution Protein Assignment and Structural–Analysis." Progress in Nuclear Magnetic Resonance Spectroscopy 26: 371–419.

Lemon, S. M. and M. Honda (1997). "Internal ribosome entry sites within the RNA genomes of hepatitis C virus and other flaviviruses." Seminars in Virology 8(3): 274–288.

Liang, Y., H. Ye, et al. (2007). "Domain 2 of nonstructural protein 5A (NS5A) of hepatitis C virus is natively unfolded." Biochemistry 46(41): 11550–11558.

Macdonald, A., K. Crowder, et al. (2004). "The hepatitis C virus NS5A protein binds to members of the Src family of tyrosine kinases and regulates kinase activity." Journal of General Virology 85: 721–729.

Macdonald, A. and M. Harris (2004). "Hepatitis C virus NS5A: tales of a promiscuous protein." Journal of General Virology 85: 2485–2502.

Macdonald, A., S. Mazaleyrat, et al. (2005). "Further studies on hepatitis C virus NS5A–SH3 domain interactions: identification of residues critical for binding and implications for viral RNA replication and modulation of cell signalling." Journal of General Virology 86: 1035–1044.

Majumder, M., A. K. Ghosh, et al. (2002). "Hepatitis C virus NS5A protein impairs TNF–mediated hepatic apoptosis, but not by an anti–FAS antibody, in transgenic mice." Virology 294(1): 94–105.

Manning, M. C. and R. W. Woody (1991). "Theoretical Cd Studies of Polypeptide Helices – Examination of Important Electronic and Geometric Factors." Biopolymers 31(5): 569–586.

Masumi, A., H. Aizaki, et al. (2005). "Reduction of hepatitis C virus NS5A phosphorylation through its interaction with amphiphysin II." Biochem Biophys Res Commun 336(2): 572–578.

Mayer, B. J. (2001). "SH3 domains: complexity in moderation." Journal of Cell Science 114(7): 1253–1263.

McAlister, M. S. B., H. R. Mott, et al. (1996). "NMR analysis of interacting soluble forms of the cell–cell recognition molecules CD2 and CD48." Biochemistry 35(19): 5982–5991.

Montelione, G. T., B. A. Lyons, et al. (1992). "An Efficient Triple Resonance Experiment Using C–13 Isotropic Mixing for Determining Sequence–Specific Resonance Assignments of Isotopically–Enriched Proteins." J Am Chem Soc 114(27): 10974–10975.

Moradpour, D., M. J. Evans, et al. (2004). "Insertion of green fluorescent protein into nonstructural protein 5A allows direct visualization of functional hepatitis C virus replication complexes." J Virol 78(14): 7400–7409.

Mullis, K. B. and F. A. Faloona (1987). "Specific synthesis of DNA in vitro via a polymerase–catalyzed chain reaction." Methods Enzymol 155: 335–350.

Nanda, S. K., D. Herion, et al. (2006). "Src homology 3 domain of hepatitis C virus NS5A protein interacts with Bin1 and is important for apoptosis and infectivity.(vol 130, pg 794, 2006)." Gastroenterology 131(2): 687–687.

Norwood, T. J., J. Boyd, et al. (1990). "Comparison of Techniques for H–1–Detected Heteronuclear H–1–N–15 Spectroscopy." Journal of Magnetic Resonance 87(3): 488–501.

Olejniczak, E. T., R. X. Xu, et al. (1992). "A 4d–Hcch–Tocsy Experiment for Assigning the Side–Chain H–1–Resonance and C–13–Resonance of Proteins." J Biomol NMR 2(6): 655–659.

Parkin, D. M. (2006). "The global health burden of infection –associated cancers in the year 2002." International Journal of Cancer 118(12): 3030–3044.

Patil, A., K. Kinoshita, et al. (2010). "Hub Promiscuity in Protein–Protein Interaction Networks." International Journal of Molecular Sciences 11(4): 1930–1943.

Penin, F., V. Brass, et al. (2004). "Structure and function of the membrane anchor domain of hepatitis C virus nonstructural protein 5A." Journal of Biological Chemistry 279(39): 40835–40843.

Pineda–Lucena, A., C. S. W. Ho, et al. (2005). "A structure–based model of the c–Myc/Bin1 protein interaction shows alternative splicing of Bin1 and c–Myc phosphorylation are key binding determinants." J Mol Biol 351(1): 182–194.

Polyak, S. J., D. M. Paschal, et al. (1999). "Characterization of the effects of hepatitis C virus nonstructural 5A protein expression in human cell lines and on interferon–sensitive virus replication." Hepatology 29(4): 1262–1271.

Poynard, T., M. F. Yuen, et al. (2003). "Viral hepatitis C." Lancet 362(9401): 2095–2100.

Rasia, R. M., E. Lescop, et al. (2011). "Rapid measurement of residual dipolar couplings for fast fold elucidation of proteins." J Biomol NMR 51(3): 369–378.

Reinehr, R. and D. Haussinger (2012). "CD95 death receptor and epidermal growth factor receptor (EGFR) in liver cell apoptosis and regeneration." Arch Biochem Biophys 518(1): 2–7.

Ren, G., P. Vajjhala, et al. (2006). "The BAR domain proteins: Molding membranes in fission, fusion, and phagy." Microbiology and Molecular Biology Reviews 70(1): 37–+.

Rijnbrand, R. C. A. and S. M. Lemon (2000). "Internal ribosome entry site–mediated translation in hepatitis C virus replication." Hepatitis C Viruses 242: 85–116.

Sakamuro, D., K. Elliott, et al. (1999). "Programmed cell death by c–Myc: Evidence of a caspase–independent effector signaling role for the c–Myc–interacting adaptor protein Bin1." Clinical Cancer Research 5: 3757s–3757s.

Sakamuro, D., K. J. Elliott, et al. (1996). "BIN1 is a novel MYC–interacting protein with features of a tumour suppressor." Nat Genet 14(1): 69–77.

Saksela, K., G. H. Cheng, et al. (1995). "Proline–Rich (Pxxp) Motifs in Hiv–1 Nef Bind to Sh3 Domains of a Subset of Src Kinases and Are Required for the Enhanced Growth of Nef(+) Viruses but Not for down–Regulation of Cd4." Embo Journal 14(3): 484–491.

Sattler, M., J. Schleucher, et al. (1999). "Heteronuclear multidimensional NMR experiments for the structure determination of proteins in solution employing pulsed field gradients." Progress in Nuclear Magnetic Resonance Spectroscopy 34(2): 93–158.

Schmidt, H., S. Hoffmann, et al. (2007). "Solution structure of a Hck SH3 domain ligand complex reveals novel interaction modes." J Mol Biol 365(5): 1517–1532.

Shelton, H. and M. Harris (2008). "Hepatitis C virus NS5A protein binds the SH3 domain of the Fyn tyrosine kinase with high affinity: mutagenic analysis of residues within the SH3 domain that contribute to the interaction." Virology Journal 5.

Shen, Y., F. Delaglio, et al. (2009). "TALOS plus : a hybrid method for predicting protein backbone torsion angles from NMR chemical shifts." J Biomol NMR 44(4): 213–223.

Shi, S. T., S. J. Polyak, et al. (2002). "Hepatitis C virus NS5A colocalizes with the core protein on lipid droplets and interacts with apolipoproteins." Virology 292(2): 198–210.

Shirota, Y., H. Luo, et al. (2002). "Hepatitis C virus (HCV) NS5A binds RNA–dependent RNA polymerase (RdRP) NS5B and modulates RNA–dependent RNA polymerase activity." Journal of Biological Chemistry 277(13): 11149–11155.

Shoemaker, B. A., J. J. Portman, et al. (2000). "Speeding molecular recognition by using the folding funnel: The fly–casting mechanism." Proc Natl Acad Sci U S A 97(16): 8868–+.

Singh, G. P., M. Ganapathi, et al. (2007). "Role of intrinsic disorder in transient interactions of hub proteins." Proteins 66(4): 761–765.

Street, A., A. Macdonald, et al. (2004). "The hepatitis C virus NS5A protein activates a phosphoinositide 3–kinase–dependent survival signaling cascade." Journal of Biological Chemistry 279(13): 12232–12241.

Tan, S. L. and M. G. Katze (2001). "How hepatitis C virus counteracts the interferon response: The jury is still out on NS5A." Virology 284(1): 1–12.

Tan, S. L., H. Nakao, et al. (1999). "NS5A, a nonstructural protein of hepatitis C virus, binds growth factor receptor–bound protein 2 adaptor protein in a Src homology 3 domain/ligand–dependent manner and perturbs mitogenic signaling." Proc Natl Acad Sci U S A 96(10): 5533–5538.

Tanji, Y., M. Hijikata, et al. (1995). "Hepatitis–C Virus–Encoded Nonstructural Protein Ns4a Has Versatile Functions in Viral Protein Processing." J Virol 69(3): 1575–1581.

Telfer, J. F., J. Urquhart, et al. (2005). "Suppression of MEK/ERK signalling by Myc: Role of Bin–1." Cellular Signalling 17(6): 701–708.

Tellinghuisen, T. L., J. Marcotrigiano, et al. (2004). "The NS5A protein of hepatitis C virus is a zinc metalloprotein." Journal of Biological Chemistry 279(47): 48576–48587.

Tellinghuisen, T. L., J. Marcotrigiano, et al. (2005). "Structure of the zinc–binding domain of an essential component of the hepatitis C virus replicase." Nature 435(7040): 374–379.

Tompa, P. (2002). "Intrinsically unstructured proteins." Trends in Biochemical Sciences 27(10): 527–533.

Uversky, V. N. (2011). "Intrinsically disordered proteins from A to Z." Int J Biochem Cell Biol 43(8): 1090–1103.

Uversky, V. N. (2011). "Intrinsically disordered proteins from A to Z." Int J Biochem Cell Biol 43(8): 1090–1103.

Uversky, V. N. (2011). "Intrinsically disordered proteins may escape unwanted interactions via functional misfolding." Biochim Biophys Acta 1814(5): 693–712.

Uversky, V. N., J. R. Gillespie, et al. (2000). "Why are "natively unfolded" proteins unstructured under physiologic conditions?" Proteins 41(3): 415–427.

Uversky, V. N., C. J. Oldfield, et al. (2008). "Intrinsically disordered proteins in human diseases: Introducing the D(2) concept." Annual Review of Biophysics 37: 215–246.

Verdegem, D., A. Badillo, et al. (2011). "Domain 3 of NS5A Protein from the Hepatitis C Virus Has Intrinsic alpha–Helical Propensity and Is a Substrate of Cyclophilin A." Journal of Biological Chemistry 286(23): 20441–20454.

Vucetic, S., H. B. Xie, et al. (2007). "Functional anthology of intrinsic disorder. 2. Cellular components, domains, technical terms, developmental processes, and coding sequence diversities correlated with long disordered regions." Journal of Proteome Research 6(5): 1899–1916.

Wang, Y. S., D. J. Liu, et al. (2004). "Competition STD NMR for the detection of high–affinity ligands and NMR–based screening." Magnetic Resonance in Chemistry 42(6): 485–489.

Ward, J. J., J. S. Sodhi, et al. (2004). "Prediction and functional analysis of native disorder in proteins from the three kingdoms of life." J Mol Biol 337(3): 635–645.

Wechsler–Reya, R., K. Elliott, et al. (1997). "The putative tumor suppressor BIN1 is a short–lived nuclear phosphoprotein, the localization of which is altered in malignant cells." Cancer Res 57(15): 3258–3263.

Williams, R. M., Z. Obradovi, et al. (2001). "The protein non–folding problem: amino acid determinants of intrinsic order and disorder." Pac Symp Biocomput: 89–100.

Wittekind, M. and L. Mueller (1993). "Hncacb, a High–Sensitivity 3d Nmr Experiment to Correlate Amide–Proton and Nitrogen Resonances with the Alpha–Carbon and Beta–Carbon Resonances in Proteins." Journal of Magnetic Resonance Series B 101(2): 201–205.

Wright, P. E. and H. J. Dyson (1999). "Intrinsically unstructured proteins: Re–assessing the protein structure–function paradigm." J Mol Biol 293(2): 321–331.

Wu, K. P. and J. Baum (2010). "Detection of Transient Interchain Interactions in the Intrinsically Disordered Protein alpha–Synuclein by NMR Paramagnetic Relaxation Enhancement." J Am Chem Soc 132(16): 5546–+.

Xie, H. B., S. Vucetic, et al. (2007). "Functional anthology of intrinsic disorder. 1. Biological processes and functions of proteins with long disordered regions." Journal of Proteome Research 6(5): 1882–1898.

Yao, J., H. J. Dyson, et al. (1997). "Chemical shift dispersion and secondary structure prediction in unfolded and partly folded proteins." FEBS Lett 419(2–3): 285–289.

Yu, H. T., J. K. Chen, et al. (1994). "Structural Basis for the Binding of Proline–Rich Peptides to Sh3 Domains." Cell 76(5): 933–945.

Zech, B., A. Kurtenbach, et al. (2003). "Identification and characterization of amphiphysin II as a novel cellular interaction partner of the hepatitis C virus NS5A protein." Journal of General Virology 84: 555–560.

Zuiderweg, E. R. P. (2002). "Mapping protein–protein interactions in solution by NMR Spectroscopy." Biochemistry 41(1): 1–7.

Zuiderweg, E. R. P. and S. W. Fesik (1989). "Heteronuclear 3–Dimensional Nmr–Spectroscopy of the Inflammatory Protein C5a." Biochemistry 28(6): 2387–2391.

Danksagung

Ich möchte mich bei Âllah(c.c.) für die unendliche Güte und Kraft bedanken, die er mir zukommen ließ.

An dieser Stelle möchte ich mich bei allen bedanken, die einen Teil zum Gelingen dieser Arbeit beigetragen haben. Prof. Dr. Dieter Willbold danke ich für die Schaffung der hervorragenden Arbeitsbedingungen und die Bereitstellung des sehr interessanten Themas. Für die Betreuung, die immerwährende Unterstützung und den ungebremsten Optimismus, der die Motivation stets auf einem hohen Niveau gehalten hat.

Bei Prof. Dr. Georg Groth möchte ich mich für die freundliche Übernahme des Zweitgutachtens bedanken.

Mein besonderer Dank gilt Dr. Silke Hoffman für die Betreuung und die zahlreichen Ideen bei der Entwicklung dieser Arbeit. Sie hatte stets immer ein offenes Ohr und stand mir tatkräftig mit ihrer Hilfe zur Seite. Darüber hinaus möchte ich mich für die Hilfe bei der Interpretation von Messdaten bedanken.

Dr. Matthias Stoldt danke ich für die Einführung in die NMR Spektroskopie und die Hilfe bei der Planung und Durchführung der NMR Experimente. Auch gilt hier mein Dank Dr. Rudolph Hartmann, der mir mit den Spektrometern immer wieder geholfen hat, wenn das „tunen und matchen“ wieder einmal nicht klappen wollte.

Für die Einführung und Unterstützung im Umgang mit Huh 7 Zellen und anschließender aufschlussreicher Diskussion in der Problematik der Zellkultur möchte ich mich bei Dr. Juliane Karthe herzlichst bedanken.

Besonders bei meinen Bürokollegen Dr. Karen Hänel und Dr. Jeannine Mohrlüder möchte ich mich stets für die freundliche Atmosphäre und die vielen lustigen sowie auch manchmal ernsthaften Gespräche über privates sowie wertvolle Ratschläge für die kleinen Pannen im Labor bedanken.

Ausserdem möchte ich mich bei Dr. Pallavi Thiagarajan für die wundervolle Zeit als meine Mitbewohnerin und als wertvolle Kollegin bedanken. Privat sowie im beruflichen Sinne haben wir uns prima verstanden und waren ein unzertrennliches Team. An dieser Stelle möchte ich mich auch bei ihrer Familie bedanken, die uns in Indien so herzlich aufgenommen haben.

Bei Dr. Julian Glück möchte ich mich für seine geduldige Einführung in die Biacore T200 Systeme bedanken.

Dr. Sophie Feuerstein und Dr. Bernhard Brutscher Danke ich für die fruchtbare Zusammenarbeit in dem NS5A Projekt. Dr. Melanie Schwarten danke ich für ihre Hilfe in dem Bin1 SH3 Projekt.

Den Mitgliedern unserer Gruppe HIV/HCV, Olga Valdau, Sussane Mödder, Alexandra Gorgels Dr. Ellen Kammula und Yufu Hung bedanke ich mich für die Hilfsbereitschaft und offenen Diskussionen in unserer Gruppe.

Bei Dr. Lei Wang, Dr. Yeliz Cinar, Dr. Ellen Kammula, Yufu Hung, Sameer Singh, Carsten Krichel, Marina Pavlidou, Cristina Asensio Jimenez, Zhanna Santybayeva, Dr. Tobias Rosenkranz, Jide Olubiye, Cheetan Poojari, Dr. Hoa Do Quynh, Silke Dornieden und Louis Möckel möchte ich mich für die privat verbrachte Zeit auf Konzerten, Dinner- und Filmabenden, den Gitarrenstunden und amüsanten Heimfahrten bedanken.

Anschließend möchte ich mich beim gesamten ICS-6 für die wundervolle Zeit und Arbeitsatmosphäre bedanken.

Mein Dank gilt auch meiner Freundin Jennifer Li, die sich geduldig alle meine Sorgen und Freuden angehört hat und mir aufmunternd zur Seite stand.

Meinen Eltern Süleyman und Ayse Aladağ gilt mein ganz besonderer Dank, weil Sie mich ohne zu zögern in meinem Leben und bei meinen Entscheidungen immer unterstützt haben. Zusammen mit meinen Geschwistern Sevim Tavşan, Nuriye Koçak, Zehra Aladağ und Fatima Aladağ waren sie immer eine Quelle von Stärke und Inspiration. Meiner Kusine Elmas Aladağ danke ich für ihr aufheiterndes Wesen.

Hiermit erkläre ich, dass ich die vorliegende Arbeit selbständig angefertigt habe. Es wurden nur die in der Arbeit ausdrücklich benannten Quellen und Hilfsmittel benutzt. Wörtlich oder sinngemäß übernommenes Gedankengut habe ich als solches kenntlich gemacht. Es wurden zuvor keine Promotionsversuche unternommen.

Jülich, den 09.03.2012

Amine Aladağ